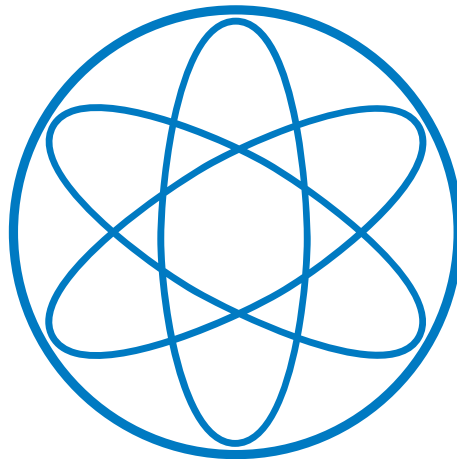# AGN Probes of Dark Matter Scenarios with t-channel Mediators

AGN Untersuchungen von Dunkler Materie
Szenarien im t-channel Austausch

Christoph Hornstein

Department of Physics
Technical University Munich

Master thesis presented for the degree
M. Sc. in Physics

Supervised by
Prof. Dr. Alejandro Ibarra

Submitted on 03rd November 2023

Abstract

It has been realised for a long time that supermassive black holes at the centre of each galaxy could form a dense dark matter spike. As a result, the density of dark matter could be enhanced in the centre of a galaxy. The particles produced inside the spike could interact more frequently with the dark matter than usually. Active Galactic Nuclei (AGN) are expected to emit neutrinos or photons with high energy. If the photons or neutrinos are produced inside the spike, they have to travel through the dense dark matter spike on their way to earth.

As a result, the flux of photons and neutrinos could get attenuated, when traversing the dense dark matter spike around an AGN. The aim of this master thesis is to calculate possible interactions between dark matter and neutrinos, as well as, photons. We focus on the case of a scalar dark matter candidate and Majorana fermion which both can be realised in the t-channel mediator model. Further, we investigate the elastic and inelastic scatterings in large and low energy regimes. These interactions are used to examine the possible flux attenuation, depending on the dark matter column density of the spike.

For the attenuation of the neutrino flux, we consider a scenario where the dark matter is a spinless scalar particle with an fermionic mediator, as well as, the scenario where the dark matter particle is a spin $1/2$ Majorana fermion with a scalar mediator. For the attenuation of the photon flux, we consider a scenario where the dark matter is a spin $1/2$ fermion that interacts with the photon via a scalar mediator.

We will mainly investigate the inelastic scatterings that can attenuate the photon and neutrino fluxes. Also, the direct production of the mediator could be possible given the very high photon and neutrino energies. Especially, the inelastic scatterings with the gauge bosons could lead to absorption effect. As an application, we are investigating the implications on the t-channel mediator model and the Scotogenic model of neutrino mass generation, as well as on its Scale Invariant extensions. We will show that the scatterings between the photons and neutrinos could lead to absorption of over 65% for certain dark matter column densities in the t-channel mediator model. We will further roughly estimate the black hole masses that are needed to achieve the column densities.

The calculations are being done analytically using standard tools of quantum field theory, and with the help of Mathematica and also Python for the numerical calculations.

Declaration

I hereby declare that the thesis submitted is my own unaided work. All direct or indirect sources used are acknowledged as references.

Ich versichere hiermit, dass ich die von mir eingereichte Abschlussarbeit selbstständig verfasst und keine anderen als die angegebenen Quellen und Hilfsmittel benutzt habe.

Munich, 03rd November 2023

List of Abbreviations

ΛCDM Standard Model of Cosmology

AGN Active Galactic Nuclei

BLR Broad Line Region

CKM Cabibbo-Kobayashi-Maskawa

CM Centre of Mass

CMB Cosmic Microwave Background

CRESST Cryogenic Rare Event Search with Superconducting Thermometers

DM Dark Matter

EHT Event Horizon Telescope

GR General Relativity

KATRIN Karlsruhe Tritium Neutrino Experiment

LFV Lepton Flavour Violation

LHC Large Hadron Collider

MACHO Massice Compact Halo Object

MOND Modified Newtonian Dynamics

MSSM Minimal Supersymmetric Standard Model

NFW Navarro-Frenk-White

QCD Quantum Chromodynamics

SM Standard Model

WIMP Weakly Interacting Massive Particle

Contents

Chapter 1

Introduction

Since ancient Greece, people have been asking themselves what the earth and the universe are made of. Natural philosophers, such as Aristotle or Plato asked questions about the origin of life and our planet. This is precisely why the term *physics* comes from the ancient Greek word *physis*, which can essentially be translated as nature and describes the nature of things [1].

For the presocratic philosophers *physis* is used for the whole cosmos as such and comprises the whole physical world. Interestingly, the two philosophers of that period, Democritus and Leucippus, postulated that the world is made of small indivisible substances, which they called atoms. The only property of the atoms is that they are indivisible. They interact which each other mechanically through collision or they may accumulate. But the two philosophers never presented any empirical evidence fpr their theory because they simply postulated it. They were not typical scientists as we know them today.

Nevertheless, this simple theory is surprisingly similar to the modern view of physicists. It reminds one very much of the Standard Model (SM) of particle physics. It is the current best theory that we have about the fundamental particles of which the world and the cosmos is built up. The particles in the SM are also not divisible, as in the theory of Democritus and Leucippus. But they can interact via the four fundamental forces, namely the electrical, the weak, the strong and the gravitational interaction. The SM is very popular in modern physics and is measured very precisely [2].

On the other hand, we have evidence that the Standard Model of particle physics is not complete and not sufficient to explain the evolution of the universe. The Standard Model of Cosmology (ΛCDM) describes the structure formation of the universe as we currently observe it and states that we need some non-luminous matter, called dark matter, in order to achieve the structures that we see today. This unknown matter is not contained in the SM of particle physics and the SM is therefore incomplete. One needs to extend the SM by dark matter. But one big questions that remains until now. What is the particle nature of dark matter and what are its properties?

There is ongoing research on dark matter for years and we have not unravelled the mystery of dark matter yet. As always in physics, it is a game of trial and error. But every negative result brings us closer to the actual dark matter scenario that is realised in our universe. So, physicist do not give up and and continue with research by testing dark matter scenarios. This inspires us to write and present the following

master thesis.

The aim of the thesis is to probe dark matter scenarios with t-channel mediators and the help of AGNs. Neutrinos and photons are emitted close to the AGN and scatter with dark matter particles along their way to the earth. Therefore, AGNs are powerful probes for dark matter scenarios and give current limits on the scattering between dark matter and neutrinos or photons [3, 4]. This motivates us to calculate the interaction between a specific choice of a dark matter model and neutrinos or photons and test the current constrains.

In this regard, the structure of the thesis is as follows. First, we will review the evidences for dark matter in Ch. 2 that lead to the conclusion that we need some non-luminous matter in our universe. We will have a look at the astrophysical and cosmological observations that point towards dark matter.

Next, in Ch. 3, we will dive into the theory of dark matter by beginning with different prominent dark matter candidates. This is followed by the basic assumptions for particle dark matter. We will also present shortly the thermodynamics of the early universe and the Boltzmann equation. In a further step we want to understand the impact of the dark matter particles in the early universe to gain insights on the dark matter abundance today and their interaction strength.

In Ch. 4 we change the topic and we will talk about scattering in Quantum Field Theory. We are going to define the scattering cross section that will be of great use in our analysis. This is followed by a motivation of why we are interested in scatterings between dark matter particles and standard model particles in Ch. 5. We will have a look at AGNs that are of great interest for probing the particle nature of dark matter. The dark matter spike that one expects around black holes is also introduced.

Then, in Ch. 6 we start our phenomenological investigations by introducing a simple toy model. This is followed by a brief introduction about two dark matter models, namely the t-channel mediator model and the Scotogenic Model. After that, we will compute the scattering cross sections between two different scenarios of dark matter particles and photons or neutrinos. Further, we will use the cross section to examine possible attenuation of the photon and neutrino fluxes, due to their interaction with dark matter, in the vicinity of black holes.

Finally, in Ch. 7 we will summarise our investigations and give state a conclusion. We will also give brief outlook for future work.

Chapter 2

Evidence for Dark Matter

The ΛCDM is the Standard Model of Cosmology, where CDM stands for cold dark matter and Λ for the cosmological constant which takes into account the accelerated expansion of the universe. Cold means that the dark matter is non relativistic. Hence, in the standard cosmological scenario we assume that there exists non luminous matter which we call Dark Matter (DM). It does not interact with light and is therefore "invisible" but it can interact via gravity. Dark matter was first stated by Franz Zwicky in 1933 [5] by looking at the redshift of the distant nebula's. Later in the 1970s, Vera Rubin discovered one of the strongest hints for dark matter by observing the rotation curves of the Andromeda nebula [6]. Today we know that dark matter contributes up to 25% to the energy density in our universe and makes up to 85% of all ordinary matter. Dark matter is an integral part of contemporary cosmology and astrophysics and we have several evidences for its the existence.

The first evidence that we will discuss are the so called rotation curves. The angular velocity in the outer regions of a galaxy is higher than expected. This phenomenon can be explained by postulating more matter than we can actually see in a galaxy. The second hint for dark matter is the mass to light ratio in the coma cluster and was found by Franz Zwicky. The visible mass of the coma cluster is to small for the velocities of the galaxies inside the cluster. The third evidence for dark matter is gravitational lensing. The fourth evidence is the so called Cosmic Microwave Background (CMB). All of them together give a clear significance that dark matter exists in our universe. In the following sections we will briefly go through these main evidences of dark matter and explain them.

2.1 Rotation Curves

One of the most popular hint for dark matter are definitely the rotation curves of the galaxy NGC6503. In our solar system the planets rotate around the centre and obey the Keplerian laws. They state that the rotation velocity v_{rot} should be proportional to 1 over the square root of the distance R, which can be quantified by

$$v_{\text{rot}} = \sqrt{\frac{GM(R)}{R}}, \tag{2.1}$$

where $M(r) = 4\pi \int \rho(r)r^2 dr$ is the total mass of the mass density distribution $\rho(r)$ and G the gravitational constant. Elliptical galaxies spiral inside a plane that can

be approximated as a disk. Outside of the disk the mass should be constant and therefore $v_{\text{rot}} \propto \sqrt{1/R}$. By only assuming this simple relation we can state that the velocity of the stars further outside should decrease.
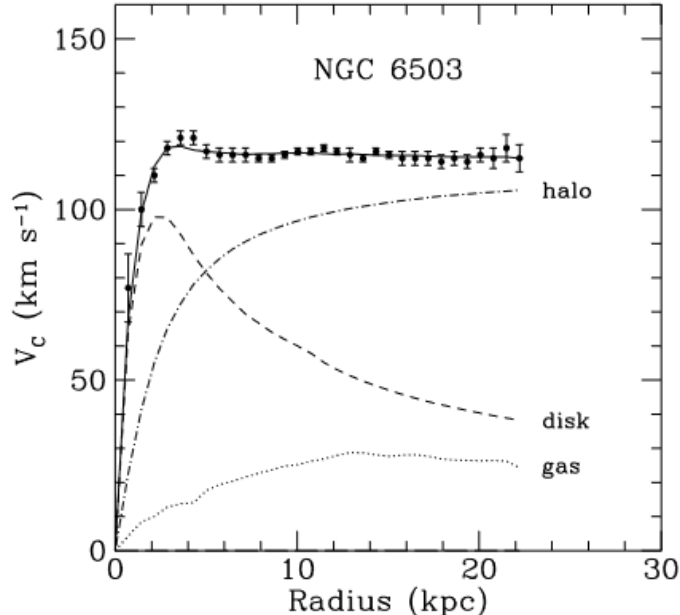
Figure 2.1: Rotation curve of the dwarf spiral galaxy NGC 6503. It shows the different contribution of gas, disk and a dark matter halo to the rotation curve. Dark Matter is postulated in order to explain that the rotation velocity becomes constant for $R > 4$ kpc. The picture was taken from [7]

But this does not happen as we can see in Fig. 2.1. In contrary, the rotation velocity stays constant outside the visible galaxy. One possible explanation for this phenomenon is that there is non-visible matter outside the visible galaxy that only interacts via gravitation and the weak force. Hence, dark matter is the reason why the velocity curve stays constant. Therefore, the density profile should scale as $\rho \propto 1/r^2$. A first hint for dark matter is born at galactic scales.

Of course, there could also be other explanations to this phenomenon. For example, this effect could be due to our ignorance about gravity and the Newtonian laws. The theory of Modified Newtonian Dynamics (MOND) states also an explanation for the increase of the velocity curve [8]. In [8] Milgrim modifies Newtons laws such that for high distances $F = ma^2/a_0$ with a_0 being a constant. For a stable system the centrifugal force equals the gravitational force. Hence, $GMm/r^2 = m/a_0 \cdot (v^2/r)^2$. This results in a constant velocity for large distances given by $v = (GMa_0)^{1/4}$. But frankly, we have more than just this one piece of evidence for dark matter. We also have the three other evidences which account for this redundancy and leave no doubt about the existence of dark matter.

2.2 Mass to Light Ratio in the Coma Cluster

In 1933 and 1937 the Swiss physicist Franz Zwicky published two papers about the Coma cluster where he uses the redshift to determine the velocity dispersion of

the galaxies inside the Coma cluster [5, 9]. For a stationary cluster the viral theorem states that $2E_{\text{kin}} + U_{\text{pot}} = 0$, where E_{kin} is the kinetic and U_{pot} the potential energy. If the galaxies inside the cluster are distributed uniformly, the potential energy is given by $U_{\text{pot}} = 3GM^2/5R$ [9]. Taking the kinetic energy simply to be $E_{\text{kin}} = M\overline{v^2}/2$, where $\overline{v}$ is the average velocity. [1] The viral theorem connects the potential and kinetic energy. Thus, Zwicky obtained that $M = 5R\overline{v^2}/3G$. Comparing the theoretical mass of the Coma cluster to explain the velocity dispersion to the amount of luminous matter in the Coma cluster Zwicky came to the result that the former is exceeded by the latter by about a factor of 400:

$$\left(\frac{M}{L}\right)_{\text{Coma}} \sim 400 \left(\frac{M_\odot}{L_\odot}\right). \tag{2.2}$$

So, Zwicky found that the velocity dispersion of the galaxies inside the cluster is so high that the visible matter is not sufficient enough to keep the system stable [10]. The same analysis was done for the Virgo cluster. With the same result that there is a discrepancy in the mass [11]. Hence, Zwicky deduced that there must be non visible matter in order to describe the mass discrepancy. He called the non visible matter Dark Matter. Later, gas was discovered in the Coma cluster that is only visible in the X-ray bands. But the mass of the gas is not sufficient to explain the high velocity dispersion relation. Nevertheless, until the 1960s and 1970s dark matter was not the only solution to the problem. Large amount of dwarf galaxies or black holes were ideas to name only two of them [10].

2.3 Gravitational Lensing

A third type of evidence for dark matter can be obtained via gravitation. In General Relativity (GR) the spacetime around massive objects is bend. If there is matter in the line of sight between a distant source and the observer, the matter can act as a lens if its mass is large enough. The light gets bend and the image is distorted around the lens. This effect is called gravitational lensing. One can use the gravitational lensing effect to scan galaxy clusters and can therefore examine the mass that should be present inside a cluster, due to the gravitational potential of the cluster. It is a perfect way of observing dark matter because the gravitational influence of dark matter is more "visible" or detectable than its particle nature [12].

The most striking and well known example of this method is the galaxy cluster 1E 0657-56 the "bullet cluster" [13]. The bullet cluster is a galaxy cluster that formed because two clusters merged [12]. During this collision the baryonic matter strongly interacts with each other. But the dark matter should not interact because it only couples to gravity and the weak force. Thus, we should have a strong separation between the ordinary matter and the dark matter as shown in Fig. 2.2.

---

[1] strictly speaking Zwicky used the average of the averaged velocity. See [9] for further information
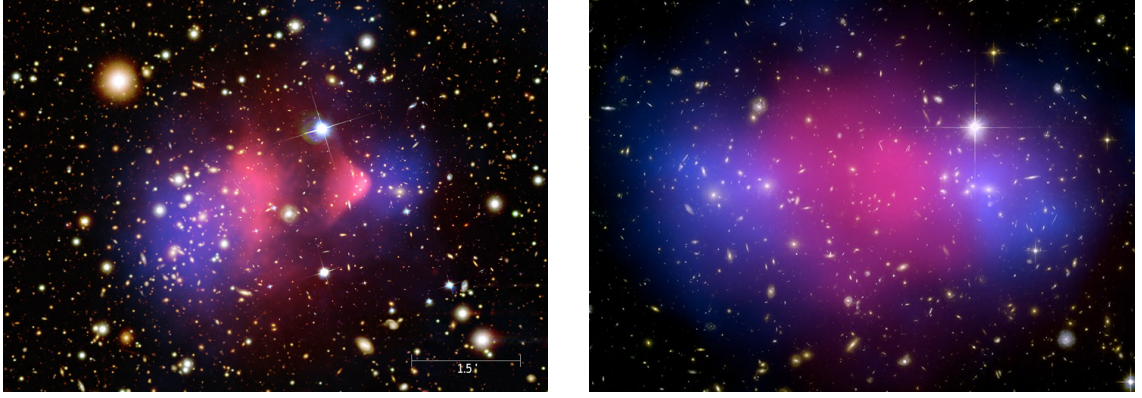
Figure 2.2: The "bullet cluster" 1E0657-56 (left) and the "baby bullet" MACSJ0025.4-1222 (right) as composition. In the background galaxies are visible mostly in yellow. The hot gas emission in the X-ray band is shown in pink. The blue feature shows the reconstruction of the total mass distribution in the galaxy cluster measured via gravitational lensing. We see clearly in both figures that the masses responsible for the gravitational potential lie further outside and are separated. Whereas the visible matter is found in the middle emitting the X-rays. This is consistent with the picture that during the merging process the dark matter does not interact and the ordinary matter does. The dark matter halo "lost" its hot gas during the collision. The mass lying outside of the visible region is larger than the total mass of all the present galaxies. Therefore it is a strong hint for dark matter. Figure Credit: Left: [14]; Right: [15].

This separation can be reconstructed with gravitational lensing. The pink region in Fig. 2.2 shows the X-ray emission of the galaxy cluster from the intergalactic plasma. The blue regions shows the gravitational potential revealed by the lensing effect. It is consistent with the location of the galaxies. The large gravitational potential cannot be explained only by the present galaxies [12]. We therefore have a strong hint for dark matter inside the bullet and baby bullet cluster.

So, we have seen that it turns out that the visible mass is again not enough to explain the effect of the gravitational lensing. Thus, we have a third evidence for dark matter in our universe that this time cannot be explained by the MOND theory [16]. Let us now turn our interest to the last evidence.

2.4   Cosmological Evidence

We have seen so far, that there are hints for dark matter in the scale of galaxies (rotation curves) and galaxy clusters (mass to light ratio in the Coma cluster and gravitational lensing effects). But there exists are fourth type of DM evidence on cosmological scales. It rose up due to the discovery of the CMB [17].

The detection of CMB through Penzias and Wilson was a real breakthrough in cosmology. It supports the theory of an expanding universe over of a steady state scenario of the universe. In the big bang model the universe starts to expand from a hot and dense initial state. During the expansion it cools off and nuclei and atoms start to form after the photons decoupled from the hot plasma. Therefore, the big bang model predicts a background radiation as a relic from the early state [18].

The CMB is a perfect black body spectrum with a temperature of $T = 2.726$ K and small temperature fluctuation at the order of 10^{-5}[7]. These fluctuations are the imprint of the density contrast in the early universe. In the 1980s Peebles pointed out that dark matter is necessary to explain how these anisotropies in the CMB lead to the large scale structure formation that we observe today [19]. Dark matter does not interact with the photons and can form large gravitational potentials since there is no pressure counteracting on it. As soon as the photons decouple the baryonic matter falls into the potential wells of the dark matter and begins to form larger structures. The presence of DM accelerates the process of galaxy and galaxy cluster formation.

To extract information from the CMB, the temperature fluctuations are expanded in spherical harmonics $Y_{lm}(\theta, \phi)$ in terms of the multipole moments l which correspond to the angle in the sky:

$$\frac{\delta T}{T}(\theta, \phi) = \sum_{l=1}^{\infty} \sum_{m=-l}^{l} a_{lm} Y_{lm}(\theta, \phi). \tag{2.3}$$

The multipole moments l can be related to the angle via $\Delta\Theta \sim \pi/l$. The variance of the coefficients a_{lm} is called C_l. Normally, $D_l = l(l+1)C_l/2\pi$ is plotted as a function of l which we call the angular power spectrum of the temperature. It is shown in Fig. 2.3[7].
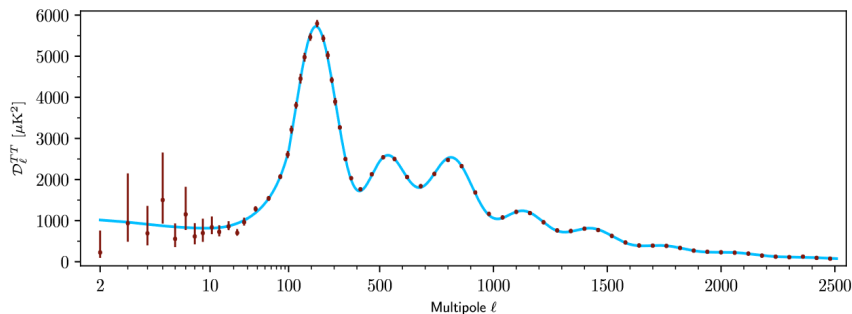
Figure 2.3: Angular power spectrum of the temperature D_l, where TT means temperature. The blue line shows the best fit to the Plank data. From this fit one can extract the total amount of matter in the universe and the amount of dark matter. The figure is taken from [20].

One fits the graph with a chosen cosmological model and the associated free parameters [21]. The best current fit of the Plank data supports the ΛCDM model with

$$\Omega_{\mathrm{DM}} h^2 = 0.120 \pm 0.001 \tag{2.4}$$

and $\Omega_{\mathrm{b}} h^2 = 0.0224 \pm 0.0001$, where Ω is the density parameter which measures the energy density in our universe and $h = H_0/(100\mathrm{km/s/Mpc})$ is the factor that makes the density parameter independent of the Hubble constant H_0 [22]. Ω_{b} is the baryonic density which means in this context the energy density of ordinary matter. Thus, the observation of the CMB indicates that dark matter makes up to 85% of the total matter in our universe.

In summary, we can conclude that we have strong evidences for the existence of dark matter in our universe from galactic to cosmological scales. Dark matter

provides a convincing solution to all of the astrophysical problems discussed above and perfectly fits to the angular power spectrum of the CMB. Thanks to the newest Plank observation we know the amount of dark matter in the universe and its impact on large scale structure formation, as well as, on the evolution of the universe. We know that every galaxy is contained in a larger DM halo. But we still do not know many other properties of dark matter. It is unclear whether dark matter interacts only via gravity or also weakly with other matter. There are many different candidates for dark matter. In this master thesis we will assume that dark matter is a particle and that it interacts weakly and that it is massive. This dark matter candidate is also known as Weakly Interacting Massive Particle (WIMP). In the next section we will mention a few other dark matter candidates and dive into the theory of dark matter.

Chapter 3

Theory of Dark Matter

Having summarised the most popular evidences of dark matter one open question still exits until now. What actually is dark matter and what is it composed of? The answer to this question is not yet found and an open question in physics. Since the realisation that most of the matter in the universe is dark matter the searches began. In the following section, we will name a few dark matter candidates and mention them only briefly. This is followed by theoretical descriptions on the particle nature of dark matter and a consideration on its relic abundance. So let us start with the different candidates.

3.1 Dark Matter Candidates

3.1.1 Massive Compact Halo Objects

One very attractive solution to the problem of the missing mass outside the visible galaxies is the postulation that so called "Massice Compact Halo Object (MACHO)" exist. A MACHO is for example a neutron star, large planets, brown dwarfs or primordial or ordinary black holes. Hence, the missing mass in the galaxy clusters are objects that we have not detected so far, because they are not easy detectable. For the detection one uses the so called weak lensing effect which is a subclass of the gravitational lensing effect. An astonishingly simple and intriguing theory. What makes this candidate so attractive is that one does not have to introduce some new particles to explain the phenomenons of dark matter. We do not have to extend the Standard Model of particle physics. One just has to search for this astrophysical objects and the problem is solved [23].

However, it is not so straight forward as it sounds. The detection of the MACHOs via weak lensing is not easy and MACHOs as a viable dark matter candidate are very constrained [24]. Furthermore, we have other problems in physics that we need to tackle by extending the Standard Model. But still MACHOs are not fully excluded yet and ongoing researches about primordial black holes will enlighten us in the future about the role of primordial black holes as dark matter candidate [25].

3.1.2 Axions

The strong CP problem is one of the unsolved mysteries in physics. Here, C stands for charge conjugation and P for parity. In Quantum Chromodynamics

(QCD) there is no indication why the CP symmetry should be conserved. In fact, one has to manually set the CP breaking term to zero which is quite unsatisfying. The CP breaking can be measured through the electric dipole moment of the neutron but it has never been observed so far [26]. To kill two birds with one stone, the axion particle was postulated that tackles the strong CP problem and is a viable dark matter candidate too [7, 26].

Axions are expected to interact very weakly with SM particles and are constrained to be very light. They satisfy all present-day constrains what makes them a suitable dark matter candidate [7]. The key detection is via their interaction with photons and current searches are ongoing around the world [27, 28]. Axion are among the most popular dark matter candidates.

3.1.3 Neutrinos

Since the detection of the neutrino oscillation [29] which was awarded with the Nobel price in 2015, we know that neutrinos must have a small mass. They only interact weakly and do not have an electromagnetic charge. So they can be a perfect dark matter candidate without introducing some beyond Standard Model (BSM) physics. However, we can make a simple consideration to disapprove them. We know that there exit three neutrino species; electron, muon and tau neutrinos. The mass hierarchy of the neutrinos is not known [30]. The total relic abundance of the neutrinos can be calculated as follows [7]

$$\Omega_\nu h^2 = \sum_{i=1}^{3} \frac{m_i}{93 \text{ eV}}. \tag{3.1}$$

The best current constrains for the neutrino mass comes from the Karlsruhe Tritium Neutrino Experiment (KATRIN). They use tritium $\beta-$decay spectra to determine upper limits on the neutrino mass. Their acutual result gives a limit of [31]

$$m_\nu < 0.8 \text{ eV} \quad (90\% \text{ C.L.}). \tag{3.2}$$

This limit concerns all three mass eigenstates because the mass difference of the neutrinos is very small. Hence, the total relic abundance is constrained to be

$$\Omega_\nu h^2 \lesssim 0.026, \tag{3.3}$$

which is lower than the dark matter value of $\Omega_{\text{DM}} h^2 = 0.120$. This means that the neutrinos are not abundant enough in our universe in order to be dark matter. Another argument against neutrinos as dark matter candidate is that the neutrinos would be so called hot dark matter because they decouple from the thermal bath when they are still relativistic (see ch. 3.5 for more details). This would influence the large scale structure formation in the universe. It would favour that large structures were formed first and the smaller structures form via fragmentation processes [32]. But the local group seems to be younger than our own galaxy [33]. Therefore, large structures form after small structures, due to gravitational attraction. Thus, we have a further argument against neutrinos as dark matter.

In summary, we can say that the ordinary neutrinos that we know from the SM can not be the dark matter because they are not abundant enough and they would be hot dark matter.

As the neutrinos are massive there must be a right handed neutrino. They can simply be added as an extension of the standard model. These new neutrinos are often called sterile neutrinos and they can actually be a viable dark matter candidate [34, 35]. The mass range of sterile neutrinos can be from keV up to TeV. However, the mixing angles and the mass of the right-handed neutrino is very constrained [35, 36]. But still they can be a dark matter candidate in opposite of the ordinary neutrinos. They are very attractive because they can be used to explain the small masses of the neutrinos via the seesaw mechanism.

3.1.4 WIMPs

The current best cosmological model (the ΛCDM model) favours the dark matter to be cold which means that the dark matter is non-relativistic at the time of the freeze-out. So, one solution to the dark matter problem can be obtained by extending the standard model by particles that only interact weakly and are very massive. These weakly interacting massive particles are called WIMPs and are a very popular dark matter candidate [37]. The dark matter abundance of the WIMPs can be very well calculated with the freeze-out mechanism in the early universe. It predicts perfectly well the dark matter abundance of today when the dark matter mass is at order of the weak scale. This is called the "WIMP miracle" [38].

Furthermore, the WIMPs are very well motivated in theory. The supersymmetric extension of the standard model predicts that every boson has a fermionic and every fermion a bosonic partner. In the Minimal Supersymmetric Standard Model (MSSM) the neutralino is the most discussed dark matter candidate [39]. Another possibility to realise WIMPs, is to simply extend the SM by another Higgs doublet. This model is also called the inert Higgs model, where the lightest neutral particle of the doublet can play the role of the dark matter particle. [40].

Most of the common dark matter detection techniques can be divided into three groups [41, 42]:

1. Direct Searches
2. Indirect Searches
3. Production Searches

Direct searches focus on detecting nuclear recoil energy. If the dark matter particle interacts with the nucleus inside the detector it deposits energy in form of recoil energy. This energy can be detected and has to be discriminated from the background. An example for a common experiment is the Cryogenic Rare Event Search with Superconducting Thermometers (CRESST) in Gran Sasso. Indirect searches focus on the detection of secondary particles from dark matter annihilation processes. For example, two dark matter particles can annihilate into two photons. Due to the photonic absorption bands of the atmosphere one goes normally into the outer space via satellites. The Fermi-LAT is one telescope that tries to detect dark matter indirectly. Production searches want to produce dark matter particles through particle collision. For example through proton-proton collision at the Large Hadron Collider (LHC) [42]. Despite the ongoing searches, no dark matter has been detected so far. The detection technique presented in this master thesis can be sorted into the 2. group.
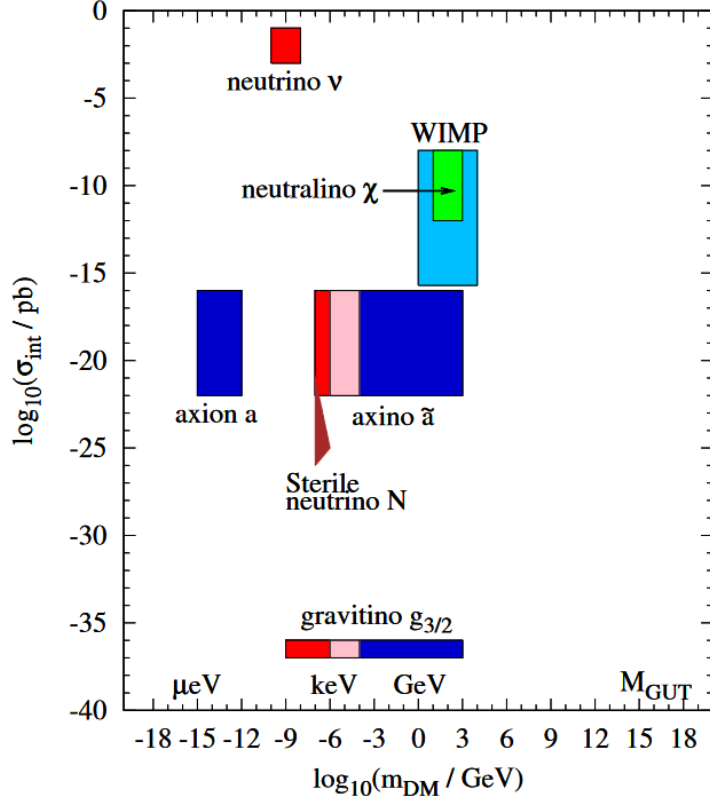
Figure 3.1: Ranges of the interaction cross section between DM and SM particles in terms of the dark matter mass. Some typical dark matter candidates are shown like the axions, the sterile neutrinos and the WIMPs as well as the SUSY particles gravitino and neutralino. The red, pink and blue colours stand for hot, warm or cold dark matter, respectively. The masses of the dark matter candidates vary from several eV up to TeV. In this master thesis we will focus on WIMPs which have mass between hundred GeV and TeV. The picture is taken from [39].

In summary, as shown in Fig. 3.1, there are several viable dark matter candidates that would solve the dark matter problem. Their masses range from several eV up to TeV. In this master thesis we will focus on dark matter being WIMPs that lie in the range of GeV up to TeV. However, there has never been a detection of a WIMP so far, despite of the ongoing searches for years. But still it is a very well motivated and attractive candidate for dark matter.

3.2 Dark Matter Properties

As mentioned before, in this thesis we will focus on the dark matter as WIMPs. In order to work with this candidate we have to impose four key assumptions on the them which are the following:

1. The WIMPs must be stable in cosmological timescales. Which means that the lifetime of the dark matter should be longer than the age of the universe. If the WIMP is not stable we would not observe the dark matter in our universe because it already decayed to some secondary particles. But we do observe the effects of dark matter and therefore the assumption that dark matter is stable is well motivated.

2. The WIMPs interact in pairs with the SM particles. These interactions are needed in order to detect dark matter particles via direct, indirect or production searches. The dark matter can either scatter with, annihilate into or be produced by standard model particles which is shown by the following sketch:
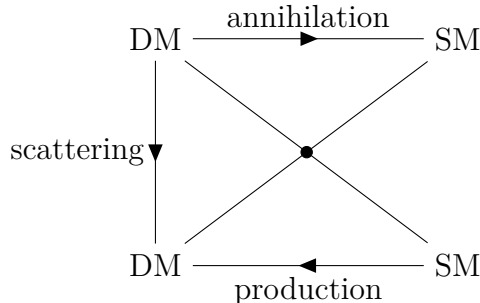
3. The WIMP interaction strength is large enough to keep the DM in thermal equilibrium at high temperatures. In the early universe we have a thermal equilibrium between standard model particles and dark matter particles. If the dark matter particles decouple to early from the thermal bath we overproduce them. On the other hand, if they decouple to early they are underproduced. That is why we need the next assumption.

4. The WIMP interaction strength is small enough to ensure that the DM particles decouple from the thermal plasma in the early universe sufficiently early.

With these four assumptions we can now continue to investigate the impact of dark matter in the early universe.

3.3 Thermodynamics and the Evolution of the Early Universe

In this section we will briefly go through the thermodynamic of the early universe. They are the key to understand the "*WIMP miracle*" that we will discuses in the next chapter. However, for a more detailed discussion see [43, 44]. We will follow [43] in this section.

According to the ΛCDM model the universe seems to be isotropic and homogeneous at large scales. We furhter assume the universe to be flat. Therefore the universe can be described by the Friedman-Lemaitre-Robertson-Walker (FLRW) metric:

$$ds^2 = dt^2 - a^2(t)(dr^2 + d\Omega^2), \tag{3.4}$$

where t describes the cosmic time and $a(t)$ is the dimensionless scale factor. The dynamics of the universe are given by the Einstein field equations

$$R_{\mu\nu} - \frac{1}{2}g_{\mu\nu}R = 8\pi G T_{\mu\nu} \tag{3.5}$$

with $R_{\mu\nu}$ being the Riemannian curvature tensor, R the Rici scalar, $g_{\mu\nu}$ the metric, $T_{\mu\nu}$ the energy-momentum tensor and $G = 6.72 \cdot 10^{39}$ GeV^{-2} Newtons gravitational constant. When we use the energy-momentum tensor of a perfect fluid together with the FLRW metric we obtain the Friedman equation

$$H(t)^2 = \left(\frac{\dot{a}}{a}\right)^2 = \frac{8\pi G}{3}\rho_{\text{tot}}, \qquad (3.6)$$

where $H(t)$ is the Hubble parameter and ρ_{tot} the total energy density of the universe. The three main contributions to the energy density are given by radiation, matter (containing ordinary and dark matter) and dark energy. During different epochs of the universe the dominating energy density changes. In the early universe radiation is the dominant quantity, while today the dark energy density predominates. We can also define the density parameter given by the following:

$$\Omega_i = \frac{8\pi G}{3H_0}\rho_i, \qquad (3.7)$$

where H_0 is the Hubble constant and ρ_i the energy density of the different species.

In the early universe radiation dominates. But the particles that contribute to the radiation density are various. There are photons, electron, protons, etc. Thus, we need a framework where we can work out the different contributions of the particles. This is done via the phase space distribution function $f(t, \vec{k})$ for a homogeneous and isotropic universe which is a probability distribution function.

So, we start by considering a gas of particles with mass m, phase space distribution $f(\vec{k})$ and g internal degrees of freedom. Thus, we obtain for the number density n_i, the energy density ρ_i and the pressure P_i of a species i the following equations:

$$n_i(t) = \frac{g}{(2\pi)^3} \int d^3k \cdot f(t, \vec{k})$$

$$\rho_i(t) = \frac{g}{(2\pi)^3} \int d^3k \cdot E \cdot f(t, \vec{k}) \qquad (3.8)$$

$$P_i(t) = \frac{g}{(2\pi)^3} \int d^3k \cdot \frac{|\vec{k}|}{3E} \cdot f(t, \vec{k}).$$

We mostly deal with fermions and bosons. The phase space distribution function is given by the Fermi-Dirac (fermion) and Bose-Einstein (boson) distribution

$$f(\vec{k}) = \frac{1}{e^{\frac{E-\mu}{T}} \pm 1}, \qquad (3.9)$$

where $+$ is for fermions and $-$ for bosons. Here μ is the chemical potential and T the temperature. The energy is given by $E = k^2 + m^2$. Due to the isotropy of the universe we can carry out the angular integration to be $\int d^3k = 4\pi \int_0^\infty k^2 dk$. Through the energy-momentum relation we can express $\vec{k}$ in terms of the energy and the mass and get that $EdE = kdk$. In the early universe all of the particles are relativistic up to a certain limit, when $T \gg m$. Hence, for the energy density we obtain

$$\rho_i = \begin{cases} \dfrac{\pi^2}{30} \cdot g_i \cdot T_i^4, & \text{Bosons} \\[2ex] \dfrac{7}{8} \cdot \dfrac{\pi^2}{30} \cdot g_i \cdot T_i^4, & \text{Fermions} \end{cases} \qquad (3.10)$$

14

For the total energy density we have to sum over the different species

$$
\begin{aligned}
\rho_{\text{tot}}(T) &= \sum_{\text{rel. bosons}} \rho_i \quad + \sum_{\text{rel. fermions}} \rho_i \\
&= \sum_{\text{rel. bosons}} \frac{\pi^2}{30} \cdot g_i \cdot T_i^4 \quad + \sum_{\text{rel. fermions}} \frac{7}{8} \cdot \frac{\pi^2}{30} \cdot g_i \cdot T_i^4 \\
&= \frac{\pi^2}{30} g_*(T) T^4,
\end{aligned}
\tag{3.11}
$$

where we used the effective number of relativistic degrees of freedom $g_*(T)$ in the last step which is giveyn by

$$
g_*(T) = \sum_{\text{rel. bosons}} g_i \cdot \left(\frac{T_i}{T}\right)^4 \quad + \sum_{\text{rel. fermions}} \frac{7}{8} \cdot g_i \cdot \left(\frac{T_i}{T}\right)^4.
\tag{3.12}
$$

In the SM the species contribute to $g_*(T)$ differently because they have different degrees of freedom depending on the temperature. For example, the neutrinos have 6 degrees of freedom because they are 3 families with 2 components for temperatures above several hundreds of GeV. The effective degree of freedom is taking into account that particles may contribute differently to the energy density at different temperatures.

Therefore, if we combine Eq. (3.6) with Eq. (3.11) we obtain the Hubble parameter for the early universe

$$
H(T) = 1.66 \cdot \sqrt{g_*(T)} \frac{T^2}{M_{\text{P}}},
\tag{3.13}
$$

where $M_{\text{P}} = 1/\sqrt{G} = 1.22 \cdot 10^{19}$ GeV is the Planck mass. With this equation we are also able to relate the cosmic time t to the temperature T at the epoch of radiation domination. During this time the Hubble parameter is given by $H = 1/(2t)$. Thus, we get the simple relation of $t \sim T^{-2}$. So, as time goes on the universe cools down. As a consequence, the temperature of the universe T reaches after some time the same value as the mass m and particles become non-relativistic. Non-relativistic particles are Boltzmann suppressed by the factor $\sim e^{-m/T}$. Thus, in the case of dark matter the number density droops as $T \sim m_{\text{DM}}$.

3.4 Boltzmann Equation

So far we have neglected the time dependence of the phase space distribution function. The time evolution is described by the Boltzmann equation and its general form reads

$$
L[f] = C[f],
\tag{3.14}
$$

where L is the Liouville operator which contains the time dependence of f and can be written as df/dt. Note that we here have the total time derivative. The term on the right hand side is the Collision operator. It gives us the information about the creation and destruction of the particles involved in the process. In principle the distribution function f is a vector and the Boltzmann equation describes a system of coupled differential equations.

In special relativity we are dealing with four vectors. So, the phase space distribution function becomes $f(x^\mu, p^\mu)$, where x^μ is the spatial four vector and p^μ the momentum four vector. We also define that $|\vec{p}| \equiv p$. The total derivative is with respect to the proper time τ in the relativistic case instead of t. Carrying out the derivatives we obtain the covariant relativistic expression for the Liouville operator as follows:

$$L[f] = \frac{\mathrm{d}f}{\mathrm{d}\tau} = p^\mu \frac{\partial f}{\partial x^\mu} - \Gamma^\mu_{\rho\sigma} p^\rho p^\sigma \frac{\partial f}{\partial p^\mu}, \tag{3.15}$$

where $\Gamma^\mu_{\rho\sigma}$ are the Christoffel symbols. In the FLRW universe the phase-space distribution function is homogeneous and isotropic. Therefore f is independent of $\vec{x}$ and $\vec{p}/|\vec{p}|$ and reduces to $f(t, E)$. The Christoffel symbols contain the derivative of the metric and can be calculated for the FLRW metric. But it is quite tedious, so we just give the final result of the Liouville operator here. For the FLRW metric we obtain that

$$L[f] = E \frac{\partial f}{\partial t} - H|\vec{p}|^2 \frac{\partial f}{\partial E}. \tag{3.16}$$

Using this equation and rearrange it together with Eq. (3.14) we get the following differential equation:

$$\frac{\partial f}{\partial t} - \frac{H}{E}|\vec{p}|^2 = \frac{1}{E} C[f]. \tag{3.17}$$

With this expression we are now able to obtain the differential equation for any of the quantities from above. For example, we get the number or energy density by simply multiply Eq. (3.17) with the terms that are missing and integrating over the whole phase space. As a concrete example we can multiply Eq. (3.17) with $g/(2\pi)^3$ to obtain the differential equation of the number density n_i of a certain species i as

$$\frac{g}{(2\pi)^3} \int d^3 p \frac{\partial f}{\partial t} - \frac{g}{(2\pi)^3} \int d^3 p \frac{H}{E}|\vec{p}|^2 \frac{\partial f}{\partial E} = \frac{g}{(2\pi)^3} \int d^3 p \frac{C[f]}{E}. \tag{3.18}$$

The first term is just simply the time derivative of the number density $\mathrm{d}n/\mathrm{d}t$. The second term can be partially integrated over the momentum $dp|\vec{p}|^2$ by using that $\partial/\partial E = (E/p)\partial/\partial p$. This leads to the final expression of the number density, namely

$$\frac{\mathrm{d}n_i}{\mathrm{d}t} + 3H n_i = \frac{g_i}{(2\pi)^3} \int d^3 p \frac{C[f]}{E}. \tag{3.19}$$

Note that we may also use the notation $\dot{n} = \mathrm{d}n/\mathrm{d}t$ in this section.

We can now make sense of the Collision term by simply putting $C[f] = 0$ which means that we have no production or destruction of particles. Hence, the total number of particles should be conserved. We see that by multiplying the left hand side by the volume $V = a^3$. Thus, we get

$$\frac{\mathrm{d}N_i}{\mathrm{d}t} = \frac{\mathrm{d}(n_i \cdot a^3)}{\mathrm{d}t} = 0. \tag{3.20}$$

We can quickly check our result by carrying out the derivative and obtain that $\mathrm{d}(na^3)/\mathrm{d}t = \dot{n}a^3 + 3a^2\dot{a}n = a^3(\dot{n} + 3Hn)$. So, the total number of particles inside a comoving volume a^3 stays constant as long as we have no production or destruction of particles. But the number density gets diluted by a^{-3} because of the expanding universe.

Now, we want to continue with the right hand side of Eq. (3.19) and massage the collision term $C[f]$. The collision term for a process $a + b \longrightarrow i + j$ is given by

$$
\begin{aligned}
\frac{g}{(2\pi)^3} \int d^3p \frac{C[f]}{E} &= \sum_{\text{spins}} \int \frac{d^3p_a}{(2\pi)^3 2E_a} \frac{d^3p_b}{(2\pi)^3 2E_b} \frac{d^3p_i}{(2\pi)^3 2E_i} \frac{d^3p_j}{(2\pi)^3 2E_j} \\
&\quad \cdot (2\pi)^4 \delta^{(4)}(p_a + p_b - p_i - p_j) \\
&\quad \cdot \big[|\mathcal{M}_{i+j \longrightarrow a+b}|^2 f_i f_j (1 \pm f_a)(1 \pm f_b) \\
&\quad - |\mathcal{M}_{a+b \longrightarrow i+j}|^2 f_a f_b (1 \pm f_i)(1 \pm f_j) \big] \\
&= \text{rate of production} - \text{rate of destruction},
\end{aligned}
\tag{3.21}
$$

where $\mathcal{M}_{i+j \longrightarrow a+b}$ is the matrix amplitude which gives the transition rate for an initial state $i + j$ going into a final state $a + b$. It can be obtained with the Feynman rules.[1] The collision term makes sense because the matrix element gives us the transition amplitude of our processes. We can either have that the particles a and b annihilate into i and j or that i and j produce our particles a and b. For WIMPs the process of $a + b \longleftarrow i + j$ would be the annihilation into SM particles. In the early universe we do not have a controlled system like in an experiment. Thus, the particles do not have fixed momenta, nor a fixed space coordinate. Therefore they follow the distribution f. The delta distribution function guarantees the four momentum conservation of the process. The last thing to do is to integrate over the full Lorentz-invariant phase space.

There are two simplifications that we can make. The first one is, that CP is conserved or respectively T because of the CPT theorem. Therefore, the squares of the matrix element are the same for production and destruction, regardless of the direction. Remember that CP is not conserved in the SM but the symmetry breaking phase in the Cabibbo-Kobayashi-Maskawa (CKM) matrix is so small that the effect is hardly noticed. So, in our case we can assume that CP is approximately conserved. The second assumption is that the gas is sufficiently diluted such that we can neglect quantum effects and treat the gas as classical gas. Hence, we can replace the phase-space distribution function f with the Boltzmann distribution function $f(E_i) = \exp(-(E_i - \mu_i)/T)$. This also means that $f \ll 1$ and that $1 \pm f \approx 1$. So, the collision term reduces to

$$
\begin{aligned}
\frac{g}{(2\pi)^3} \int d^3p \frac{C[f]}{E} &= \sum_{\text{spins}} \int \frac{d^3p_a}{(2\pi)^3 2E_a} \frac{d^3p_b}{(2\pi)^3 2E_b} \frac{d^3p_i}{(2\pi)^3 2E_i} \frac{d^3p_j}{(2\pi)^3 2E_j} \\
&\quad \cdot (2\pi)^4 \delta^{(4)}(p_a + p_b - p_i - p_j) |\mathcal{M}_{a+b \longrightarrow i+j}|^2 \cdot \big[f_i f_j - f_a f_b \big].
\end{aligned}
\tag{3.22}
$$

We now want to consider the case of dark matter particles a and b annihilating into standard model particles i and j. Or in other words $\text{DM}_a + \text{DM}_b \longrightarrow \text{SM}_i + \text{SM}_j$. This process is well described in [45]. To continue, it is important to assume that the annihilation products i and j go into thermal equilibrium with the background very quickly. This is mostly the case when i and j are charged particles because they interact with the large amount of photons and it is also in most cases true for neutral particles. Hence, the chemical potential is zero and we may write $f_i^{\text{eq}} = \exp(-E_i/T)$.

---

[1]Note that we will later take more care about the matrix element. It is also sometimes denoted by T.

Due to energy conservation we obtain that

$$f_i^{\text{eq}} f_j^{\text{eq}} = \exp(-(E_i + E_j)/T) = \exp(-(E_a + E_b)/T) = f_a^{\text{eq}} f_b^{\text{eq}}. \tag{3.23}$$

We can define the unpolarised cross section

$$\sigma = \frac{1}{4F g_a g_b} \sum_{\text{spins}} \int \frac{d^3 p_i}{(2\pi)^3 2E_i} \frac{d^3 p_j}{(2\pi)^3 2E_j} |\mathcal{M}_{a+b \longrightarrow i+j}|^2 (2\pi)^4 \delta^{(4)}(p_a + p_b - p_i - p_j), \tag{3.24}$$

where F is the flux and g_a, g_b come from the spin average over the initial spins. We will later discuss the flux and the cross section in a more stringent manner in ch. 4.2. The invariant flux F is given by $F = [(p_a \cdot p_b)^2 - m_a^2 m_b^2]^{-1/2}$. We are also able to define the Møller velocity by

$$v_{\text{Møller}} = \frac{F}{E_a E_b} = \left[|\vec{a} - \vec{b}|^2 - |\vec{a} \times \vec{b}|^2 \right]^{1/2}. \tag{3.25}$$

With the unpolarised cross section and the Møller velocity we can simplify Eq. (3.22) together with Eq.(3.23) to get

$$\frac{g}{(2\pi)^3} \int d^3 p \frac{C[f]}{E} = -g_a g_b \int \frac{d^3 p_a}{(2\pi)^3} \frac{d^3 p_b}{(2\pi)^3} (f_a f_b - f_a^{\text{eq}} f_b^{\text{eq}})(\sigma v_{\text{Møller}}). \tag{3.26}$$

The thermally averaged cross section can be written as

$$\begin{aligned}
\langle \sigma v_{\text{Møller}} \rangle &= \frac{g_a g_b \int d^3 p_a d^3 p_b f_a^{\text{eq}} f_b^{\text{eq}} (\sigma v_{\text{Møller}})}{g_a g_b (\int d^3 p_a f_a^{\text{eq}})(d^3 p_b f_b^{\text{eq}})} \\
&= \frac{g_a g_b \int d^3 p_a d^3 p_b f_a^{\text{eq}} f_b^{\text{eq}} (\sigma v_{\text{M øller}})}{(2\pi)^6 n_a^{\text{eq}} n_b^{\text{eq}}}.
\end{aligned} \tag{3.27}$$

We further assume that the particles a and b are in kinetic equilibrium with the standard model particles through scatterings. We can relate the equilibrium phase-space distribution function with the Boltzman phase-space distribution function in the following way:

$$\frac{f_a}{f_a^{\text{eq}}} = e^{-\frac{E_a - \mu_a}{T}} \cdot e^{\frac{E_a}{T}} = e^{\frac{\mu}{T}} = \frac{n_a}{n_a^{\text{eq}}}. \tag{3.28}$$

With this consideration we can reduce the collision term further to

$$\begin{aligned}
\frac{g}{(2\pi)^3} \int d^3 p \frac{C[f]}{E} &= -g_a g_b \big(e^{\frac{\mu_a + \mu_b}{T}} - 1 \big) \int \frac{d^3 p_a}{(2\pi)^3} \frac{d^3 p_b}{(2\pi)^3} f_a^{\text{eq}} f_b^{\text{eq}} (\sigma v_{\text{Møller}}) \\
&= -\big(e^{\frac{\mu_a + \mu_b}{T}} - 1 \big) \langle \sigma v_{\text{Møller}} \rangle n_a^{\text{eq}} n_b^{\text{eq}} \\
&= -\langle \sigma v_{\text{Møller}} \rangle (n_a n_b - n_a^{\text{eq}} n_b^{\text{eq}}).
\end{aligned} \tag{3.29}$$

So we obtain the final result for the evolution of the particle density [45]:

$$\frac{\mathrm{d} n_a}{\mathrm{d} t} + 3H n_a = -\langle \sigma v_{\text{Møller}} \rangle (n_a n_b - n_a^{\text{eq}} n_b^{\text{eq}}). \tag{3.30}$$

It makes sense that the Boltzmann equation depends on the cross section because if $\sigma = 0$ no interaction takes place and the total number of particles is conserved. Let us highlight that we derived this equation by assuming that CP is conserved.

We neglected quantum effects and treated the gas classically. Further, we assumed that the dark matter particles are in kinetic equilibrium with the standard model particles via scatterings.

A quantity that we have not mentioned so far is the entropy. The entropy density is defined as $s = S/V$, whereby S is the total entropy. With the second law of thermodynamics we see that the entropy density is related to the energy density, the pressure and the temperature in the following way:

$$s = \frac{S}{V} = \frac{\rho + P}{T} \tag{3.31}$$

In the early universe the entropy can be explicitly expressed via the energy density and the pressure given at that time for relativistic fermions and bosons as

$$s = \frac{2\pi^2}{45} g_{*s}(T)T^3, \tag{3.32}$$

where

$$g_{*s}(T) = \sum_{\text{rel. bosons}} g_i \cdot \left(\frac{T_i}{T}\right)^3 + \sum_{\text{rel. fermions}} \frac{7}{8} \cdot g_i \cdot \left(\frac{T_i}{T}\right)^3 \tag{3.33}$$

is the effective number of degrees of freedom for the entropy. It looks quite similar to the total energy density ρ_{tot} in Eq. (3.11).

Finally, it is very useful and convenient to normalise the entropy density to another quantity that scales out the effect of the expanding universe. This is done by defining the yield as

$$Y \equiv \frac{n}{s}. \tag{3.34}$$

The total entropy is conserved $dS/dt = 0$ if $\sigma = 0$ as well as the total number of particles. Thus, also the yield Y is conserved if we assume that $\sigma = 0$. Later, we will make great use of the yield.

3.5 Dark Matter Thermal Freeze-out

3.5.1 Freeze-out Mechanism

We now want to calculate the dark matter abundance as a thermal relic of the early universe. We have seen that the particle density in the early universe becomes Boltzmann suppressed when $T \sim m_{\text{DM}}$. Hence, if the dark matter particles would stay in equilibrium with the background there would be no dark matter left due to the exponential suppression of the Boltzmann distribution for non-relativist particles. But we observe a significant abundance of dark matter. Hence, the WIMPs must have decoupled from the thermal bath at a certain point which is called the freeze-out. We now want to use the formalism from the previous section for the freeze-out mechanism of the WIMPs.

We first start by taking the time derivative of the yield and obtain

$$\frac{dY}{dt} = \frac{\dot{n}s - \dot{s}n}{s^2} = \frac{-3Hns - \langle\sigma v\rangle s(n_a n_b - n_a^{\text{eq}} n_b^{\text{eq}}) + 3Hsn}{s^2}, \tag{3.35}$$

where we inserted $\dot{s} = 3Hs$. This yields the Boltzmann equation for the yield of a particle a as

$$\frac{\mathrm{d}Y_a}{\mathrm{d}t} = -s\langle\sigma v\rangle(Y_a Y_b - Y_a^{\mathrm{eq}}Y_b^{\mathrm{eq}}). \qquad (3.36)$$

Note that we have dropped the subscript Møller for the velocity v out of convenience. Let us define the quantity $x = m/T$. In the epoch of radiation domination the scale factor $a \sim t^{1/2}$ and $t \sim T^{-2}$. Thus, the scale factor is inversely proportional to the temperature $a \sim T^{-1}$. We further conclude that the scale factor times the temperature is constant. Therefore it does not matter if we multiply or divide the constant by the mass m. So, a/x is also constant. In other words $0 = \mathrm{d}(ax^{-1})/\mathrm{d}t = \dot{a}/x - (a/x^2)\dot{x}$ which yields that $\mathrm{d}x/\mathrm{d}t = xH$. This little exercise is useful because we can now get an expression for the yield with respect x. Using $\mathrm{d}Y/\mathrm{d}t = \mathrm{d}Y/\mathrm{d}x \cdot \mathrm{d}x/\mathrm{d}t$ we get

$$\frac{\mathrm{d}Y_a}{\mathrm{d}x} = -\frac{s\langle\sigma v\rangle}{xH}(Y_a Y_b - Y_a^{\mathrm{eq}}Y_b^{\mathrm{eq}}), \qquad (3.37)$$

where Y_a is the actual number of particles a per comoving volume and Y_a^{eq} the equilibrium number of a´s in the comoving volume.

We can calculate the equilibrium number density specifically for the special cases of the ultra relativistic and non-relativistic limit and obtain the following relations:

$$n^{\mathrm{eq}} \sim \begin{cases} T^3, & \text{relativistic} \\ (mT)^{3/2} \cdot e^{-\frac{m}{T}}, & \text{non-relativistic} \end{cases} \qquad (3.38)$$

The entropy is given by $s = 2\pi^2 g_{*s}(T)T^3/45$. The yield is the number density divided by the entropy. Thus we obtain

$$Y^{\mathrm{eq}} = \begin{cases} 0.278\dfrac{g_{\mathrm{eff}}}{g_{*s}}, & x \gg 3 \\ 0.145\dfrac{g}{g_{*s}}(x)^{3/2}e^{-x}, & x \ll 3, \end{cases} \qquad (3.39)$$

where $g_{\mathrm{eff}} = g$ for bosons and $g_{\mathrm{eff}} = 3g/4$ for fermions. From this equation we see that the equilibrium yield for ultra relativistic particles is constant. But then, when the particles become non-relativist at $x \sim 1$ the yield starts to decrease and gets Boltzmann suppressed by e^{-x}. We can further massage Eq. (3.37) by dividing by Y_a^{eq} and multiplying by x such that

$$\begin{aligned} \frac{x}{Y_a^{\mathrm{eq}}}\frac{\mathrm{d}Y_a}{\mathrm{d}x} &= -\frac{s\langle\sigma v\rangle Y_b^{\mathrm{eq}}}{H(x)}\left(\frac{Y_a(x)}{Y_a^{\mathrm{eq}}}\frac{Y_b(x)}{Y_b^{\mathrm{eq}}} - 1\right) \\ &= -\frac{\Gamma_{\mathrm{ann}}}{H(x)}\left(\frac{Y_a(x)}{Y_a^{\mathrm{eq}}}\frac{Y_b(x)}{Y_b^{\mathrm{eq}}} - 1\right), \end{aligned} \qquad (3.40)$$

where we have used the fact that $sY_b^{\mathrm{eq}} = n_b^{\mathrm{eq}}$ and that $\Gamma = n_b^{\mathrm{eq}}\langle\sigma v\rangle$ which is the annihilation rate. The important part of this equation is the fraction of the annihilation rate over the Hubble expansion rate. It connects particle physics with cosmology and determines when the decoupling process takes place.

Now we want to study the freeze-out of dark matter. Therefore, we consider a stable dark matter particle χ that can annihilate with its antiparticle $\overline{\chi}$ into SM

particles. Hence, we have the annihilation channel $\chi\overline{\chi} \longrightarrow \text{SM}\overline{\text{SM}}$. We will simply use Y instead of Y_χ and obtain that

$$\frac{x}{Y^{\text{eq}}}\frac{\mathrm{d}Y}{\mathrm{d}x} = -\frac{\Gamma_{\text{ann}}}{H(x)}\left(\frac{Y^2(x)}{Y_{\text{eq}}^2} - 1\right). \tag{3.41}$$

The Hubble parameter scales with $H \sim T^2$ and the annihilation rate $\Gamma = n_{\text{eq}}\langle\sigma v\rangle$ is proportional to the number density at equilibrium. So, for large temperatures, when $T \gg m$ the annihilation rate scales with $\Gamma \sim T^3$ and therefore $\Gamma/H \gg 1$. In this case the yield is constant and the reaction can take place in both directions, namely $\chi\overline{\chi} \to \text{SM}\overline{\text{SM}}$. If the temperature is small compared to the mass $T \ll m$, the annihilation rate scales with $\Gamma \sim T^{3/2}\exp(-m/T)$. Thus, for small temperatures $\Gamma/H \ll 1$. So, in both scenarios the annihilation rate decreases as the temperature decreases. But roughly around $\Gamma \sim H$ the annihilation starts to become less efficient and becomes impotent. As a consequence, the dark matter particles "freeze-out" at x_{fo} and decouple from the thermal bath because their abundance gets frozen. We call such particles thermal relics.
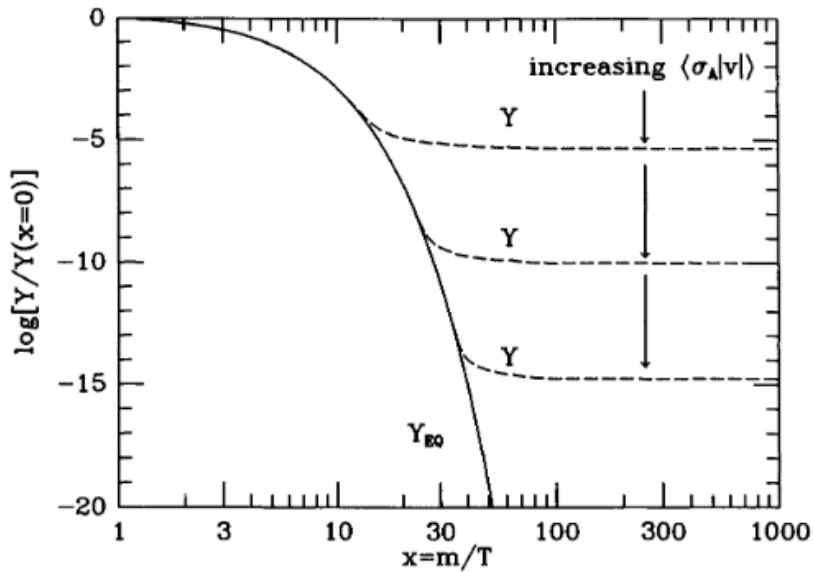
Figure 3.2: The freeze-out of a massive particle. The equilibrium yield is shown as a solid line and the dashed line is the actual abundance of the particle. As the thermal averaged annihilation cross section increases, the abundance of the massive particle decreases. The figure is taken from [43]

The physical interpretation of this behaviour is straight forward. As the hot universe evolves it grows in size. In the beginning the dark matter particles are in thermal equilibrium with the standard model particles. They annihilate and get produced in an equal amount. But as the universe cools down, while increasing, the dark matter particle become non-relativistic at the point where $T \sim m$. Then, the number of particles decreases because the number density is Boltzmann suppressed and therefore the annihilation is more efficient and the production of dark matter particles stops. Then, when the Hubble expansion rate is large compared to the

annihilation rate the particles freeze-out as we can see in Fig. 3.2. This happens because the size of the universe is so large that the dark matter particles can not interact with each other anymore to annihilate sufficiently. In order words, they do not find another partner do annihilate because the universe is to large. Note, that the relic abundance of the dark matter particles is determined by the thermal averaged annihilation cross section because $\Gamma = n_{\rm eq}\langle\sigma v\rangle$. The higher the annihilation cross section, the lower is the relic abundance of the dark matter particles. If the annihilation cross section is very large than the annihilation takes place a longer period and therefore the relic abundance is lower as we can see in Fig. 3.2.

We have seen that the relic abundance of dark matter particles strongly depends on the thermal averaged annihilation cross section $\langle\sigma v\rangle$. The annihilation cross section can be decomposed in partial waves

$$\sigma v \propto \sum v^p = a + bv^2 + cv^4 + ..., \tag{3.42}$$

where $p = 0$ is the s-wave, $p = 2$ the p-wave and $p = 4$ the d-wave and a, b and c are coefficients. Since we know from thermodynamics that $3k_{\rm b}T/2 = mv^2/2$, where $k_{\rm b}$ is the Boltzmann constant we realise that $\langle v\rangle \sim T^{1/2}$. Thus, $\sigma v \propto T^n$ with $n = 0$ for the s-wave and $n = 1$ for the p-wave. Thus, we can conclude that $\langle\sigma v\rangle \sim x^{-n}$. It is convenient to rewrite the thermally averaged annihilation cross section such that $\langle\sigma v\rangle(x) = \langle\sigma v\rangle(x = 1)x^{-n} = \sigma_0 x^{-n}$, where $x = 1$ is the time when $T = m$. In fact it is advantageous to do the same with the Hubble parameter and the entropy. So, we define the following parameter

$$\lambda = \left[\frac{s(x)\langle\sigma v\rangle(x)}{H(x)}\right]_{x=1} \approx 0.264\left(\frac{g_{*s}}{g_*^{1/2}}\right)M_{\rm P}\cdot m\cdot\sigma_0. \tag{3.43}$$

So we can rewrite the Boltzman equation in the following way:

$$\frac{{\rm d}Y}{{\rm d}x} = -\lambda x^{-n-2}(Y^2(x) - Y_{\rm eq}^2(x)), \tag{3.44}$$

where $Y_{\rm eq}(x) \approx 0.145(g/g_{*s})\cdot x^{3/2}\cdot e^{-x}$. It is further very practical to define the parameter $\Delta \equiv Y(x) - Y_{\rm eq}(x)$ which measures the deviation of the yield from the equilibrium yield. The derivative of Δ with respect to x yields

$$\begin{aligned}\frac{{\rm d}\Delta}{{\rm d}x} &= -\lambda x^{-n-2}(Y^2(x) - Y_{\rm eq}^2(x) - \frac{{\rm d}Y_{\rm eq}}{{\rm d}x} \\ &= -\lambda x^{-n-2}\Delta(\Delta + 2Y_{\rm eq}) - \frac{{\rm d}Y_{\rm eq}}{{\rm d}x}.\end{aligned} \tag{3.45}$$

At early times between $1 < x \ll x_{\rm fo}$ we expect the deviation from the equilibrium to be small and therefore also its derivative. So with $|{\rm d}\Delta/{\rm d}x| \ll 1$, $|\Delta| \ll 1$ and $({\rm d}Y_{\rm eq}/{\rm d}x)/Y_{\rm eq} = -1 + 3/(2x) \approx -1$ it follows for Eq. (3.45) that

$$\Delta = -\frac{\frac{{\rm d}Y_{\rm eq}}{{\rm d}x}}{2\lambda Y_{\rm eq}}x^{n+2} \approx \frac{x^{n+2}}{2\lambda} \tag{3.46}$$

at early times. At late times for $x \gg x_{\rm fo}$ the deviation form the equilibrium yield is very large such that $Y_{\rm eq} \ll Y \approx \Delta$. Therefore we obtain for Eq. (3.45)

$$\frac{{\rm d}\Delta}{{\rm d}x} = -\lambda x^{-n-2}\Delta^2. \tag{3.47}$$

This differential equation needs to be integrated from the time of the freeze-out x_{fo} until today where $x = \infty$. By doing so we get

$$Y_\infty = \Delta_\infty = \frac{n+1}{\lambda} x_{\text{fo}}^{n+1} = \frac{3.79(n+1)x_{\text{fo}}^{n+1} g_*}{g_{*s} M_{\text{P}} m \sigma_0}. \tag{3.48}$$

Hence, we notice that $\Omega h^2 \sim \langle \sigma v \rangle^{-1}$. With the number density of dark matter particles of today $n_0 = s_0 Y_\infty$, where $s_0 = 2970$ cm^{-3} we get

$$\Omega_{\text{DM}} h^2 = \frac{2 \cdot 10^{-10} \text{GeV}^{-2}}{\langle \sigma v \rangle}. \tag{3.49}$$

With a dark matter density of roughly $\Omega_{\text{DM}} h^2 \sim 0.1$ one would obtain that $\langle \sigma v \rangle \sim 10^{-9} \cdot \text{GeV}^{-2}$. Hence, we realise that the dark matter freeze-out mechanism influences the annihilation cross section of our specific dark matter model and sets limits if we want to obtain the correct relic abundance.

3.5.2 Three Exceptions

We have seen that the freeze-out mechanisms a powerful tool to produce the correct relic abundance of particle species like dark matter by making assumptions about the thermally averaged annihilation cross section. For dark matter this is of high importance because it influences the indirect searches of dark matter. However, there are three main exceptions to the freeze-out mechanism which were first mentioned 1991 by Griest and Seckel [46] (see also [7]).

The first exception happens when there exists particles similar to the relic particle with roughly the same mass. The classical calculation tend to fail because we have a richer dark sector. We call this phenomenon "coannihilation". Let us assume that we have a class of particles χ_i with $i = 1, ..., N$ which differ from the SM particles by a conserved quantum number. We further assume the masses to be $m_i < m_j$ for $j > i$. A typical example for the conserved quantum number is the Z_2 symmetry. So, χ_1 is the lightest particle and our dark matter candidate, while χ_2 is the second lightest particle and so on. We further denote the standard model particles by X and Y. We can have three reactions that influence our relic abundance, namely

$$\begin{aligned}
\chi_i \chi_j &\longrightarrow XY \\
\chi_i X &\longrightarrow \chi_j Y \\
\chi_i &\longrightarrow \chi_j XY.
\end{aligned} \tag{3.50}$$
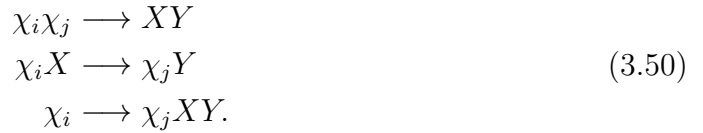
The first and second reaction are inelastic scatterings denoted by σ_{ij} and σ'_{ij}. The last reaction is an annihilation denoted by Γ_{ij}. The reactions $\chi_i \chi_j \longrightarrow \chi_k X$ and $\chi_i X \longrightarrow XX$ are forbidden by the assumed symmetry. The Boltzmann equation (3.30) for these three reactions of the particle i becomes

$$\begin{aligned}
\frac{\mathrm{d}n_i}{\mathrm{d}t} = -3Hn_i - \sum_{j,X,Y} \Big[&\langle \sigma_{ij} v_{ij} \rangle (n_i n_j - n_i^{\text{eq}} n_j^{\text{eq}}) \\
&- (\langle \sigma'_{ij} v_{ij} \rangle n_i n_X - \langle \sigma'_{ji} v \rangle_{ji} n_j n_Y) \\
&- \Gamma_{ij} (n_i - n_i^{\text{eq}}) \Big],
\end{aligned} \tag{3.51}$$

where the first term on the right hand sides denotes the dilution of the number density due to the expansion of the universe. The second, third and fourth terms are due to the reactions in (3.50). The velocity is given by

$$v_{ij} = \frac{\sqrt{(p_i \cdot p_j)^2 - m_i^2 m_j^2}}{E_i E_j}. \tag{3.52}$$

After the coupling all of the χ_i in the dark sector, that survived the annihilation, decay into the lightest particle χ_1. Thus, the total number of the dark sector is given by $n = \sum_i n_i$. Hence, we obtain

$$\frac{dn}{dt} = -3Hn - \sum_{i,j=1}^{N} \langle \sigma_{ij} v_{ij} \rangle (n_i n_j - n_i^{\text{eq}} n_j^{\text{eq}}). \tag{3.53}$$

We have to remark that we assumed that the χ particles are either scalars or Majorana fermions such that they can annihilate with themselves and are not asymmetric [46]. We can define the effective thermal averaged cross section by

$$\langle \sigma_{\text{eff}} v \rangle = \frac{\sum_{i,j} \langle \sigma_{ij} v_{ij} \rangle n_i^{\text{eq}} n_j^{\text{eq}}}{(\sum_i n_i^{\text{eq}})^2}. \tag{3.54}$$

With the effective thermal averaged cross section we can rewrite Eq. (3.53) and get

$$\frac{dn}{dt} = -3Hn - \langle \sigma_{\text{eff}} v \rangle (n^2 - n_{\text{eq}}^2), \tag{3.55}$$

where we can still Taylor expand the cross section in the following way: $\sigma_{\text{eff}} v = a_{\text{eff}} + b_{\text{eff}} v^2 + \dots$. But now we see that the dark matter density is given by

$$\Omega_{\text{DM}} h^2 = \frac{2 \cdot 10^{-10} \text{GeV}^{-2}}{\langle \sigma_{\text{eff}} v \rangle}. \tag{3.56}$$

We notice that this equation is similar to Eq. (3.49) but the denominator is now the effective averaged thermal cross section instead of the ordinary one which modifies our relic abundance.

The second exception to the standard freeze-out scenario is due to resonances. This is the case when the cross section has a pole. That might happen when two dark matter particles annihilate into standard model particles via a Z boson or some scalar mediator particle through the s-channel. So, the reaction that we consider is the following:
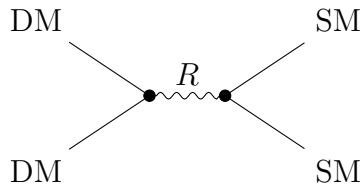
We will denote the mediator particle simply with and subscript R. Hence, in the matrix element we will have the expression of $1/(s - m_R^2)$ which becomes zero if

$s = m_R^2$. This pole is called the resonance. We can express the Mandelstam variable s as follows:

$$s = 2m_\chi^2 + 2(E_1 E_2 - \vec{p_1} \cdot \vec{p_2}), \quad (3.57)$$

where $E_{1/2}$ are the energies of the dark matter particles and $\vec{p}_{1/2}$ the momenta. The WIMPs are non-relativistic and therefore we can simply us $E_1 \approx m_\chi + m_\chi v_1^2/2$ and $\vec{p_1} = m\vec{v_1}$. With this assumptions we get that $s = 4m_\chi + m_\chi^2 |\vec{v_1} - \vec{v_2}|^2$. Thus we obtain $|\vec{v_1} - \vec{v_2}| = (m_R^2 - 4m_\chi^2/m_\chi^2)$. This motivates us to make the following consideration for the annihilation cross section close to the resonance:

$$\sigma v = \frac{\alpha_g^2 s}{(m_R - s)^2 + m_R^2 \Gamma_R^2}. \quad (3.58)$$

Where m_R is the mass of the mediator particle, α_g is the coupling constant of the process and Γ_R the total width of the mediator particle. We can simplify this formula with the help of the delta function. Is is known that the delta function can be written as

$$\lim_{\gamma \to 0} \frac{\gamma}{x^2 + \gamma^2} = \pi \delta(x). \quad (3.59)$$

So, we can use Eq. (3.59) and substitute it into Eq. (3.58) to get

$$\sigma v = \frac{\alpha_g^2 s}{m_R \Gamma_R} \pi \delta(m_R^2 - s). \quad (3.60)$$

The thermally averaged cross section can be calculated in the following way:

$$\langle \sigma v \rangle = \int \mathrm{d}p p^2 4\pi (\sigma v). \quad (3.61)$$

Thus, the thermally averaged cross section can be enhanced near the resonance. In our case when $2m_\chi/m_R \approx 1$. Consequently, in this region the relic abundance drops significantly. As a result, one has to be more carefully when calculating the relic abundance if one has annihilation of dark matter near a pole. For example, one can produce the correct relic abundance with small couplings due to the increase of the thermally averaged cross section near a pole [46].

The third exception takes places when the dark matter particle χ has a mass m_χ that is slightly below the mass threshold for annihilation. If the mass of the dark matter particle were a bit more massive, then it would annihilate into secondary particles ϕ with mass m_ϕ. So, during the freeze-out the the reaction $\phi\phi \longrightarrow \chi\chi$ can occur because $m_\phi > m_\chi$. However, the number density of n_ϕ is Boltzmann suppressed and the number of particles ϕ decreases faster than n_χ because $n_\phi \sim \exp(-m_\phi/T)$. On the other hand, we can have the annihilation of $\chi\chi \longrightarrow \phi\phi$, if χ has sufficient kinetic energy to overcome the threshold. In other words, the dark matter particle can annihilate into forbidden channels, if the kinetic energy is large enough. We will now follow [47] for a more detailed discussion of this phenomenon.

The Boltzmann equation for the dark matter particle χ in our case reads

$$\frac{\mathrm{d}n_\chi}{\mathrm{d}t} + 3Hn_\chi = -\langle \sigma v \rangle_{\chi\chi} n_\chi^2 + \langle \sigma v \rangle_{\phi\phi} (n_\phi^{\mathrm{eq}})^2. \quad (3.62)$$

In equilibrium the right hand side of the Boltzmann equation vanishes because we have a detailed balance of annihilation and creation. Hence, we obtain that

$$\langle \sigma v \rangle_{\chi\chi} = \langle \sigma v \rangle_{\phi\phi} \frac{(n_\phi^{\mathrm{eq}})^2}{(n_\chi^{\mathrm{eq}})^2} \quad (3.63)$$

Furthermore, we notice that $n_\phi^{\text{eq}}/n_\chi^{\text{eq}} \sim \exp(-(m_\phi - m_\chi)/T)$. So we can reduce the Boltzmann equation to the following:

$$\frac{\mathrm{d}n_\chi}{\mathrm{d}t} + 3Hn_\chi = -\langle \sigma v \rangle_{\phi\phi} e^{-2(m_\phi - m_\chi)/T}(n_\chi^2 - (n_\chi^{\text{eq}})^2). \tag{3.64}$$

This is what we call the Boltzmann equation for the forbidden channel. As we already have seen the dark matter relic abundance can be determined via the Boltzmann equation. Therefore, we can relate the dark matter abundance with the forbidden channel to the abundance without the forbidden channel and obtain

$$\frac{\Omega_\chi^{\text{forbidden}}}{\Omega_\chi} \sim e^{\frac{2(m_\phi - m_\chi)}{T_{fo}}} = e^{\frac{2(m_\phi - m_\chi)}{\chi} \cdot x_{fo}}. \tag{3.65}$$

Since the mass of particle ϕ is heavier than the mass of particle χ, the relic abundance of χ can be larger for the case with the forbidden channel than without. As a consequence, one can obtain the correct relic abundance with lighter dark matter mass than one usually would expect which makes this exception very attractive for theorists [46, 47].

3.5.3 The WIMP Miracle

From the freeze-out mechanism we know that dark matter can be a thermal relic of the early universe. The dark matter decouples from the hot plasma roughly when $\Gamma \sim H$, so when the expansion rates is similar to the annihilation rate. Therefore, the dark matter particle interaction rate with the standard model particles needs to be large enough for $x > x_{\text{fo}}$ such that the particles are in thermal equilibrium. On the other side, the interaction needs to be weak enough such that for $x > x_{\text{fo}}$ the dark matter particles do not annihilate anymore into standard model particles. Together with the assumption that the dark matter particle must be stable and interact in pairs weakly. These are all the properties for the WIMP that we mentioned before. Hence, we have a consistent picture. We will now derive the WIMP miracle.

The WIMPs are non-relativistic at the time of the freeze-out. That is why they are cold dark matter. Hence, the evolution of the number density yields $n \sim (mT)^{3/2} \exp(-m/T)$. So, n is exponentially suppressed. During the freeze-out we are in the era of radiation domination and the Hubble parameter is given by $H \approx 1.66\sqrt{g_*(T)T^2/M_{\text{P}}}$ (see Eq. (3.13)). The annihilation rate gamma is $\Gamma = n\langle \sigma v \rangle$. So, by demanding that $\Gamma \sim H$ we get

$$n\langle \sigma v \rangle \sim 1.66\sqrt{g_*(T)}\frac{T^2}{M_{\text{P}}}. \tag{3.66}$$

As before we use $x = m/T$ and want to determine x_{fo} at the time of the freeze-out. The above equation reduces to

$$\sqrt{x_{\text{fo}}} = e^{-x_{\text{fo}}} \sim \frac{1.66\sqrt{g_*(T)}}{\langle \sigma v \rangle m M_{\text{P}}}. \tag{3.67}$$

This equation has to be solved numerically. But before we have to make an assumption on the cross section σ. When $x < 1$ we only the interaction of dark matter annihilating into standard model particles. Thus, we have the following interaction:
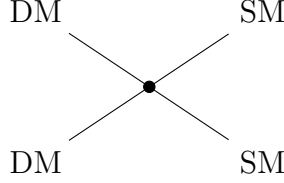
Since we have assumed the WIMPs to interact weakly, the cross section should scale with Fermi's constant G_{F}. Also it should scale with the Mandelstam variable s which encodes the energy dependence. In the non-relativistic regime $m < T$, s scales proportional to the dark matter mass m, namely $s \sim m^2$. Hence, the cross section can be approximated by $\sigma \sim G_{\mathrm{F}}^2 m^2$. Now we have everything we need to solve Eq. (3.67). We want the dark matter to be massive around several GeV. For a mass about $m \sim 100$ GeV we obtain that (3.67) reduces to $\sqrt{x_{\mathrm{fo}}} \exp(-x_{\mathrm{fo}}) \sim 10^{-14}$. This yields $x_{\mathrm{fo}} \sim 34$. For a dark matter mass of 1GeV we would get $x_{\mathrm{f0}} \sim 20$.

So let us determine whether we obtain the correct dark matter abundance for WIMP relics at $x_{\mathrm{fo}} = 20 - 30$. The dark matter density parameter today is given by

$$\Omega_{\mathrm{DM}} = \frac{8\pi G}{3H_0} \rho_{\mathrm{DM}} = \frac{8\pi G}{3H_0} \cdot m n_0, \qquad (3.68)$$

where n_0 is the particle density of today given by $n_0 = n_{\mathrm{fo}}(T_0/T_{\mathrm{fo}})^3$ and T_0 the dark matter particle temperature of today. We know that $n_{\mathrm{fo}}\langle \sigma v \rangle = H(T_{\mathrm{fo}}) = 1.66\sqrt{g_*(T_{\mathrm{fo}})}T_{\mathrm{fo}}^2/M_{\mathrm{P}}$ because $\Gamma \sim H$. So, we obtain for the dark matter density parameter the following:

$$\Omega_{\mathrm{DM}} = \frac{1.66 m \sqrt{g_*}}{\rho_{\mathrm{c}} \langle \sigma v \rangle} \frac{T_{\mathrm{fo}}^2}{M_{\mathrm{P}}} \frac{T_0^3}{T_{\mathrm{fo}}^3}. \qquad (3.69)$$

With ρ_{c} being the critical density given by $\rho_{\mathrm{c}} = 3H_0/(8\pi G)$. Eq. (3.69) basically shows that that the density parameter is determined by some physical factors, namely the dark matter mass, x_{fo} and the thermally averaged cross section $\langle \sigma v \rangle$.

Hence, if we put everything together it reduces in the end all to

$$\Omega_{\mathrm{DM}} \sim 0.2 \left(\frac{x_{\mathrm{FO}}}{20}\right) \left(\frac{3 \cdot 10^{-26} \mathrm{cm}^3/\mathrm{s}}{\langle \sigma v \rangle}\right). \qquad (3.70)$$

To sum up, we started with an weakly interacting particle with mass around $m \sim 1 - 100$GeV and we ended up with approximately the correct abundance of dark matter in our current universe if the annihilation cross section is roughly about $\langle \sigma v \rangle \sim 3 \cdot 10^{-26} \mathrm{cm}^3/\mathrm{s}$. This is what we call the "WIMP miracle". It is why the WIMPs are so famous among the dark matter candidates. We remark that the decomposition of $\langle \sigma v \rangle$ is justified because the WIMP freeze-out happens when the particles are non-relativistic [38]. We can quickly check that by using that $v_{\mathrm{fo}} = \sqrt{3/x_{\mathrm{fo}}} \sim 0.3$.

To conclude this section, we have seen throughout this chapter that WIMPs are well motivated in theory. With some simple considerations we can compute the correct relic abundance with the freeze-out mechanism. But we have to be aware of the exceptions. It is therefore not exceptional that the WIMPs are one of the most famous dark matter candidates.

Chapter 4

Cross Section

Until now, we have looked at the evidences and at dark matter and its properties. In this thesis, we assume to have particle dark matter, namely WIMPs. So far, we only studied the theory of dark matter particles. But the important way of observing dark matter is via their interaction with standard model particles. In this section we briefly want to cover how one can calculate the interaction between two particles in general and give a formula for the scattering cross section. The introduction is quite briefly and mainly follows [48].

4.1 The S-matrix

In this thesis we will look at processes that occur in the vicinity of black holes far away from our planet. In particular at interactions between dark matter and photons or neutrinos. The neutrinos and photons scatter with the dark matter particles when passing through a dark matter halo. They are well separated from the DM particles before and after the interaction. Even when the scattering is inelastic the outgoing particles form separated particle states and do not interact anymore among themselves. The time of interaction is very short compared to distance that the photon or neutrino travels before and after the interaction. So, the time duration of the interacting does not matter. Therefore, we can treat the interactions between dark matter and photons or neutrinos as two separated initial states or two separated wave packets at $t \longrightarrow -\infty$. Further, the particle states interact or the wave packets overlap during the interaction. Then, at $t \longrightarrow +\infty$ we have again two or even more separated final states or wave packets. We call the initial state $|\psi_i\rangle$ and the final states $|\psi_f\rangle$.

If we could set up a detector near the reaction, then we would be able to measure all the particles with the respective momenta. So in summary, in the beginning the two particles are far apart and do not yet interact and we end with particles that stopped interacting with each other. Thus, let us begin with the formalism.

One wave packet can be expressed as

$$|\psi\rangle = \int \frac{\mathrm{d}^3 p}{(2\pi)^3 2E_{\vec{p}}} f(\vec{p})|p\rangle, \tag{4.1}$$

where $f(\vec{p})$ is the Fourier transform of the wave function and $|p\rangle$ is a one-particle state of momentum $\vec{p}$.

We want to have the asymptotic states before and after the interaction in the interacting theory. With them we are able to compute quantities that we can measure in our experiments. Usually, one starts with a full Lagrangian that can be decomposed in an interacting and a non interacting part

$$\mathcal{L} = \mathcal{L}_0 + \mathcal{L}_{\text{int}} \tag{4.2}$$

From the Lagrangian one is able to calculate the Hamiltonian H by requiring that $H = P^0$, where P^μ is the total four momentum operator. We assume that the eigenvalues of $P_\mu P^\mu = P^2 \geq 0$. The eigenvalues of P^2 are the masses m^2 which are sometimes denoted as M^2.[1]

The basis states of the operator P^2 are simply denoted as follows

$$|p\rangle. \tag{4.3}$$

We call them the one-particle or single-particle states. The name already tells us that we are only looking at one particle right now. Note that in some textbooks or lectures one uses $|p, n\rangle$, where n stands for other properties like spin or colour. For simplicity we will just leave them aside but the following derivations work similar.

The eigenvalue of the Hamiltonian $H = P^0$ in the free theory is given by $p^0 = \sqrt{m^2 + \vec{p}^2}$. Since the Schrödinger equation implies that $H|p\rangle = E|p\rangle$ we realise that $p^0 = E_{\vec{p}} = \sqrt{m^2 + \vec{p}^2}$ is the energy.

But we have to recognise one important thing: the one-particle states of the free theory are not necessary the same one-particle states of the interacting theory. A quick example is given by the following Lagrangian

$$\mathcal{L} = \frac{1}{2}\left(\partial_\mu \phi \partial^\mu \phi - m^2 \phi^2\right) + \mathcal{L}_{\text{int}}(\phi), \tag{4.4}$$

where $\mathcal{L}_{\text{int}}(\phi)$ is the interaction part of the Lagrangian depending on the field ϕ. If $\mathcal{L}_{\text{int}} = 0$, P^2 has the simple eigenvalue of $p^2 = m^2$. But if $\mathcal{L}_{\text{int}} \neq 0$ the eigenvalues get shifted or we might get new eigenvalues in form of bound states. For the case of a bound state we have the new eigenvalue $M^2 \approx (2m)^2$.

From the single-particle states we can move to many-particle states. Via tensor product we can create the Fock space of many-particle states. The many-particle states are given by

$$|\phi_\alpha\rangle = |p_1, p_2, p_3, ...\rangle. \tag{4.5}$$

We can separate the full Hamiltonian into a free Hamiltonian H_0 and a Hamiltonian containing the interaction part H_{int} such that

$$H = H_{\text{int}} + H_0. \tag{4.6}$$

The free Hamiltonian H_0 has the eigenstates $|\phi_\alpha\rangle$ with the eigenvalues

$$H_0|\phi_\alpha\rangle = E_\alpha|\phi_\alpha\rangle, \tag{4.7}$$

---

[1]Normally one uses m^2 as the eigenvalues for the masses in the free theory $\mathcal{L}_0$ and M^2 for the eigenvalues of the interacting theory.

where $E_\alpha = \sum_\alpha p_\alpha^0$. Remember that we assumed that the interaction has a short range. Therefore, the eigenstates $|\psi_\alpha\rangle$ of the full Hamiltonian H have the same eigenvalues E_α as $|\phi_\alpha\rangle$. Hence, we deduce that

$$H|\psi_\alpha\rangle = E_\alpha|\psi_\alpha\rangle, \tag{4.8}$$

where $|\psi_\alpha\rangle$ are the states of the separated wavepackets that do not interact with each other with $\alpha = p_1, p_2, p_3, ...$

Now we can define the in- and out-states for $t \longrightarrow -\infty$ and $t \longrightarrow +\infty$ as eigenstates of the full Hamiltonian H:

$$|\psi_\alpha^{\text{in}}\rangle \quad \text{and} \quad |\psi_\alpha^{\text{out}}\rangle. \tag{4.9}$$

The in- and out-states are an ensemble of particles that are spatially separated. With them we define the scattering matrix (S-matrix):

$$S_{\beta\alpha} = \langle \psi_\beta^{\text{out}}|\psi_\alpha^{\text{in}}\rangle, \tag{4.10}$$

where $|\psi_\beta^{\text{out}}\rangle$ and $|\psi_\alpha^{\text{in}}\rangle$ are again the well separated free particle states of the in- and out state. Hence, the S matrix describes the transition of asymptotic free particles α at $t \longrightarrow -\infty$ to a system of free particles β at $t \longrightarrow +\infty$.

In the next step we want to connect the in- and out-states with our many-particle states. Let us therefore start at early times with a state

$$H_0|\phi\rangle = E|\phi\rangle. \tag{4.11}$$

If we assume that the energies are continuous there will be an eigenstate of the full theory with the same eigenvalue

$$(H_0 + H_{\text{int}})|\psi\rangle = E\psi\rangle. \tag{4.12}$$

Hence, we can write

$$|\psi\rangle = |\phi\rangle + \frac{1}{E - H_0}H_{\text{int}}|\psi\rangle \tag{4.13}$$

Let us quickly check the result of Eq. (4.13). We multiply both sides by $(E - H_0)$ and obtain

$$(E - H_0)|\psi\rangle = (E - H_0)|\phi\rangle + H_{\text{int}}|\psi\rangle = H_{\text{int}}|\psi\rangle, \tag{4.14}$$

which we can reshuffle such that $E|\psi\rangle = (H_0 + H_{\text{int}}|\psi\rangle = H|\psi\rangle$. The first term is zero because $H_0|\phi\rangle = E|\phi\rangle$ in the free theory.

But we need to be more careful because we divide by $(E - H_0)$ and E is an eigenvalue of H_0 and therefore $1/(E - H_0)$ is singular. The solution simple solution is to shift the singularity. The final expression is the Lippmann-Schwinger equation given by

$$|\psi_\alpha^{\text{in}}\rangle = |\phi_\alpha\rangle + \frac{1}{E_\alpha - H_0 + i\epsilon}H_{\text{int}}|\psi_\alpha^{\text{in}}\rangle. \tag{4.15}$$

Note that one has to be more careful when deriving the Lippman-Schwinger equation. But we will not derive it in more detail. For a more rigorous derivation the reader is recommended to read [49]. The out-state can be obtained by replacing $+i\epsilon \longrightarrow -i\epsilon$. We see that for $H_{\text{int}} = 0$ the eigenstates $|\psi_\alpha^{\text{in}}\rangle = |\psi_\alpha^{\text{out}}\rangle = |\phi_\alpha\rangle$ are the same.

The Lippman-Schwinger equation states that the in- and out-states have to satisfy the followingvcondition:

$$e^{-iHt} \int \mathrm{d}x g(x) |\psi_\alpha^{\text{in/out}}\rangle \quad \underrightarrow{t \to \mp\infty} \quad e^{-iH_0 t} \int \mathrm{d}x g(x) |\phi_\alpha\rangle \qquad (4.16)$$

The condition can be rewritten as

$$|\psi_\alpha^{\text{in/out}}\rangle = \Omega^{\text{in/out}} |\phi_\alpha\rangle, \qquad (4.17)$$

where

$$\Omega^{\text{in/out}} = \lim_{t \to \mp\infty} e^{iHt} e^{-iH_0 t} \qquad (4.18)$$

are called Møller operators. Now we can return to the scattering matrix defined in Eq. (4.10) and define the scattering operator S with the help of Eq. (4.17) as

$$S_{\beta\alpha} = \langle \psi_\beta^{\text{out}} | \psi_\alpha^{\text{in}} \rangle \equiv \langle \phi_\beta | S | \phi_\alpha \rangle, \qquad (4.19)$$

such that

$$S = (\Omega^{\text{out}})^\dagger \Omega^{\text{in}} = \lim_{t_2 \to +\infty} \lim_{t_1 \to -\infty} e^{iH_0 t_2} e^{-iH(t_2 - t_1)} e^{-iH_0 t_1}. \qquad (4.20)$$

For later we will use the following shorthand notation

$$\langle \phi_\beta | \phi_\alpha \rangle \equiv \delta(\beta - \alpha) = (2\pi)^3 2 E_{\vec{p}_\alpha} \delta^{(3)}(\vec{p}_\beta - \vec{p}_\alpha). \qquad (4.21)$$

To summarise, we started from the Lagrangian of the free and interacting theory. With the Lagrangian one is able to compute the full Hamiltonian H of the theory. One can split the Hamiltonian H into a free and interacting Hamiltonian. We further realised that the eigenvalue E_α of the many-particle state $|\phi_\alpha\rangle$ for the free Hamiltonian H_0 is the same eigenvalue than for $|\psi_\alpha\rangle$ for the total Hamiltonian H. Therefore, we defined the in- and out-states $|\psi_\alpha^{\text{in/out}}\rangle$ that correspond to the eigenstates $|\psi_\alpha\rangle$ of H at $t \longrightarrow \mp\infty$. This motivated us to define the S-matrix $S_{\beta\alpha}$. The Lippman-Schwinger equation helped us to connect the eigenstates $|\psi_\alpha^{\text{in/out}}\rangle$ and $|\phi_\alpha\rangle$ through the Møller operators $\Omega^{\text{in/out}}$. With them we were able to rewrite the scattering matrix $S_{\beta\alpha}$ in terms of the scattering operator S. In the next chapter we will make use of this derivation to obtain a full expression for the scattering cross section that is calculable.

4.2 Scattering Cross Section

What we really measure in experiments is the cross section of a process. The cross section denoted by σ is measure of the probability that some process will take place. Or in other words, the probability that two particles will react in a certain way. For example the process of shooting a beam of α particles on a gold foil like Rutherford did. The α particles scatter off the gold nucleus. For this process you can determine the cross section which measures the probability that particles gets deflected when passing through the gold foil.

In Fig. 4.1 we can see a rough sketch of a beam of particles in the initial state α and momentum p_1 that interact with a target p_2 into a final state β with particle momenta p_1', p_2' and p_3'. In the following we want to obtain a useful expression for

the cross section that we can use for our calculations. We will closely follow [48], [50] and [51] in this chapter.
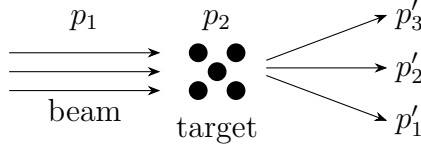
Figure 4.1: Scattering process of a beam of particles p_1 on target particles p_2 which are at rest resulting in different outgoing particles p_1', p_2' and p_3'. The initial state $\alpha = p_1, p_2$ goes to the final state $\beta = p_1', p_2', p_3'$

Another useful interpretation of the cross section is that the cross section is the fraction of time that the particles collide with the nucleus. In other words, the number of particles that scatter of in a certain time T. This leads to the follow definition of the cross section:

$$\sigma = \frac{\text{number of particles scattered}}{\text{time} \cdot \text{number density in beam} \cdot \text{velocity of particles in the beam}} = \frac{1}{T} \cdot \frac{1}{\Phi} \cdot N,$$
(4.22)

where we can identify the incoming flux of the particle beam

$$\Phi = \text{number density in beam} \cdot \text{velocity of particles in the beam.} \tag{4.23}$$

We can see the definition in another way which makes the definition above very reasonable:

$$N = \sigma \Phi T. \tag{4.24}$$

This equation states that the total number of scattered particles is the flux of particles in a time T weighted with the cross section σ. So, the cross section is indeed a measure of the probability of a certain process to happen. We can also calculate the cross section only for a solid angle $\Omega(\theta, \phi)$. This is known as the differential cross section. It gives the probability for a certain process to happen in the solid angle Ω and is given by

$$\frac{d\sigma}{d\Omega} = \text{number of particles scattered into a certain solid angle } d\Omega \tag{4.25}$$

Our main goal is now to express $d\sigma_{\beta\alpha}$ in terms of the scattering amplitude $S_{\beta\alpha}$ for a scattering of two particles $p_1 + p_2 \to p_1' + p_2' + ...$ We start by rewriting $S_{\beta\alpha}$ as

$$S_{\beta\alpha} = \langle \phi_\beta | S | \phi_\alpha \rangle \equiv \delta(\beta - \alpha) + i(2\pi)^4 \delta^{(4)}(p_\beta - p_\alpha) T_{\beta\alpha}, \tag{4.26}$$

where the first term comes from the contribution where we have no scattering. The δ-function in the second term can always be extracted because the scattering matrix commutes with P^μ which means $[S, P^\mu] = 0$. So, the total momentum is conserved and $p_\beta = p_\alpha$ with $p_\alpha = p_1 + p_2$ and $p_\beta = p_1' + p_2' + ...$.

To derive the final formula for the scattering cross section we temporarily put our system into a large but finite volume V and normalise the particle states such that

$$\langle p' | p \rangle_V = \frac{(2\pi)^3}{V} \delta^{(3)}(\vec{p} - \vec{p'}). \tag{4.27}$$

Let us quickly verify our normalisation:

$$
\begin{aligned}
\langle p | p \rangle_V &= \frac{(2\pi)^3}{V} \delta^{(3)}(0) = \frac{(2\pi)^3}{V} \frac{1}{(2\pi)^3} \int \mathrm{d}^3 x \; e^{i(\vec{p}-\vec{p})\cdot\vec{x}} \\
&= \frac{1}{V} \int \mathrm{d}^3 x = \frac{V}{V} = 1.
\end{aligned}
\tag{4.28}
$$

Thus, the normalisation is well chosen.[2] The particle states are dimensionless and normalised. Hence, $S_{\beta\alpha}^V$ is also dimensionless, which it should be as a probability amplitude.

The probability that a system in state α before the interaction is turned on, has changed to a system in state β after the interaction is turned off, is given by

$$
P(\alpha \longrightarrow \beta) = |S_{\beta\alpha}^V|^2.
\tag{4.29}
$$

In the next step, we want to compute the transition rate which is the transition probability per unit time. It is given by

$$
R_{\beta\alpha} = \frac{P(\alpha \to \beta)}{T} = \frac{|S_{\beta\alpha}^V|^2}{T} = \lim_{T\to\infty} \frac{1}{T} \left| i(2\pi)^4 \delta^{(4)}(p_\beta - p_\alpha) T_{\beta\alpha}^V \right|^2,
\tag{4.30}
$$

where we have inserted Eq. (4.26) in the third step. The first term of Eq. (4.26) is zero because we assume that $\alpha \neq \beta$. Otherwise no scattering would have happen. $T_{\beta\alpha}$ is called the T-matrix element.

We have to deal with a delta function squared which looks quite cumbersome. But we are physicist, so we can tackle this problem in typical physicist style. As mentioned earlier, we have put our system in a large volume. This allows us to interpret the delta function square as follows

$$
\begin{aligned}
|\delta^{(4)}(p_\beta - p_\alpha)|^2 &= \frac{1}{(2\pi)^4} \int \mathrm{d}^4 x e^{i(p_\beta - p_\alpha)x} \delta^{(4)}(p_\beta - p_\alpha) \\
&= \frac{VT}{(2\pi)^4} \delta^{(4)}(p_\beta - p_\alpha).
\end{aligned}
\tag{4.31}
$$

Since the particle is in a large box with volume V the integration $\int \mathrm{d}^3 x = V$ and the time integral gives $\int \mathrm{d}t = T$. The exponential $e^{i(p_\beta - p_\alpha)x} = 1$ because we have the delta function $\delta^{(4)}(p_\beta - p_\alpha)$ which guarantees us that momentum is conserved and $p_\beta = p_\alpha$. Nevertheless, this is a very sloppy way of interpreting the square of the delta function. But since this is a master's thesis written by a physicist and not a mathematician, this interpretation is sufficient at this point.

If we compare $T_{\beta\alpha}^V$ to the usual normalisation we realise that

$$
T_{\beta\alpha}^V = \prod_{i=1}^{2} \prod_{j=1}^{n'} \sqrt{\frac{N_i}{(2\pi)^3 2E_{\vec{p}_i}}} \sqrt{\frac{N_j}{(2\pi)^3 2E_{\vec{p}_j}}} T_{\beta\alpha},
\tag{4.32}
$$

where N_i and N_j are the normalisation factors given by $N_i = (2\pi)^3/V$.

---

[2]Note that we have chosen a different normalisation than in the normal canonical quantisation were one normaly uses $(2\pi)^3 2E_{\vec{p}} \delta^{(3)}(\vec{p} - \vec{p}')$.

If we combine Eq. (4.30) with Eq. (4.31) and Eq. (4.32) we obtain

$$R_{\beta\alpha} = V(2\pi)^4\delta^{(4)}(p_\beta - p_\alpha)\prod_{i=1}^{2}\prod_{j=1}^{n'}\frac{N_i}{(2\pi)^3 2E_{\vec{p}_i}}\frac{N_j}{(2\pi)^3 2E_{\vec{p}_j}}|T_{\beta\alpha}|^2. \tag{4.33}$$

The momentum is continuous. Hence, the transition rate can only be calculated in a final state with momentum $\vec{p}'_j$ in a small volume $\mathrm{d}^3 p'_j$. So, we multiply Eq. (4.33) by $\prod_{j=1}^{n'}\frac{\mathrm{d}^3 p'_j}{N_j}$ and get

$$\mathrm{d}R_{\beta\alpha} = V(2\pi)^4\delta^{(4)}(p_\beta - p_\alpha)\prod_{i=1}^{2}\prod_{j=1}^{n'}\frac{N_i}{(2\pi)^3 2E_{\vec{p}_i}}\frac{\mathrm{d}^3 p'_j}{(2\pi)^3 2E_{\vec{p}_j}}|T_{\beta\alpha}|^2. \tag{4.34}$$

The differential cross section is the differential transition rate divided by the flux and the number of the target particles

$$\mathrm{d}\sigma_{\beta\alpha} = \frac{\mathrm{d}R_{\beta\alpha}}{\Phi \cdot \text{number of target particles}}. \tag{4.35}$$

As mentioned above in Eq. (4.23) the flux is the number density of particle in the beam times the relative velocity of the particles which is given by

$$\Phi = \frac{1}{V} \cdot |\vec{v}_1 - \vec{v}_2| = \frac{N_1}{(2\pi)^3} \cdot |\vec{v}_1 - \vec{v}_2|. \tag{4.36}$$

The number of particles in the target is simply given by $N_2 V/(2\pi)^3$. So, finally we obtain for the differential cross section the following:

$$\mathrm{d}\sigma_{\beta\alpha} = \frac{1}{4E_{\vec{p}_1}E_{\vec{p}_2}|\vec{v}_1 - \vec{v}_2|}\prod_{j=1}^{n'}\frac{\mathrm{d}^3 p'_j}{(2\pi)^3 2E_{\vec{p}_j}}(2\pi)^4\delta^{(4)}(p_\beta - p_\alpha)|T_{\beta\alpha}|^2. \tag{4.37}$$

The factors V and T have dropped out and we can take the limit of $T \longrightarrow \infty$ and $V \longrightarrow \infty$.

In the frame where the two incoming particles collide head on head and therefore $\vec{p}_1 = -\vec{p}_2$ and $\vec{v}_i = \vec{p}_i/E_i$ we obtain that

$$\frac{1}{4E_{\vec{p}_1}E_{\vec{p}_2}|\vec{v}_1 - \vec{v}_2|} = \frac{1}{4\sqrt{(p_1 \cdot p_2)^2 - m_1^2 m_2^2}}. \tag{4.38}$$

We can also define the so called Lorentz invariant phase space

$$\mathrm{d}\Pi_{\mathrm{LIPS}} \equiv \prod_{j=1}^{n'}\frac{\mathrm{d}^3 p'_j}{(2\pi)^3 2E_{\vec{p}_j}}(2\pi)^4\delta^{(4)}(p_\beta - p_\alpha). \tag{4.39}$$

Note that normally the spin orientation J is random and not known. Therefore one has to take the average of the initial state. If we further do not measure the spin s of the final state we also have to sum over all final states. So we have to modify the cross section as follows:

$$\mathrm{d}\sigma_{\beta\alpha} \longrightarrow \frac{1}{(2J_1 + 1)(2J_2 + 1)}\sum_{s_1, s_2}\mathrm{d}\sigma_{\beta\alpha}. \tag{4.40}$$

Finally, formula of the cross section for a $p + k \longrightarrow p' + k'$ process can be written as

$$d\sigma = \frac{1}{4E_{\vec{p}}E_{\vec{k}}|\vec{v}_p - \vec{v}_k|} \frac{d^3p'}{(2\pi)^3 2E_{\vec{p'}}} \frac{d^3k'}{(2\pi)^3 2E_{\vec{k'}}} (2\pi)^4 \delta^{(4)}(p + k - p' - k')\overline{|T|^2}, \quad (4.41)$$

where

$$\overline{|T|^2} = \frac{1}{(2J_1 + 1)(2J_2 + 1)} \sum_{s_1, s_2} |T|^2 \quad (4.42)$$

is the spin averaged matrix element. Note that it is also quite common to use $\mathcal{M}$ as notation for the matrix element.

Usually one follows the following path to compute the cross section:

1. Start with the Lagrangian $\mathcal{L}$

2. Calculate the Feynman rules for the Lagrangian

3. Draw the Feynman diagrams of a specific process

4. Calculate the matrix element T

5. Compute the total cross section for a specific reference frame

In this master thesis the FeynArts [52] package of Mathematica was used to draw the diagrams and FeynCalc [53, 54, 55] to compute the matrix element. Finally the total cross section was calculated with the help of Python.

Quite often it is useful to work in Centre of Mass (CM) frame. In the following, we want to derive the cross section of the CM frame. For the process $1 + 2 \to 3 + 4$ we can define the variables as follows:
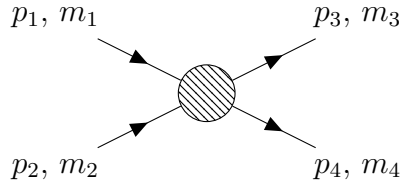
With the masses m_1 and m_2 and four momenta p_1 and p_2 of the incoming particles which scatter into the particles with masses m_3 and m_4 and four momenta p_3 and p_4. We can define the Lorentz-invariant Mandelstam variables by

$$\begin{aligned} s &= (p_1 + p_2)^2 = (p_3 + p_4)^2 \\ &= m_1^2 + m_2^2 + 2E_1E_2 - 2\vec{p}_1 \cdot \vec{p}_2 \end{aligned} \quad (4.43)$$

$$\begin{aligned} t &= (p_1 - p_3)^2 = (p_2 - p_4)^2 \\ &= m_1^2 + m_3^2 - 2E_1E_3 + 2\vec{p}_1 \cdot \vec{p}_3 \end{aligned} \quad (4.44)$$

$$\begin{aligned} u &= (p_1 - p_4)^2 = (p_2 - p_3)^2 \\ &= m_1^2 + m_4^2 - 2E_1E_4 + 2\vec{p}_1 \cdot \vec{p}_4. \end{aligned} \quad (4.45)$$

The Mandelstam variables satisfy the useful relation

$$s + t + u = \sum_i m_i^2 = m_1^2 + m_2^2 + m_3^2 + m_4^2. \quad (4.46)$$

Hence, we can always replace one of the three Mandelstam variables by the other two such that our cross section only depends on two Mandelstams. In the CM frame the incoming momentum $|\vec{p}_1| = |\vec{p}_{1\text{CM}}| = |\vec{p}_2|$ because $\vec{p}_1 = -\vec{p}_2$. Thus, the velocity $v_1 = |\vec{p}_{1\text{CM}}|/E_1 = v_2$ and $s = (p_1 + p_2)^2 = (E_1 + E_2)^2$. Note that correctly we should write $E_{1\text{cm}}$ but we will drop the subscript cm in the following discussion. Later one, we will restore it. So the flux becomes

$$
\begin{aligned}
4E_{\vec{p}_1} E_{\vec{p}_2} |\vec{v}_1 - \vec{v}_2| &= 4E_1 E_2 (v_1 + v_2) \\
&= 4E_1 E_2 (|\vec{p}_{1\text{CM}}|/E_1 + |\vec{p}_{1\text{CM}}|/E_1) \\
&= 4|\vec{p}_{1\text{CM}}|(E_1 + E_2) \\
&= 4|\vec{p}_{1\text{CM}}|\sqrt{s}.
\end{aligned}
\tag{4.47}
$$

We have to deal with the four dimensional delta function $\delta^{(4)}(p_1 + p_2 - p_3 - p_4)$ that ensures the energy and momentum conservation. We can decompose the delta function:

$$
\begin{aligned}
\delta^{(4)}(p_1 + p_2 - p_3 - p_4) &= \delta(E_1 + E_2 - E_3 - E_4)\delta^{(3)}(\vec{p}_1 + \vec{p}_2 - \vec{p}_3 - \vec{p}_4) \\
&= \delta(\sqrt{s} - E_3 - E_4)\delta^{(3)}(\vec{p}_3 + \vec{p}_4),
\end{aligned}
\tag{4.48}
$$

where we have used that we are in the CM frame in the second step. So, the cross section can be reduced to

$$
\mathrm{d}\sigma = \frac{1}{4|\vec{p}_{1\text{CM}}|\sqrt{s}} \frac{\mathrm{d}^3 p_3}{(2\pi)^3 2E_3} \frac{\mathrm{d}^3 p_4}{(2\pi)^3 2E_4} (2\pi)^4 \delta(\sqrt{s} - E_3 - E_4)\delta^{(3)}(\vec{p}_3 + \vec{p}_4)\overline{|T|^2}. \tag{4.49}
$$

We can now take the integral over $\vec{p}_4$ by using the δ-function. Therefore, we get $\vec{p}_3 = -\vec{p}_4$ and can write $p_f = |\vec{p}_{3\text{cm}}| = |\vec{p}_3| = |\vec{p}_4|$. So, we are left with the integration over $\mathrm{d}^3 p_3 = \mathrm{d}\Omega \mathrm{d}p_f p_f^2$. It is useful to change the variables from p_f to $x(p_f) = E_3 + E_4 - \sqrt{s}$, where $E_3 = \sqrt{m_3^2 + |\vec{p}_{3\text{cm}}|^2}$ and $E_4 = \sqrt{m_4^2 + |\vec{p}_{3\text{cm}}|^2}$ so that $x(0) = m_3 + m_4 - \sqrt{s}$. The derivative yields

$$
\frac{\mathrm{d}x}{\mathrm{d}p_f} = \frac{p_f}{E_3} + \frac{p_f}{E_4} = \frac{E_3 + E_4}{E_3 E_4} p_f. \tag{4.50}
$$

Inserting the change of variables into the cross section we obtain

$$
\begin{aligned}
\mathrm{d}\sigma &= \frac{1}{4|\vec{p}_{1\text{CM}}|\sqrt{s}} \frac{1}{16\pi^2} \mathrm{d}\Omega \int_{m_3+m_4-\sqrt{s}}^{\infty} \mathrm{d}x \frac{p_f}{E_3 + E_4} \delta(x)\overline{|T|^2} \\
&= \frac{1}{64\pi^2 |\vec{p}_{1\text{CM}}|\sqrt{s}} \mathrm{d}\Omega \frac{p_f}{\sqrt{s}} \overline{|T|^2} \theta(\sqrt{s} - m_3 - m_4),
\end{aligned}
\tag{4.51}
$$

where here $\theta(x)$ is the Heaviside function with $\theta(x) = 1$ if $x > 1$ and 0 otherwise. If we define $|\vec{p}_{1\text{cm}}| = p_i$ as the initial momentum and rearrange the formula it simplifies to

$$
\left(\frac{\mathrm{d}\sigma}{\mathrm{d}\Omega}\right)_{\text{CM}} = \frac{1}{64\pi^2 s} \frac{|\vec{p}_f|}{|\vec{p}_i|} \overline{|T|^2} \theta(\sqrt{s} - m_3 - m_4). \tag{4.52}
$$

This formula only holds in the CM frame. Note, that $\mathrm{d}\Omega$ is the solid angle in the CM frame. We want to gain a Lorentz-invariant expression for the cross section. For simplicity (or we can call it laziness) we will neglect the term of the Heaviside function in the following calculations. The Mandelstam variable $t = (p_1 - p_3)^2 = m_1^2 + m_3^2 - 2E_1 E_3 + 2|\vec{p}_1||\vec{p}_3|\cos\theta$, where θ is the scattering angle in the CM frame.

The derivative with respect to the scattering angle yields $dt = 2|\vec{p}_1||\vec{p}_3|d(\cos\theta)$. Therefore $d\Omega = d(\cos\theta)d\phi = dtd\phi/(2|\vec{p}_1||\vec{p}_3|)$. Remember that $|\vec{p}_1| = |\vec{p}_i|$ and $|\vec{p}_3| = |\vec{p}_f|$. If we assume that the matrix element $\overline{|T^2|}$ does not depend on ϕ we obtain an additional factor of 2π because of the integration. So finally, for the two body reaction the cross section formula can be simplified to [56]:

$$\frac{d\sigma}{dt} = \frac{1}{64\pi s}\frac{1}{|p_{1cm}|^2}\overline{|T|^2}, \tag{4.53}$$

where we have restored the subscript CM for $\vec{p}_1$. This formula is Lorentz-invariant and can therefore be applied in any reference frame. In the centre of mass frame we can write for t:

$$t = (E_{1cm} - E_{3cm})^2 - (\vec{p}_{1cm} - \vec{p}_{3cm})^2 - 4|\vec{p}_{1cm}||\vec{p}_{3cm}|\sin^2(\theta_{cm}/2), \tag{4.54}$$

where the particle momenta read

$$\vec{p}_{icm} = \sqrt{E_{icm}^2 - m_i^2}. \tag{4.55}$$

The limiting values are $\theta_{cm} = 0$ which we call t_0 and $\theta_{cm} = \pi$ which we call t_1. The centre of mass energies are given by

$$E_{1cm} = \frac{s + m_1^2 - m_2^2}{2\sqrt{s}}, \quad E_{3cm} = \frac{s + m_3^2 - m_2^4}{2\sqrt{s}}. \tag{4.56}$$

Hence for our $2 \rightarrow 2$ scattering we get the limiting values by

$$t_0/t_1 = \left(\frac{m_1^2 - m_3^2 - m_2^2 + m_4^2}{2\sqrt{s}}\right)^2 - (|\vec{p}_{1cm}| \mp |\vec{p}_{3cm}|)^2, \tag{4.57}$$

So, for a two body process we can express the phase factor in terms of s which is quite useful because it is independent of the integration variable t. We have to evaluate the matrix element $\overline{|T|^2}$ and integrate it over t. The total cross section then only depends on the Mandelstam variable s and we can transform into the rest frame of the dark matter particle, where $s = m_{DM}^2 + 2Em_{DM}$ with E the energy of the incoming particle that scatters off the dark matter particle which is at rest.

In summary, we have obtained a general relation for the scattering cross section and another relation in the CM frame. We will make great use of the derivations in ch. 6. We will now continue by motivating, why we are interested in scatterings between dark matter particles and photons or neutrinos.

Chapter 5

Dark Matter Spike

After reviewing the scattering theory we now want to give a motivation why we are interested in scatterings between dark matter and elementary particles. We have evidence for the existence of dark matter particles at galactic scales. Hence, we will first give an overview of the most common dark matter profiles inside a galaxy. Furthermore, we will give an overlook on Black Holes and Active Galactic Nuclei. In almost every centre of a galaxy we assume to have supermassive black holes. They emit photons and neutrinos through various mechanism. Thereafter, we will examine what will happen with the common dark matter profile close to the black hole at the centre of a galaxy. The dark matter density is expected to increase and form a spike. Lastly, we will conclude that the enhanced dark matter density profile can lead to flux attenuation for the neutrinos or photons in the vicinity of a black hole due to their interaction with the dark matter.

5.1 Dark Matter Profiles

We have evidence that dark matter exists at galactic scales. One of the key detection were the rotation curve of the galaxies. We pointed out earlier that the dark matter density has to scale with $\rho_{\mathrm{DM}} \sim r^2$ in order to obtain that $v_{\mathrm{rot}} = \mathrm{const.}$ outside the visible galaxy. This means that the density increases towards the centre of the galaxy. The dark matter distribution is not precisely known but it can be inferred from numerical N-body simulations. They assume the dark matter halos to grow via mergers in an expanding universe [57].

One of the most popular choice for the dark matter density profile is the Navarro-Frenk-White (NFW) profile [58]:

$$\rho_{\mathrm{DM}}(r) = \frac{\rho_0}{\frac{r}{r_s}(1 + \frac{r}{r_s})^2},\tag{5.1}$$

where $r_s = 24$ kpc is the scaling radius of the Milky Way and ρ_0 is the normalisation factor to reproduce the local dark matter density $\rho_\odot = 0.39$ GeV $\cdot$ cm^{-3} [59]. Note that the scaling radius and the normalisation factor differ from halo to halo. For the Milky Way the dark matter density can be approximated as [57]:

$$\rho_{\mathrm{DM}}(r) \approx 10^2 M_\odot \mathrm{pc}^{-3} \left(\frac{\rho_\odot}{10^{-2} M_\odot \mathrm{pc}^{-3}}\right)\left(\frac{R_\odot}{8 \text{ kpc}}\right)\left(\frac{r}{1 \text{ pc}}\right)^{-1},\tag{5.2}$$

where $R_\odot$ is the radius of the solar circle. Another popular dark matter density profile as alternative to the NFW profile is the Einasto profile [60]:

$$\rho_{\text{DM}}(r) = \rho_0 \exp\left[-\frac{2}{\alpha}\left(\frac{r}{r_s}\right)^\alpha\right], \tag{5.3}$$

where $\alpha = 0.17$ and $r_s = 24$ kpc. The higher the value of α, the faster shallows the density profile for small radii. And last but not least, we present the isothermal profile [61]:

$$\rho_{\text{DM}}(r) = \frac{\rho_0}{1 + \frac{r^2}{r_s^2}}, \tag{5.4}$$

where $r_s = 4.4$ kpc. The variety of dark matter density profiles clearly illustrates that the dark matter distribution is not completely known. Typically, the N-body simulations ignore the effect that stars and gas may dominate the inner regions of the galaxy [57]. For example, in the vicinity of black holes the slope of the density profile can change dramatically and result in a much more steeper slope as we will see later. Nevertheless, it is pretty clear that the slope should increase as we move towards the centre of the galaxy. But the power law index of the slope is still under debate [57].

5.2 Black Holes and Active Galatic Nuclei

In 1915 Einstein published his famous work about general relativity [62]. In 1916, shortly after Einsteins publication Karl Schwarzschild presented the first solution to Einsteins field equations for a non rotating point mass. The solution is called Schwarzschild metric and it has two interesting properties: First, the metric becomes singular at the origin because gravity is so strong that it bends the spacetime such that the curvature goes to infinity. Second, it states the so called event horizon for gas and even light. Light crossing the event horizon is not able to escape anymore from the gravitational field of the black hole and moves inevitably towards the singularity at the origin. Hence, the solution of Karl Schwarzschild predicts what we call a black hole.

Figure 5.1: A picture of the black hole of our own Milky way (left) and of the galaxy M87 (right). They are the first visual evidence of a black hole in our universe. The event horizon of the black hole is clearly visible. The picture was taken from the Event Horizon Telescope Figure Credit: Left: [63]; Right: [64]

Since the 1990s astrophysics suspect a black hole at the centre of our own galaxy [65, 66]. But it took years to directly proof this hypothesis. In the Milky Way there

are lot of indirect evidences through the motion of stars around the galactic centre [67]. In 2022 the Event Horizon Telescope (EHT) published an article where they showed a picture of the black hole in the centre of the milky way [68]. Three years before, the EHT collaboration published the first picture ever taken from a black hole in the centre of the galaxy M87 [69]. Hence, we have no doubt that black holes exists in our universe. In Fig. 5.1 both picture of the EHT are shown. One clearly see the event horizon of the black hole and large emissions of photons around it.

An active galactic nuclei (AGN) is the region in the centre of a galaxy that has very high luminosity compared to other stellar objects. AGNs can even shine brighter than their host galaxy. Theory indicates that there exist black holes from $10^6 M_\odot$ to $10^{10} M_\odot$ in the centre of galaxies and even in the galactic centre [70] which is shown in Fig. 5.2. Four our studies it is important that the black hole is supermassive because the gravitational attraction of the surrounding particles is higher and therefore the particle density can be denser than expected, as we will see in the next section.

Figure 5.2: The image shows the galactic centre. In the centre there is a supermassive black hole with approximately $10^6 M_\odot$. The galatic center and in general the AGNs are good locations and unique laboratories in our universe to probe various dark matter models. Image was taken from [71]

A special class of AGN is the blazar. Blazars are characterised by their emission of strong relativistic beams [72]. They are promising sources to probe dark matter models because we expect them to emit high-energetic neutrinos and photons. For example, the blazar TXS $0506 + 056$ is a candidate for high-energetic neutrino emission which is also known for its gamma-ray emission [73, 74]. The IceCube collaboration also states to have found neutrinos associated to the AGN NGC 1068

at a 4.2σ significance [75]. The detection is a strong hint for TeV neutrinos. For the same AGN the FermiLAT found evidence for high energetic photons which are consistent with hadronic emissions[76]. Thus, we have observational evidence, that the AGNs are sources for high-energetic photons ans neutrinos.

The high energy neutrinos can be produced via inelastic *pp* collisions or *pγ* interactions [77, 78]. In the case of the hadronic *pp* collision the proton produces charged pions. These charged pions then decay into muons ans muon neutrinos. The muons also decay in a furhter process into electrons and electron neutrinos. Hence, the process is $\pi^+ \longrightarrow \mu^+ + \nu_\mu \longrightarrow e^+ + \nu_e + \overline{\nu}_\mu + \nu_\mu$ for positively charges pions and $\pi^- \longrightarrow \mu^- + \overline{\nu}_\mu \longrightarrow e^- + \overline{\nu}_e + \overline{\nu}_\mu + \nu_\mu$ for negatively charges pions. The other interaction is between protons and gamma rays. In general the AGNs are surrounded by a geometrically thin accretion disc [79]. The accretion disc is hot an emits thermal radiation which produces observable features [80]. Stellar protons get accelerated close to the black hole and interact with the photons via $p\gamma \longrightarrow n\pi^+$. The π^0 decays into two gammas and the π^+ decays as described above. The way to discriminate between the *pp* and *pγ* emission through the amount of electron antineutrinos [81]. In the *pγ* process one expects to have less electron antineutrinos.

Gamma rays can be produced through four main mechanisms. If a charged particle like an electron or proton is deflected in a magnetic field it losses energy and emits synchroton radiation. Also, if a charged particle like an electron or proton gets deflected by the field of an atomic nucleus it emits photon as bremsstrahlung. The third mechanism is the pion decay. When two protons collide they can form a π^0 particle that decays into two γ's. But the π^0 can also be produce through in intermediate Δ^+ particle, namely $p + \gamma \longrightarrow \Delta^+ \longrightarrow p + \pi^0$ [78]. The fourth and last reaction is the inverse Compton scattering. If we have a low energy photons from another process like synchotron radiation, it can increase its energy due to the scattering with an electron. Normally, the low energetic photons are produced by the accretion disc of the black hole and up scattered via inverse Compton scattering. But also the π^0 decay produces high energy γ's [76].

During their way to the earth the flux of photons attenuates due to electromagnetic processes, e.g. $\gamma\gamma \longrightarrow e^+e^-$. On the other side, the neutrinos only interact weakly with the matter and suffer less attenuation on their way. Nevertheless, if we extend the SM there could be new sources of gamma-ray or neutrino interactions which can affect their propagation. We have seen, that we need an extension of the SM to explain dark matter as WIMPs. So, the interaction between the WIMPs and the gamma-rays and photons can influence their propagation too if the interaction strength is large enough.

In summary, we can tell that black holes are among the most interesting and important objects in the sky because they are assumed to be the source of high energy cosmic neutrinos and photons [82]. These high energetic particles provide useful information's about their environment and their surroundings. Furthermore one can use the information's to probe various dark matter models as we will see in the next section.

5.3 Dark Matter Spike

One of the most promising methods to probe dark matter models is to look at the neutrino and photon flux of distant objects [3]. The neutrinos and photons have to propagate through the surrounding medium and scatter with the particles on the way to the earth. If the particle density of dark matter is high enough, the neutrinos or photons interact more frequently with the dark matter particles. This could reduce the expected neutrino or photon flux significantly. The flux attenuation can then be detected here on earth. But, for this phenomenon one needs a large dark matter density. Normally, the WIMP density is not high enough to archive remarkable flux reductions. But, close to a black holes one expects DM to form a dense dark matter spike due to gravitational attraction of the black hole [83]. Our goal is now to introduce the dark matter spike.

The first person mentioning a spike was Peebles in the year 1972 [84]. He was interested in the question whether the density profile of baryons gets enhanced near a black hole. He conclusion was rather simple. There can not be any conclusion as long as we do not know that black holes exists. But nowadays we have observational proof for black holes in our universe as stated above. In [85] the idea of Peebles was given a more robust framework. Also, for the idea of a spike of baryons close to a black hole. They concluded that for a non-isothermal cusp the baryon density is steeper. The results of [85] were reinterpreted in the late 90s from Gondolo and Silk for the formation of a dark matter spike in the vicinity of a black hole [83]. They postulated that the black holes accretes the surrounding particle dark matter into a dense spike. Further they concluded that the dark matter annihilation must be very strong inside the spike. Hence, the dark matter spike is a compact source for photons, electrons, etc. and a powerful probe for the nature of dark matter [3, 4, 83, 86].

We will not fully derive the final dark matter density close to a black hole after its formation. It involves knowledge about general relativity that we do not want to recapitulate at this point. The reader is refereed to the paper of Gondolo and Silk in [83]. We just want to stress that one can derive the spike density by assuming that the black holes grows adiabatic which means that the black hole grows slowly over time compared to the time of a typical orbital period of the surrounding mater [87]. Then, with the help of general relativity and angular momentum conservation one is able to obtain the final result of the dark matter spike density as follows [83]:

$$\rho_{\rm sp}(r) = \rho_R g_\gamma(r) \Big(\frac{R_{\rm sp}}{r}\Big)^{\gamma_{\rm sp}}, \qquad (5.5)$$

where $R_{\rm sp} = \alpha_\gamma r_0 (M_{\rm BH}/(\rho_0 r_0^3))^{1/(3-\gamma)}$ defines the size of the spike with $\alpha_\gamma \simeq 0.293\gamma^{4/9}$ for $\gamma \ll 1$ and $M_{\rm BH}$ being the black hole mass. The cuspiness of the dark matter spike is described by the spike parameter $\gamma_{\rm sp} = (9 - 2\gamma)/(4 - \gamma)$. Between $0 \leq \gamma \leq 2$ the spike parameter only varies between 2.25 and 2.5 [83]. For $0 < \gamma < 2$ we can approximate the function $g_\gamma(r)$ by $g_\gamma \approx \big(1 - \frac{4R_{\rm S}}{r}\big)$, where $R_{\rm S}$ is the Schawrzschild radius. For $\gamma > 1$ the factor α_γ must be obtained numerically. For $\gamma = 1$ we find that $\alpha_\gamma \approx 0.122$ [83]. Finally, $\rho_{\rm R} = \rho_0 (R_{\rm sp}/r_0)^{-\gamma}$ is a normalisation factor chosen to match the density profile outside the spike. The value ρ_0 is determined by the uncertainty of the black hole mass [88].

The spike parameter can also be derived through scaling relations. We will quickly

have a look at it because it gives a good understanding of the spike parameter in combination with the black hole growth condition [7]. The black hole is assumed to accrete masses adiabatic. Hence, the initial mass distribution reads $\rho \propto r^{-\gamma}$. The final dark matter distribution is given by $\rho \propto r^{-\gamma_{\rm sp}}$. With angular momentum conservation and the conservation of mass we obtain the following relation:

$$\rho_i r_i^2 {\rm d}r_i = \rho_f r_f^2 {\rm d}r_f. \tag{5.6}$$

This equation simply states the angular momentum conservation. With the initial and final distribution of the dark matter profile we therefore obtain that r_i scales as

$$r_i \propto r_f^{(3-\gamma_{\rm sp})/(3-\gamma)}. \tag{5.7}$$

Besides, we also have an equation due to the conservation of mass which is given by

$$r_i M_i = r_f M_f \approx r_f M_{\rm BH}. \tag{5.8}$$

When can express the inital mass M_i in terms of the initial volume which is proportional to r_i^3 times the initial density $\rho_i \propto r_i^{-\gamma}$. Thus, we get:

$$r_i \propto r_f^{1/(4-\gamma)}. \tag{5.9}$$

So, we have two different relations for the initial radius in terms of the final radius from our two conservation laws. They must be equal and therefore we obtain by rearranging for the spike parameter

$$\gamma_{\rm sp} = \frac{9 - 2\gamma}{4 - \gamma}. \tag{5.10}$$

This little exercise shows us that the spike parameter is very well motivated by the conservation of mass and angular momentum [7].

When we allow self annihilation of the dark matter particles inside the spike, the density saturates as

$$\rho_{\rm sat} = \frac{m_{\rm DM}}{\langle \sigma v \rangle t_{\rm BH}}, \tag{5.11}$$

where $\langle \sigma v \rangle$ is the annihilation cross section, $m_{\rm DM}$ the dark matter mass and $t_{\rm BH}$ the age of the black hole. Further, we notice that the dark matter spike profile extends to a certain maximal radius $R_{\rm sp}$. Afterwards, the dark matter distribution follows the existing dark matter profile inside the galaxy [3].

If we now take the dark matter density profile outside the spike to be the NFW profile such that $\gamma = 1$, the general density profile of dark matter reads [83]

$$\rho(r) = \begin{cases} 0, & r \leq 4R_S \\ \dfrac{\rho_{\rm sp}(r)\rho_{\rm sat}}{\rho_{\rm sp}(r) + \rho_{\rm sat}}, & 4R_{\rm S} \leq r \leq R_{\rm sp} \\ \rho_0 \left(\dfrac{r}{r_0}\right)^{-1}\left(1 + \dfrac{r}{r_0}\right)^{-2}, & r \geq R_{\rm sp}. \end{cases} \tag{5.12}$$

Below the radius of $r \leq 4R_S$ the dark matter gets captured and is swallowed by the black hole. Note that we have a combination of particle physics and astrophysical

knowledge in the spike density. The saturation of the dark matter spike is given by the annihilation cross section of the dark matter particles and their mass that has to be determined by particle physicists. While the black hole mass, the initial dark matter profile and various other properties have to be determined by astrophysicists.

Furthermore, we have some uncertainties in the density profile. We assume that the black hole growth is adiabatic but, until now, it is not fully understood how black holes form and grow at the centre of galaxies [87, 89]. Further, it could also be that the black hole does not lie in the centre of the density spike [89]. Both cases would weaken the spike profile. It was also shown that the dark matter spike can be destroyed by hierarchical mergers. The merging between two supermassive black holes lead to the formation of black hole binaries and lower the density of the dark matter or even destroy it [90]. Another effect that could alter the spike profile is stellar heating [91, 92]. In total, the spike profile might be different than the one proposed from Gondolo and Silk. Nevertheless, we will stick to their description because it is well motivated.

Now, we want to make a concrete example how a dark matter spike can look like. We assume that the dark matter spike is given by Eq. (5.12). We consider a black hole of mass $M_{\mathrm{BH}} \approx 3 \cdot 10^8 M_\odot$ such that $R_S \approx 3 \cdot 10^{-5}$ pc and $t_{\mathrm{BH}} = 10^9$ yr. Further, we take $r_0 = 10$ kpc and $\rho_0 \approx 7 \cdot 10^3$ GeV/cm^3. We assume a NFW profile for the dark matter profile inside the galaxy with $\gamma = 1$. Consequently, we get $\gamma_{\mathrm{sp}} = 7/3$. This situation can be realised for the blazar TXS 0506+056 [3]. The result is shown in Fig. 5.3.
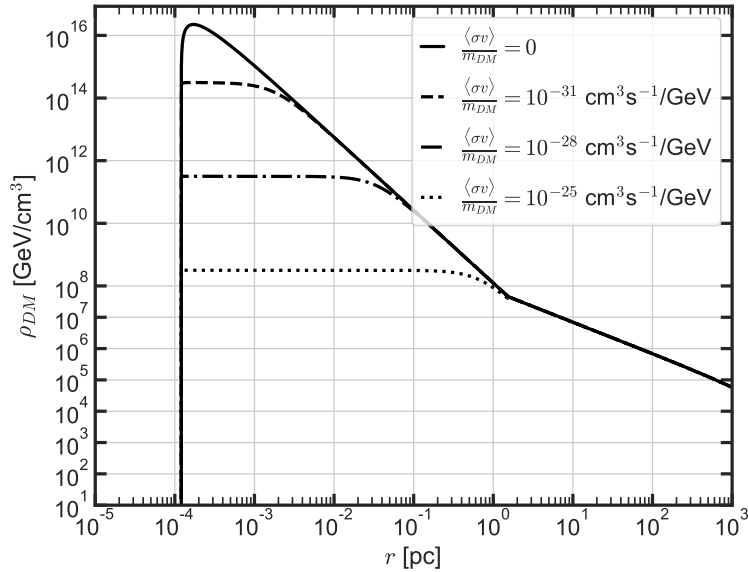
Figure 5.3: Dark matter density profile around the black hole with $M_{\mathrm{BH}} = 3 \cdot 10^8 \mathrm{M}_\odot$ and $t_{\mathrm{BH}} = 10^9$ yr. The initial dark matter distribution is given by a NFW profile with $\gamma = 1$. The spike parameter is $\gamma_{\mathrm{sp}} = 7/3$. The profile is shown for different annihilation cross sections normalised by the dark matter mass. The dark matter is expected to form a dense spike according to Eq. 5.12.

We see in Fig. 5.3 that the dark matter density increases extremely by two up to even eight orders of magnitude after roughly one parsec. This is exactly the case when $r \leq R_{\mathrm{sp}}$. The dashed lines show different scenarios for the dark matter

annihilation cross section. The higher the annihilation cross section the less denser is the spike. This is expected because the dark matter spike saturates proportional to the annihilation cross section. If the annihilation cross section is large, more dark matter particles annihilate due to the compression of the dark matter particles inside the spike. If annihilation the cross section is low, the dark matter particles can be compressed even more without annihilating. As a consequence the spike density increases to lower radii. Note that the typical value of the annihilation cross section for WIMPs is $\langle \sigma v \rangle \approx 3 \cdot 10^{-26}$ cm^{3}s^{-1}. But this is only the case when we have $s-$wave annihilation. There can be cases where the $s-$wave annihilation is suppressed and we have $p-$wave annihilation. So, there can be exceptions for which the dark matter annihilation cross section is lower than $3 \cdot 10^{-26}$ cm^{3}s^{-1}. See ch. 3.5 for more details.

In summary, we have seen that in the vicinity of a black hole the dark matter density profile can be much steeper than expected. The dark matter particles could form a dense spike around the black hole. As a results, the density is much sharper than the usual NFW profile of the host galaxy. In the following section we will make use of the spike to motivate why we are interested in scattering cross sections between dark matter particles and neutrinos or photons. Also,we want to mention that [93] claims to have indirect evidence for dark matter spikes around stellar mass black holes. Hence, dark matter spikes could exist in our universe. This makes the study of dark matter spikes even more attractive.

5.4 Flux Attenuation in the vicinity of a Black Hole

Neutrinos or photons can be produce close to the black hole. In the vicinity of a black hole we expect the dark matter to form a dense spike. Therefore, the neutrinos or photons have to traverse the dark matter spike when travelling to our detector on earth. On their journey they scatter with the dark matter particles χ along their way [82]. Hence, the neutrino or photon flux on earth gets attenuated. We will now discuss this scenario for neutrinos but the photon case works analogously.

The attenuation of the neutrino flux can be described by a Boltzmann equation that is called cascade equation [86, 94]:

$$\frac{\mathrm{d}\Phi}{\mathrm{d}\tau} = -\sigma_{\nu\chi}\Phi + \int_{E_\nu}^{\infty} \mathrm{d}E_\nu' \frac{\mathrm{d}\sigma_{\nu\chi}}{\mathrm{d}E_\nu} \Phi(E_\nu'), \tag{5.13}$$

where E_ν is the neutrino energy and $\sigma_{\nu\chi}$ the model dependent scattering cross section of the dark matter particle χ and the neutrino. Φ is the neutrino flux and τ the accumulated dark matter column density Σ over the dark matter mass m_χ given by $\tau = \Sigma(r)/m_\chi$. The first term on the right hand side describes the decrease of the neutrino flux due to their interaction with the surrounding dark matter particles. The second term corresponds to the effect that the neutrino energies get redistributed from high to low energy [4].

If the cross section is independent of the energy, the second term vanishes and the equation reduces to

$$\frac{\mathrm{d}\Phi}{\mathrm{d}\tau} = -\sigma_{\nu\chi}\Phi. \tag{5.14}$$

This equation can easily be integrated. We obtain an exponential attenuation of the flux given by

$$\Phi(E_\nu) \sim \Phi_\nu(E_\nu) e^{-\frac{\sigma_{\nu\chi}\Sigma_\chi}{m_\chi}}, \tag{5.15}$$

where $\Phi(E_\nu)$ is the observed flux a the detector and $\Phi_\nu(E_\nu)$ is the initial flux at the source. Note that the second term in Eq. (5.13) states the redistribution of the neutrino energies due to their elastic scattering. If one assumes that most of the dark matter particles get absorbed in the dark matter spike due to their interaction with the dark matter, the second term can also be neglected. Hence, we obtain the same result for the neutrino flux in the case of inelastic absorption. The similar analysis can also be done for photons.

Hence, we can now define the flux attenuation coefficient μ_i for different species i due to their interaction with dark matter as follows:

$$\mu_i\big|_{\mathrm{DM}} = \frac{\sigma_{\mathrm{DM\text{-}i}}\Sigma_{DM}}{m_{\mathrm{DM}}}. \tag{5.16}$$

The attenuation coefficient is the crucial quantity to calculate the absorption of the particles when travelling through the dark matter spike and we will make great use of it later in ch. 6. The definition of the coefficient makes sense because the higher the interaction of dark matter particles with species i, the more is the attenuation effect that we observe on earth of particle i. Also, the higher the dark matter density, the more scatterings can occur which will also lead to an reduction of the flux. On the other side, the heavier the dark matter particles, the fewer lie on the way between the particle i and the detector, when the particle i traversing the dark matter spike. As a consequence, it is less likely for the particle i to scatter with the dark matter particle and the attenuation of the flux gets depleted.

Note that μ is highly model dependent because the scattering cross section as well as the dark matter mass depend on the dark matter model. The mass and the cross section must be determined by particle physics for a specific model. Furthermore, the column density Σ depends on astrophysical parameters, e.g. the black hole mass. The particle physicist have to rely on the observations made by the astrophysicists. Thus, we can conclude that the attenuation coefficient combines particle physics with astrophysics.

In the vicinity of a black hole we assume the dark matter to form a dense spike. Hence, the typically small value of the scattering cross section between dark matter particles and photons or neutrinos can be compensated by the large dark matter density of the spike. This might lead to flux attenuation of 65% for neutrinos or photons if the attenuation coefficient is around $\mathcal{O}(\mu) \sim 1$. The physical interpretation is that the neutrinos or photons can interact more frequently inside the spike because there are more dark matter particles than in the rest of the host galaxy.

Let us express the dark matter column density more explicitly for the dark matter spike. We will closely follow [3] during the derivation. A long the line of sight the column density is given by [3, 4]

$$\Sigma_{\mathrm{DM}} = \int_{R_{\mathrm{em}}}^{r} \mathrm{d}r' \rho_{\mathrm{DM}}(r'), \tag{5.17}$$

where R_{em} is the distance from the black hole to the position where the neutrino or photons is likely to be produced. ρ_{DM} is given by Eq. (5.12). We assume that

the impact of the absorption only takes place inside the dark matter spike and the host galaxy. We neglect the contributions from the intergalactic medium and the Milky Way. Including this contributions is left over for future work. So, we can approximate [3]:

$$\Sigma_{\mathrm{DM}} \simeq \Sigma_{\mathrm{DM}}\big|_{\mathrm{spike}} + \Sigma_{\mathrm{DM}}\big|_{\mathrm{host}} \simeq \int_{R_{\mathrm{em}}}^{R_{\mathrm{sp}}} \mathrm{d}r \rho_{\mathrm{DM}}(r) + \int_{R_{\mathrm{sp}}}^{\infty} \mathrm{d}r \rho_{\mathrm{DM}}(r). \tag{5.18}$$

If we assume that the photon and neutrino emission region is $R_{\mathrm{em}} \gg 4R_S$, then $g_\gamma(r) \simeq 1$. Furthermore, when the neutrinos or photons are emitted in regions below the saturation density we can neglect the annihilation of the dark matter particles. In this case the dark matter profile is given by $\rho_{\mathrm{DM}}(r) \simeq \rho_{\mathrm{sp}}(R_{\mathrm{em}})(r/R_{\mathrm{em}})^{-\gamma_{\mathrm{sp}}}$. Substituting into Eq. (5.18) yields [3]

$$\Sigma_{\mathrm{DM}}\big|_{\mathrm{spike}} \simeq \int_{R_{\mathrm{em}}}^{R_{\mathrm{sp}}} \mathrm{d}r \rho_{\mathrm{sp}}(R_{\mathrm{em}}) \left(\frac{r}{R_{\mathrm{em}}} \right)^{-\gamma_{\mathrm{sp}}} \simeq \frac{\rho_{\mathrm{sp}}(R_{\mathrm{em}}) R_{\mathrm{em}}}{(\gamma_{\mathrm{sp}} - 1)} \left[1 - \left(\frac{R_{\mathrm{sp}}}{R_{\mathrm{em}}} \right)^{1-\gamma_{\mathrm{sp}}} \right] \tag{5.19}$$

We are interested in the cases where the neutrinos and photons are produced inside the spike such that $R_{\mathrm{em}} \ll R_{\mathrm{sp}}$ and $\gamma_{\mathrm{sp}} > 1$. Hence, we can neglect the second term in Eq. (5.19). For an initial NFW profile $\gamma = 1$ and $\gamma_{\mathrm{sp}} = 7/3$. Thus, the dark matter spike density reduces to

$$\Sigma_{\mathrm{DM}}\big|_{\mathrm{spike}, \gamma=1} \simeq \frac{3 M_{\mathrm{BH}}^{2/3} r_0^{1/3} \alpha_\gamma^{4/3} \rho_0^{1/3}}{4 R_{\mathrm{em}}^{4/3}}. \tag{5.20}$$

The more general form of the dark matter spike can also be calculated. The computation is straight forward but tedious. One just has to plug $\rho_{\mathrm{sp}}(R_{\mathrm{em}}) = \rho_0 (R_{\mathrm{sp}}/r_0)^{-\gamma} (R_{\mathrm{sp}}/R_{\mathrm{em}})^{\gamma_{\mathrm{sp}}}$ and $R_{\mathrm{sp}} = \alpha_\gamma r_0 (M_{\mathrm{BH}}/(\rho_0 r_0^3))^{1/(3-\gamma)}$ into Eq. (5.19) to get

$$\Sigma_{\mathrm{DM}}\big|_{\mathrm{spike}} = \frac{1}{\gamma_{\mathrm{sp}} - 1} \frac{\alpha_\gamma^{-\gamma+\gamma_{\mathrm{sp}}}}{R_{\mathrm{em}}^{\gamma_{\mathrm{sp}}-1}} \left(r_0^{\gamma(3-\gamma_{\mathrm{sp}})} M_{\mathrm{BH}}^{-\gamma+\gamma_{\mathrm{sp}}} \rho_0^{3-\gamma} \right)^{1/(3-\gamma)}. \tag{5.21}$$

If the cross section is very large, the density of the spike can be set equal to the saturation density which is inversely proportional to the the annihilation cross section [3]:

$$\Sigma_{\mathrm{DM}}\big|_{\mathrm{spike}} \simeq \int_{R_{\mathrm{em}}}^{R_{\mathrm{sp}}} \mathrm{d}r \rho_{\mathrm{sat}} \simeq \rho_{\mathrm{sat}} R_{\mathrm{sp}} \left[1 - \frac{R_{\mathrm{em}}}{R_{\mathrm{sp}}} \right]. \tag{5.22}$$

We now want to make a concrete example and calculate the column density of a dark matter spike. For the case of the blazar TXS 0506 + 056 the source of the neutrinos and photons has been estimated in [95] to be emitted close the Broad Line Region (BLR) $R_{\mathrm{BLR}} \sim 0.021$ pc. This means that the neutrino and photons emission lies inside the dark matter spike. As a result, they have to travel through the dense dark matter spike when reaching the earth.
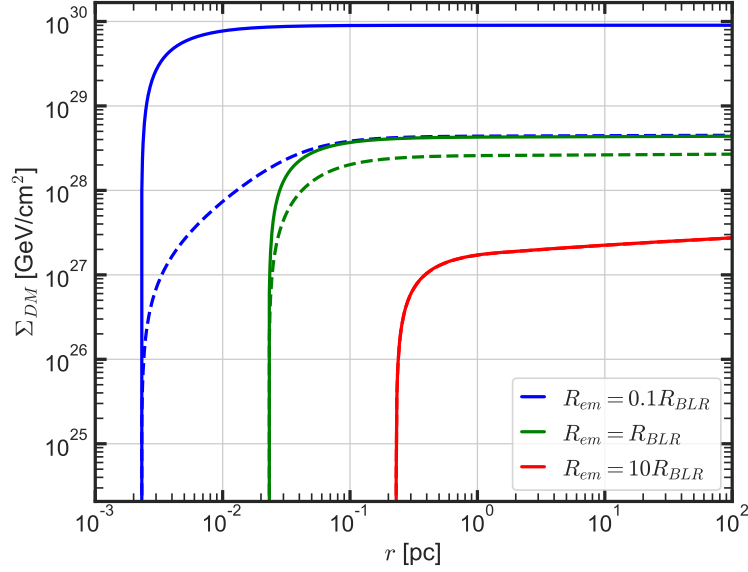
Figure 5.4: Dark matter column density for the case of $M_{\mathrm{BH}} \approx 3 \cdot 10^8 M_\odot$, $t_{\mathrm{BH}} = 10^9$ yr, $\gamma = 1$, $r_0 = 10$ kpc and $\rho_0 \approx 7 \cdot 10^3$ GeV/cm^3. Three different scenarios for R_{em} are shown in terms of the Borad Line Region $R_{\mathrm{BLR}} \approx 0.023$ pc. The dashed lines indicate the case where $\langle \sigma v \rangle / m_{\mathrm{DM}} = 10^{-28}$ cm^{3}s^{-1}/GeV while the solid line represents $\langle \sigma v \rangle / m_{\mathrm{DM}} = 0$.

In Fig. 5.3 we see the dark matter column density Σ_{DM} of the blazar TXS $0506 + 056$ for different values of $\langle \sigma v \rangle / m_{\mathrm{DM}}$ and R_{em}. We take the values of $M_{\mathrm{BH}} \approx 3 \cdot 10^8 M_\odot$, $t_{\mathrm{BH}} = 10^9$ yr with $\gamma = 1$, $r_0 = 10$ kpc and $\rho_0 \approx 7 \cdot 10^3$ GeV/cm^3. Now, we just have to integrate Eq. (5.12) to obtain the column density. We only want to consider the case of $\langle \sigma v \rangle / m_{\mathrm{DM}} = 0$ and $\langle \sigma v \rangle / m_{\mathrm{DM}} = 10^{-28}$ cm^{3}s^{-1}/GeV. For the TXS $0506 + 056$ the column density is given in Fig. 5.4 for three different cases of R_{em}. The closer the emission region of the neutrinos or photons is to the black hole, the higher is the column density. If the annihilation is sufficiently large, the dark matter density saturates. Hence, the column density is several orders of magnitude lower than without the annihilation. In the case of $R_{\mathrm{em}} = 10R_{\mathrm{BLR}}$ the column density is the same, regardless of the dark matter annihilation. This is due to effect that the dark matter spike for $\langle \sigma v \rangle / m_{\mathrm{DM}} = 10^{-28}$ saturates below $r \sim 10^{-1}$ pc. Thus, the annihilation does not influence the dark matter profile in this region (see Fig. 5.3).

If we now take the value of $\Sigma_{\mathrm{DM}} \sim 10^{28}$ GeV/cm^2 and require the attenuation coefficient to be at order one, we obtain that

$$\frac{\sigma_{\mathrm{DM\text{-}i}}}{m_{\mathrm{DM}}} \approx 10^{-28} \mathrm{cm}^2/\mathrm{GeV}. \tag{5.23}$$

This result is within the range of for high energy neutrinos that one expects to be emitted from blazars. Furthermore, we are able to constrain the dark matter-neutrino scattering cross section with dark matter spikes.

The best current results come from the blazar TXS $0506 + 056$ and the active galacxy NGC 1068 [3, 4]. For a non self-annihilation dark matter particle the upper limits are $\frac{\sigma_{\mathrm{DM\text{-}\nu}}}{m_{\mathrm{DM}}} \leq 2.0 \cdot 10^{-29}$ cm^2/GeV and $\frac{\sigma_{\mathrm{DM\text{-}\gamma}}}{m_{\mathrm{DM}}} \leq 4.1 \cdot 10^{-29}$ cm^2/GeV [3]. When the annihilation cross section increases, the limits become weaker. Hence, we do not stay in conflict with the current limits.

In summary, we have seen that in the vicinity of a black hole the dark matter density can be larger than in the rest of the galaxy. The dark matter forms a dense spike around the black hole. Further, we noticed that if particles like photons or neutrinos are emitted inside the spike their flux gets attenuated due to their interaction with the dark matter particles. The attenuation depends on the column density of the dark matter spike and the scattering cross section between the photons or neutrinos and the dark matter. One one side, the column density mainly depends on observable astrophysical quantities. On the other side, the cross section can be obtained by using standard tools of quantum field theory. One just has to chose a specific model as an extension of the standard model. With that model one is able to calculate the scattering cross section and can further estimate the impact on the absorption. This motivates us to chose a specific dark matter model in the next section and to calculate the rate of attenuation. The goal is to find a model with a high enough scattering cross section in order to obtain a large attenuation.

Chapter 6

Dark Matter Phenomenology

So far, we have reviewed the formation of a dark matter spike around a black hole that can deplete the flux of neutrinos or photons. The photons or neutrinos are emitted by the AGN and have to traverse the dense dark matter spike. Along their way to the earth they interact with the dark matter inside the spike. We have seen that the attenuation is highly model depndend, due to the cross section. We now want to make specific choices for the dark matter model to calculate concretely the scattering rate between neutrinos and photons. Hereby, we will use the techniques of quantum field theory that we have developed in ch. 4.

6.1   A simple Toy Model

Let us start our investigations with a very simple toy model that only contains a scalar dark matter particle η and a fermion χ that mediates the interaction between the dark matter particle and the neutrino. Thus, the interaction Lagrangian reads [96]:

$$\mathcal{L}_{\text{int}} = -y\eta\overline{\chi}\nu_L + \text{h.c.}, \tag{6.1}$$

where y is the Yukawa coupling between the dark matter, the fermion and the left handed neutrino. We assume the fermion to be a Majorana fermion. Note that $\nu_L = P_L\nu$, where $P_L = (1-\gamma^5)/2$ is the chirality operator. Our goal is to show that this simple model can lead to a significant absorption rate. Later, in a further step, we will put this simple toy model in a more robust theoretical framework.

The interaction $\eta\nu \to \eta\nu$ between the dark matter particle η and the neutrino result in the two Feynman diagrams shown in Fig. 6.1. We demand that $m_\chi > m_\eta$ to avoid that the dark matter decays into the mediator, due to kinematics. Note that we will later impose a Z_2 symmetry on the non standard model particles to avoid the decay of the dark matter. We assume the neutrino to be a standard model neutrino that is massless. It also makes the computation easier.

The two diagrams of the elastic scattering between η and the neutrino result in the following amplitude:

$$iT = \bar{u}(p',s')P_R\left[(iy)^2\frac{i(\not{p}+\not{k}+m_\chi)}{(p+k)^2-m_\chi^2+i\epsilon} + (iy)^2\frac{i(\not{p}-\not{k}'+m_\chi)}{(p-k')^2-m_\chi^2+i\epsilon}\right]P_Lu(p,s), \tag{6.2}$$

where $u(p,s)$ is the spinor of the neutrino with four momentum p and spin s. We adopted the Feynman slash notation where $\not{p} = \gamma_\mu p^\mu$. In the interaction we have a
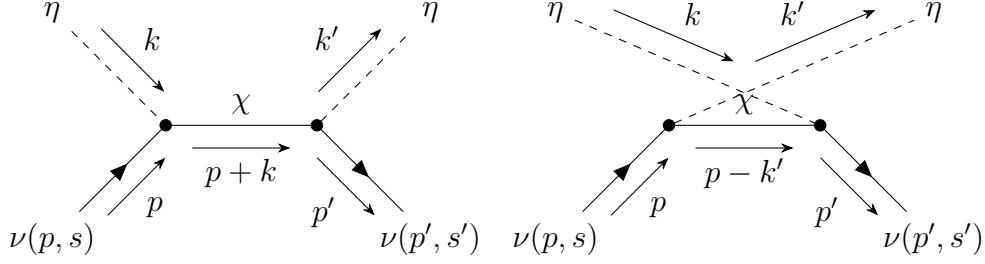
Figure 6.1: Feynman diagram of the $\nu\eta \to \nu\eta$ scattering in the s and u channel. The amplitude is given by Eq. (6.2). The time axis is the x-axis. To avoid the decay of $\eta \to \nu\chi$, we assume that the mediator mass $m_\chi > m_\eta$. So the decay of the dark matter particle is not allowed by kinematics.

$s-$channel and a $u-$channel that cause some interference. We quickly recapitulate the formula for a two body scattering cross section for a process $p + k \to p' + k'$:

$$\mathrm{d}\sigma = \frac{1}{4E_{\vec{p}}E_{\vec{k}}|\vec{v}_p - \vec{v}_k|} \frac{\mathrm{d}^3 p'}{(2\pi)^3 2E_{\vec{p'}}} \frac{\mathrm{d}^3 k'}{(2\pi)^3 2E_{\vec{k'}}} (2\pi)^4 \delta^{(4)}(p + k - p' - k')\overline{|T|^2}. \quad (6.3)$$

To continue with the computation we have to fix the kinematics for our process. We consider the neutrino to be emitted close to the black hole and that it has to travel through the dark matter spike. Hence, the dark matter particle will be at rest. So, we will calculate the cross section in the frame where η is at rest. Thus, the scattering can be sketched as follows:
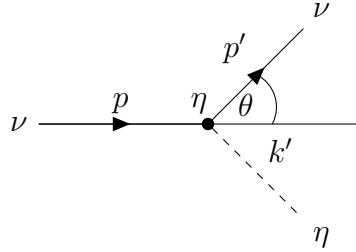
Figure 6.2: Sketch of the elastic scattering of $\nu\eta \to \nu\eta$ in the rest frame of the dark matter particle η, where θ is the scattering angle.

Here θ is the scattering angle between the incoming and the outgoing neutrino. Note that we have neglected the subscripts ν and η for the energies to make the formulas look more appealing. Our case is quite similar to the Compton scattering scenario, where a photon scatters off an electron. With the scattering angle and the conservation of energy and momentum the four momenta in the rest frame of the dark matter particle read

$$p = \begin{pmatrix} E \\ 0 \\ 0 \\ E \end{pmatrix}, \; k = \begin{pmatrix} m_\eta \\ 0 \\ 0 \\ 0 \end{pmatrix}, \; p' = \begin{pmatrix} E' \\ E'\sin\theta \\ 0 \\ E'\cos\theta \end{pmatrix}, \; k' = \begin{pmatrix} m_\eta + E - E' \\ -E'\sin\theta \\ 0 \\ E - E'\cos\theta \end{pmatrix},$$

where E is the energy of the incoming neutrino and E' the energy of the scattered neutrino. For the elastic scattering we can use the conservation laws to express the

energy E' in terms of the scattering angle θ and the incoming energy E by

$$E' = \frac{E}{1 + \frac{E}{m_\eta}(1 - \cos\theta)}. \tag{6.4}$$

Now, we have to calculate the matrix element. Therefore have to compute $|T|^2 = T^* \cdot T$ and then take the spin average of that expression. In the following we will explicitly calculate the matrix element. But, later, we will make use of Mathematica to do the job for us. Nevertheless, it is good to do it once on our own to have insides about what the program is actually doing. So, let us start.

We can express Eq. (6.2) as follows:

$$iT = i(iy)^2 \overline{u}_\alpha(p', s') M_{\alpha\beta} u_\beta(p, s), \tag{6.5}$$

where we have defined

$$M_{\alpha\beta} \equiv P_R \left[\frac{(\not{p} + \not{k} + m_\chi)}{(p+k)^2 - m_\chi^2 + i\epsilon} + \frac{(\not{p} - \not{k}' + m_\chi)}{(p-k')^2 - m_\chi^2 + i\epsilon} \right] P_L. \tag{6.6}$$

When taking the complex amplitude we are generally dealing with terms of $(\overline{u}(p', s')\gamma^{\mu_1} \cdot ... \cdot \gamma^{\mu_n} u(p, s))^*$. We remember that $\overline{u}(p', s') = u^\dagger(p', s')\gamma^0$. Furthermore, we know that $(AB)^\dagger = B^\dagger A^\dagger$, $\gamma^0(\gamma^\mu)^\dagger\gamma^0 = \gamma^\mu$ and $(\gamma^0)^\dagger = \gamma^0$. With these relations we get

$$
\begin{aligned}
&(\overline{u}(p', s')\gamma^{\mu_1} \cdot ... \cdot \gamma^{\mu_n} u(p, s))^* \\
&= u^\dagger(p', s')\gamma^0\gamma^{\mu_1} \cdot ... \cdot \gamma^{\mu_n} u(p, s))^\dagger \\
&= u^\dagger(p, s)(\gamma^{\mu_n})^\dagger \cdot ... \cdot (\gamma^{\mu_1})^\dagger\gamma^0 u(p', s') \\
&= u^\dagger(p, s)\gamma^0\gamma^0(\gamma^{\mu_n})^\dagger\gamma^0\gamma^0 \cdot ... \cdot \gamma^0\gamma^0(\gamma^{\mu_1})^\dagger\gamma^0 u(p', s') \\
&= \overline{u}(p, s)\gamma^{\mu_n} \cdot ... \cdot \gamma^{\mu_1} u(p', s'),
\end{aligned}
\tag{6.7}
$$

where we have uses that $(\gamma^0)^2 = \mathbb{1}$. We can use this expression to simplify

$$
\begin{aligned}
|T|^2 &= y^4 \left[\overline{u}(p', s') M u(p, s) \right] \left[\overline{u}(p, s)\overline{M} u(p', s') \right] \\
&= y^4 \left[u(p, s)\overline{u}(p, s) \right]_{\alpha\beta} \overline{M}_{\beta\gamma} \left[u(p', s')\overline{u}(p', s') \right]_{\gamma\delta} M_{\delta\alpha}.
\end{aligned}
\tag{6.8}
$$

The completeness relation states the standard formula for spin sums as

$$\sum_s = u(p, s)\overline{u}(p, s) = \not{p} + m. \tag{6.9}$$

For our case the photons is massless. Thus, $m = m_\nu = 0$. So, by taking the spin average of the matrix element we can apply the completeness relation for s and s'. Further, we can make use of the trace such that the matrix element reduces to

$$\overline{|T^2|} = \frac{1}{2}y^4 \text{tr}\left(\not{p}\overline{M}\not{p}'M\right). \tag{6.10}$$

The next step is to use the properties of the Dirac matrices. The well known relations yield $\{\gamma^\mu, \gamma^\nu\} = 2\eta^{\mu\nu}\mathbb{1}$ and $\{\gamma^\mu, \gamma^5\} = 0$, where $\eta_{\mu\nu}$ is the Minkowski tensor. With

these relations the gamma properties read

$$\text{tr}(\gamma^\mu) = 0 \tag{6.11}$$

$$\text{tr}(\gamma^\mu \gamma^\nu) = 4\eta\mu\nu \tag{6.12}$$

$$\text{tr}(\# \text{ odd } \gamma^\mu) = 0 \tag{6.13}$$

$$\text{tr}(\gamma^\mu \gamma^\nu \gamma^\rho \gamma^\sigma) = 4(\eta^{\mu\nu}\eta^{\rho\sigma} - \eta^{\mu\rho}\eta^{\nu\sigma} + \eta^{\mu\sigma}\eta^{\nu\rho}) \tag{6.14}$$

$$\text{tr}(\gamma^\mu \gamma^\nu \gamma^\rho \gamma^\sigma \gamma^5) = -4i\epsilon^{\mu\nu\rho\sigma}, \tag{6.15}$$

where $\epsilon^{\mu\nu\rho\sigma}$ is the Levi-Civita symbol which is zero for odd permutations, one for even permutations and zero otherwise. By using these relation we can simplify the expression for the matrix element. We encounter a lot of scalar products between the different four momenta. The expression is long and is not a feast for the eyes, so we will not explicitly write it here. But we can give the final expression in terms of the Lorentz-invariant Mandelstam variables which are

$$s = (p + k)^2 = (p' + k')^2$$
$$t = (p - p')^2 = (k - k')^2$$
$$u = (p - k')^2 = (k - p')^2.$$

They also sort of define our interaction to be called s and u channel. Together with the Mandelstam variables and the Dirac traces the matrix element reduces to

$$\overline{|T|^2} = \frac{y^4}{2}\left[\frac{-(s - m_\eta^2)(u - m_\eta^2) + m_\eta^2 t}{(s - m_\chi^2)^2} + \frac{-(s - m_\eta^2)(u - m_\eta^2) + m_\eta^2 t}{(u - m_\chi^2)^2} - \frac{(s - m_\eta^2)^2 + (u - m_\eta^2)^2 - t(2m_\eta^2 - t)}{(s - m_\chi^2)(u - m_\chi^2)} \right]. \tag{6.16}$$

The Mandelstam variables full-fill the following relation: $s + t + u = 2m_\eta^2$. Using this properties we can simplify Eq. (6.16) to

$$\overline{|T|^2} = \frac{y^4}{2}\left[\frac{(s - u)^2(m_\eta^4 - su)}{(s - m_\chi^2)^2(u - m_\chi^2)^2} \right]. \tag{6.17}$$

We can massage this term further by using the four momenta in the rest frame of the dark matter particle given by $s = m_\eta^2 + 2m_\eta E$ and $u = m_\eta^2 - 2m_\eta E'$. Hence, we get

$$\overline{|T|^2} = \frac{y^4}{2} \frac{8m_\eta^4 EE'(1 + \cos\theta)(E + E')^2}{(s - m_\chi^2)^2(u - m_\chi^2)^2}. \tag{6.18}$$

So, we have calculated the matrix element. The last thing that we have to do, is to compute the phase space factor.

In Eq. (6.3) the velocity of the dark matter particle $\vec{v}_k = 0$ and the velocity of the neutrino $\vec{v}_p = c = 1$ because we are working with neutral units. We also notice that $E_{\vec{p}} = E$, $E_{\vec{k}} = m_\eta$ and $E_{\vec{p'}} = E'$. Therefore, we can write Eq. (6.3) of the cross section as

$$d\sigma = \frac{1}{4Em_\eta} \frac{d^3 p'}{(2\pi)^3 2E'} \frac{d^3 k'}{(2\pi)^3 2E_{\vec{k'}}} (2\pi)^4 \delta^{(4)}(p + k - p' - k')\overline{|T|^2} \tag{6.19}$$

We further have to integrate out the delta function. We can decompose the four dimensional delta function $\delta^{(4)}(p+k-p'-k') = \delta^{(3)}(\vec{p}-\vec{p'}-\vec{k'})\delta(E+m_\eta-E'-E_{\vec{k'}})$. The delta function of the spatial momentum gives the relation that $\vec{k'} = \vec{p}-\vec{p'}$. Thus, the energy of $E_{\vec{k'}} = \sqrt{\vec{k'}^2 + m_\eta^2} = \sqrt{(\vec{p}-\vec{p'})^2 + m_\eta^2} = \sqrt{\vec{p}^2 + \vec{p'}^2 - (\vec{p}\cdot\vec{p'}) + m_\eta^2}$. We have elastic scattering and the mass of the η particle does not change. So, $m'_\eta = m_\eta$. Hence, we can write the delta function of the energy as

$$\delta(E + m_\eta - E' - E_{\vec{k'}}) = \delta(E + m_\eta - E' - \sqrt{m_\eta^2 + E'^2 + E^2 - 2EE'\cos\theta}). \quad (6.20)$$

In order to take the integral over the delta function we can decompose $\mathrm{d}^3p' = \mathrm{d}\phi\,\mathrm{d}\cos\theta\,\mathrm{d}E'E'^2$ because $p^2\mathrm{d}p = E^2\mathrm{d}E$ through the energy-momentum relation. Thus, the cross section reduces to

$$\mathrm{d}\sigma = \frac{2\pi}{4Em_\eta}\frac{\mathrm{d}\cos\theta}{(2\pi)^3 2E'}\frac{\mathrm{d}E'E'^2}{(2\pi)^3 2E_{\vec{p}-\vec{p'}}}$$
$$\cdot (2\pi)^4 \delta(E + m_\eta - E' - \sqrt{m_\eta^2 + E'^2 + E^2 - 2EE'\cos\theta})\overline{|T|^2}_{\vec{k'}=\vec{p}-\vec{p'}}, \quad (6.21)$$

where the 2π comes from the integration over $\mathrm{d}\phi$ and $E_{\vec{k'}} = E_{\vec{p}-\vec{p'}}$. We have to deal with a function inside the delta distribution. Therefore, one can use the following relation for a function $g(x)$ and its derivative with poles x_i:

$$\delta(g(x)) = \sum_{i=1}^n \frac{\delta(x-x_i)}{|\frac{\mathrm{d}g}{\mathrm{d}x}|_{x=x_i}|}. \quad (6.22)$$

Thus, we need to find the poles of $f(E') = E + m_\eta - E' - \sqrt{m_\eta^2 + E'^2 + E^2 - 2EE'\cos\theta}$. The root E'_0 of $f(E')$ is exactly the expression of Eq. 6.4 that one can find with the help of the energy and momentum conservation. This makes sense because the delta function is the object that guarantees the conservation of energy and momentum. So, we have the proof that we used E' correctly so far. The derivative evaluated at the pole E'_0 gives

$$\frac{\mathrm{d}f}{\mathrm{d}E'}\Big|_{E'_0=E'} = 1 + \frac{E' - E\cos\theta}{E_{\vec{p}-\vec{p'}}}, \quad (6.23)$$

where we used that $E_{\vec{p}-\vec{p'}} = \sqrt{m_\eta^2 + E'^2 + E^2 - 2E'E\cos\theta}$. Note that we basically would have an overall minus sign in the expression of the derivative. But we neglected it because we have to take the absolute value of the derivative.

Hence, we can now simplify our cross section by the expression of the delta function of the energy and obtain

$$\mathrm{d}\sigma = \frac{\mathrm{d}\cos\theta}{32\pi Em_\eta}\frac{\mathrm{d}E'E'}{E_{\vec{p}-\vec{p'}}}\frac{\delta(E'-E'_0)}{|1 + \frac{E'-E\cos\theta}{E_{\vec{p}-\vec{p'}}}|}\overline{|T|^2}|_{\vec{k'}=\vec{p}-\vec{p'}}. \quad (6.24)$$

With the conservation of energy we can use that $E_{\vec{p}-\vec{p'}} = m_\eta + E - E'$. The integration over $\mathrm{d}E'$ just yields unity because $E'_0 = E'$. We will leave out now the concrete evaluation of the matrix element because it is obvious that we have energy and momentum conservation for the matrix element. Thus, the cross section reads

$$\mathrm{d}\sigma = \frac{\mathrm{d}\cos\theta}{32\pi Em_\eta}\frac{E'}{m_\eta + E - E\cos\theta}\overline{|T|^2}. \quad (6.25)$$

We can further simplify this expression by using Eq. 6.4. By rearranging the formula we finally get

$$\frac{\mathrm{d}\sigma}{\mathrm{d}\cos\theta} = \frac{1}{32\pi m_\eta^2}\frac{E'^2}{E^2}\overline{|T|^2}. \tag{6.26}$$

Thus, we obtained a formula for the cross section that only depends on the initial energy E and the scattering angle θ. The dimension of the cross section is GeV^{-2} which is correct in natural units and can be transferred into cm^2. This is a standard formula which is known for the Compton scattering. Note, that this formula is only true for elastic scattering. We will later use a different formula for the inelastic scattering. Together with our expression for the matrix element in Eq. (6.18) we obtain

$$
\begin{aligned}
\frac{\mathrm{d}\sigma}{\mathrm{d}\cos\theta} &= \frac{y^4}{8\pi m_\eta^2}\frac{E'^2}{E^2}\frac{m_\eta^4 EE'(1+\cos\theta)(E+E')^2}{(s-m_\chi^2)^2(u-m_\chi^2)^2} \\
&= \frac{y^4 m_\eta^2}{8\pi}\frac{E'^2}{E^2}\frac{EE'(1+\cos\theta)(E+E')^2}{(m_\eta^2+2Em_\eta-m_\chi^2)^2(m_\eta^2-2E'm_\eta-m_\chi^2)^2},
\end{aligned}
\tag{6.27}
$$

where we have written in the second term the Mandelstam variables explicitly in the rest frame of the dark matter particle. The solution is in good agreement with [97]. For the total cross section we just have to integrate over the angle. This lengthy computation can be done with Mathematica. But for practical purpose we have mentioned it here to have at least one complete calculation of the cross section.

We have now an expression for the differential cross section. To obtain the total cross section of the elastic scattering between our dark matter particle η and the neutrino, we have to integrate over the angle θ. This can be done numerically by using Python and the libraries of NumPy and SciPy. For a given masses and energy one can integrate the equation.

If we now take a dark matter mass of $m_\eta = 1$ GeV and vary the mediator mass m_χ between 10 GeV and 1 TeV we can calculate the total cross section $\sigma_{\mathrm{DM}-\nu}$ for the neutrino energy E_ν. The result is shown in Fig. 6.3. The analysis is done by assuming that the coupling constant $y = 1$. First, we see that the cross section has three different regimes. It grows with E_ν^4 for $E_\nu \leq m_\eta$ and it scales with E_ν^3 for $m_\eta \leq E_\nu \leq (m_\chi^2 - m_\eta^2)/(2m_\eta)$. For $E_\nu \geq (m_\chi^2 - m_\eta^2)/(2m_\eta)$ the cross section decreases with E_ν^{-1}. Further, we denote that the cross section is smaller, the higher the dark matter mass in the low energy regime. Which makes sense because the cross section scales with m_χ^8 for low energies. We notice a peak in all of the three graphs. This happens when we hit the resonance. Hence, when $s = m_\eta^2 + 2m_\eta E_\nu = m_\chi$. This translates into $E_\nu = (m_\chi^2 - m_\eta^2)/(2m_\eta)$. The scaling behaviours are in good agreement with [97, 98].

We can obtain an analytical expressions for the large and low scale behaviours. The energy of the outgoing neutrino can be simplified under the conditions that $E_\nu \ll m_\eta$ and $E_\nu \gg m_\eta$. Further, we have to take into account that $m_\chi > m_\eta$. For low energies the $E'_\nu \to E_\nu$ and it follows for Eq. (6.27) that it reduces to

$$\frac{\mathrm{d}\sigma}{\mathrm{d}\cos\theta}\bigg|_{E\ll m_\eta} \approx \frac{y^4 E_\nu^4 m_\eta^2}{2\pi m_\chi^8}(1+\cos\theta). \tag{6.28}$$
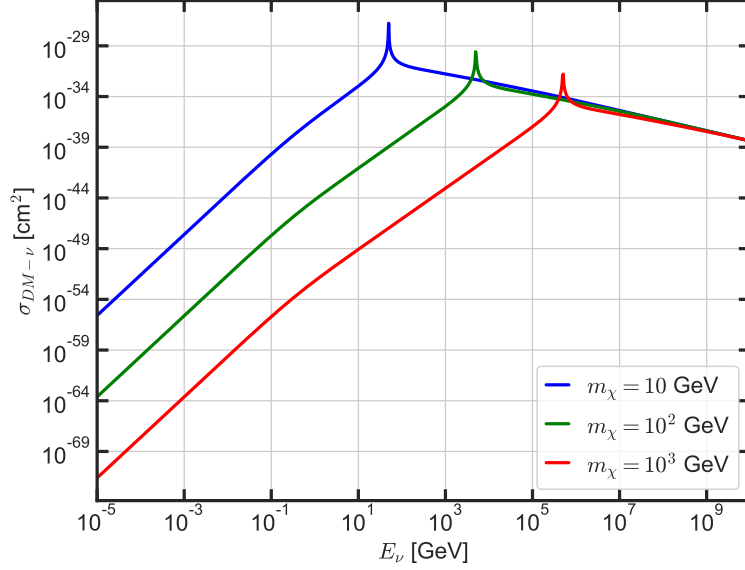
Figure 6.3: Total cross section of the dark matter neutrino scattering for different mediator masses m_χ and a dark matter mass of $m_\eta = 1$ GeV. The unit of the cross section is given by cm^2. The coupling constant was set to $y = 1$ for simplicity. We see the scaling behaviours of $\sigma \sim E_\nu^4$ for $E_\nu \leq m_\eta$, $\sigma \sim E_\nu^3$ for $m_\eta \leq E_\nu \leq (m_\chi^2 - m_\eta^2)/(2m_\eta)$ and $\sigma \sim E_\nu^{-1}$ for $E_\nu \geq (m_\chi^2 - m_\eta^2)/(2m_\eta)$ which is consistent with [97] and [98].

We can easily integrate over $\mathrm{d}\cos\theta$ from -1 to 1 and obtain

$$\sigma\big|_{E_\nu \ll m_\eta} \gtrsim \frac{y^4 E_\nu^4 m_\eta^2}{\pi m_\chi^8}. \tag{6.29}$$

For large energies the cross section is approximately given by

$$\sigma\big|_{E_\nu \gg m_\eta} \gtrsim \frac{y^4}{16\pi E_\nu m_\eta}. \tag{6.30}$$

One can see that the cross section is independent of the mediator mass in the large energy regime. Note that in more realistic scenarios we have to take lower values for the coupling constant which would decrease the cross section.

In this simple model the energy of the cross section grows until the resonance and then decreases. Now, we want to investigate the impact of absorption and the attenuation of the neutrino flux, due to their interaction with the dark matter particles. We remember that we need two quantities that measure the flux attenuation. First, the scattering cross section σ and second, the column density Σ_{DM} of the dark matter particles. In our simple toy model we only have scattering between the neutrinos and the dark matter particle η. We only have elastic scattering. So, all we need is to make an assumption for the column density. Furthermore, we assume that the neutrinos are emitted close to the black hole and have to travel through the dark matter spike that surrounds the black hole.

Let us check two different scenarios for the dark matter spike. The first one, where the dark matter does not annihilate with each other. In order words, the case of antisymmetric dark matter. For the second scenario, we assume that the dark

matter annihilation cross section is roughly given by $\langle\sigma v\rangle = 10^{-28}$ cm³s⁻¹. We take the dark matter column density that is shown in Fig. 5.4 and realised for the blazar TXS 0506 + 056 [3]. So, we use Eq. (5.20) for $\gamma = 1$ and $\gamma_{\mathrm{sp}} = 7/3$. Furthermore, $M_{\mathrm{BH}} \approx 3 \cdot 10^8 M_{\odot}$, $t_{\mathrm{BH}} = 10^9$ yr, $r_0 = 10$ kpc and $\rho_0 \approx 7 \cdot 10^3$ GeV/cm³. The only quantity which is left to define is the point of neutrino emission R_{em}. We take two different emission regions: One close to BLR, namely $R_{\mathrm{em}} = 0.1 R_{\mathrm{BLR}}$ and the other one $R_{\mathrm{em}} = R_{\mathrm{BLR}}$. The flux of the neutrinos get reduced by (see ch. 5.4):

$$\frac{\Phi_{\nu}^{\mathrm{obs}}}{\Phi_{\nu}^{\mathrm{em}}} = e^{-\mu_{\nu}} = e^{-\frac{\sigma_{\mathrm{DM}\text{-}\nu}\Sigma_{\mathrm{DM}}}{m_{\mathrm{DM}}}}. \tag{6.31}$$

We are able to use this formula because for energies larger than the dark matter mass the outgoing energy of the neutrino becomes nearly constant. Hence, we can drop the second term in the cascade equation because the cross section is independent of the outgoing neutrino energy E_{ν}'. However, for energies lower than the dark matter mass this approximation does not hold. Nevertheless, we stick do this formula for simplicity and because the goal of this simple toy model is to illustrate and motivate the calculations in the following sections. If one wants to be more precise, one needs to solve the full cascade equation given by Eq. 5.13. This can be done in a future work.

So, we choose the mass of our dark matter particle to be $m_{\mathrm{DM}} = m_{\eta}$ and vary the dark matter mass as well as the mediator mass. The result is shown in Fig. 6.4. We can see four different values of the observed neutrino flux normalised to the emitted neutrino flux. The neutrino energy is given in GeV. We see that for the case of $m_{\eta} = 1$ GeV and $m_{\chi} = 10$ GeV we obtain an sizable absorption around $E_{\nu} \sim 50$ GeV. This is roughly the resonance energy when $E_{\nu} = (m_{\chi}^2 - m_{\eta}^2)/(2m_{\eta})$. It makes sense that we have absorption around the resonance energy because the energy basically goes to infinity. Nevertheless, in the case of $\langle\sigma v\rangle = 0$ and $R_{\mathrm{em}} = 0.1 R_{\mathrm{BLR}}$ the flux also gets attenuated close to the resonance and we can distinguish it from the three other cases in the above left panel. As the mediator mass increases, the cross section decreases because the cross sections depends on the mediator mass until the resonance peak. The cross section is not large enough such that we can distinguish between the four different scenarios anymore. We only have absorption precisely at the resonance peak because the peak narrows for larger mediator masses. Furthermore, as expected, the resonance peak shifts to higher energies for higher values of m_{η} and m_{χ}. In the bottom right panel of Fig. 6.4 the resonance peak does not lead to a large value of absorption. This is due to numerical reasons because we can not chose a small enough difference between the energy points for our integration. Basically, if we just resolve around the peak with a small enough energy spacing we would also have a larger absorption rate. Note that we have uncertainties in the column density of the dark matter spike.

To sum up, we have seen that the cross section for a dark matter mass larger than 1 GeV is too small in order to lead to a reasonable absorption of the neutrino flux. The only exception is the resonance peak but. Thus, we have checked that it is possible to have some kind of reduction of the neutrino flux, due to the interaction between neutrinos and dark matter. But this model is far from being realistic. So, the next step will be to introduce some more realistic models with a concrete parameter space for dark matter and mediator masses.
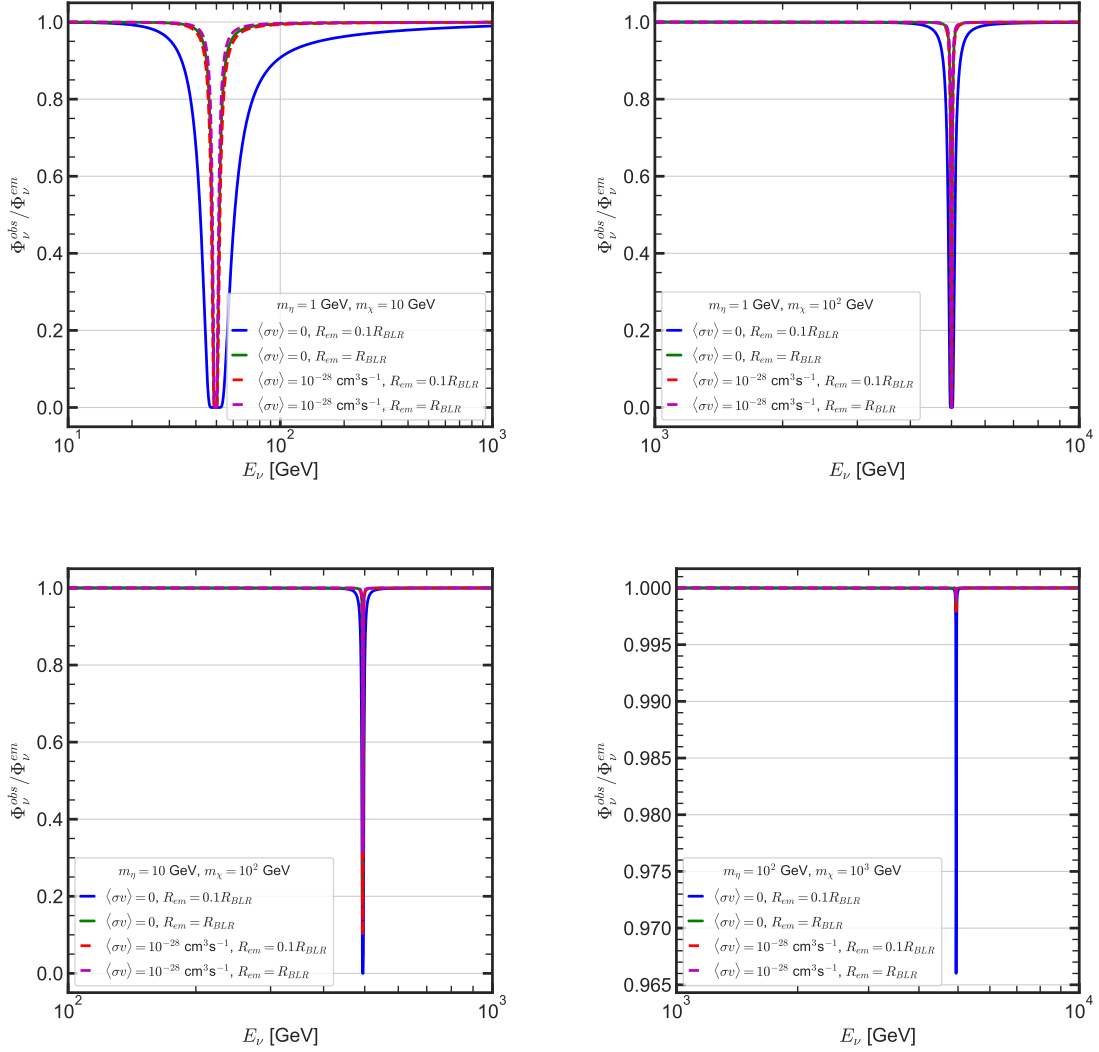
Figure 6.4: The figures show the neutrino flux attenuation of Eq. (6.31), due to the dark matter neutrino interaction given by the Lagrangian of Eq. (6.1) for four different cases. The case for the annihilation cross section $\langle \sigma v \rangle = 0$ and $R_{\mathrm{em}} = 0.1 R_{\mathrm{BLR}}$ or $R_{\mathrm{em}} = R_{\mathrm{BLR}}$ and the other case for $\langle \sigma v \rangle = 10^{-28} \mathrm{cm}^3 \mathrm{s}^{-1}$. All of the figures are for different combinations of the dark matter masses m_η and the mediator masses m_χ. For dark matter masses above the order of TeV the column density is very small. Hence, we see no decrease of the flux, expect at the resonance peak. The heavier the dark matter particle, the less particles are on the way of the neutrino to the earth because the density profile $\rho(r)$ stays the same. Hence, the column density Σ decreases because it is divided by m_{DM}. In this case it is logical that the interaction between the dark matter particle and the neutrino decreases because we have less dark matter particles between the blazar and the earth.

6.2 The t-channel Mediator Model

We want to use the dark matter spike in the vicinity of black holes to probe concrete dark matter models. In this thesis we will focus on the t-channel mediator model described in [99]. It is a simple model where the SM is extended by one colourless and electrically neutral Majorana fermion χ and a complex scalar η. The

scalar particle mediates a Yukawa interaction between the SM fermions f and the Majorana fermion χ. Therefore the general Lagrangian is given by

$$\mathcal{L} = \mathcal{L}_{\text{SM}} + \mathcal{L}_\eta + \mathcal{L}_\chi + \mathcal{L}_{\text{int}}, \tag{6.32}$$

where $\mathcal{L}_{\text{SM}}$ is the Lagrangian of the Standard Model with the Higgs doublet Φ. $\mathcal{L}_\eta$ and $\mathcal{L}_\chi$ are the Lagrangian which contain the part of the scalar particle η and χ. The Lagrangians read

$$
\begin{aligned}
\mathcal{L}_\chi &= \frac{1}{2}\overline{\chi}^c \slashed{\partial}\chi - \frac{1}{2}m_\chi \overline{\chi}^c \chi \\
\mathcal{L}_\eta &= (D_\mu \eta)^\dagger (D^\mu \eta) - m_\eta^2 \eta^\dagger \eta - \frac{1}{2}\lambda_2 (\eta^\dagger \eta)^2,
\end{aligned}
\tag{6.33}
$$

where D_μ is the covariant derivative. $\mathcal{L}_{\text{int}}$ denotes the interaction term that we can divide into the scalar interaction part $\mathcal{L}_{\text{int}}^{\text{sclar}}$ and the fermionic part of the interaction $\mathcal{L}_{\text{int}}^{\text{fermion}}$. Both of them describe the interaction of the new particles η and χ with the SM fermions and the Higgs doublet. We further impose a Z_2 symmetry under which the new particles η and χ are odd, while the SM particles are even. This ad hoc introduced discrete symmetry ensures the stability of our dark matter particle. In addition, we impose that χ and η only couple to one generation of fermions for simplicity. We will later see, why this is important. Normally, χ is to be considered as the dark matter candidate and η as the mediator. But we will later also treat η as DM candidate.

We do not want that the Majorana fermion interacts with the weak gauge bosons W^+, W^- and Z at tree level. Hence, we only treat χ as a $SU(2)_L$ singlet. To have an electrically neutral particle the hypercharge of χ has to be zero. Now, if we consider χ to be the dark matter, there exists two options for the mediator particle η. First, it can be a singlet under $SU(2)_L$ with hypercharge Y such that the particle χ couples to a right-handed lepton f_R Yukawa coupling y as follows:

$$\mathcal{L}_{\text{int}}^{\text{fermion}} = -y\overline{\chi} f_R \eta + \text{h.c.}. \tag{6.34}$$

This possibility is realised in the MSSM, when η is the selectron $\tilde{e}$ so that

$$\mathcal{L}_{\text{int}}^{\text{fermion}} = -y\overline{\chi} e_R^- \tilde{e}_R^+ + \text{h.c.}. \tag{6.35}$$

The second option is that η is a doublet under $SU(2)_L$ with hypercharge Y. Then, the Majorana fermion χ only couples to left-handed fermions f_L given by

$$\mathcal{L}_{\text{int}}^{\text{fermion}} = -y\overline{\chi} f_L i\sigma_2 \eta + \text{h.c.}, \tag{6.36}$$

where σ_2 is the Pauli matrix. We can decompose the $SU(2)_L$ doublet η in $\eta = (\eta^+, \eta^0 + iA^0)$ with η^+ being the charged and $\eta^0 + iA^0$ the neutral component. Here η^0 is a scalar and A^0 a pseudosclar. For the case of scalar dark matter η we take the lightest particle of the $SU(2)_L$ doublet to be the dark matter. Hence, if $f_L = (\nu, e^-)_L$ the interaction term reduces to

$$\mathcal{L}_{\text{int}}^{\text{fermion}} = -y(\overline{\chi}\nu_L \eta^0 + i\overline{\chi}\nu_L A^0 - \overline{\chi}e_L^- \eta^+) + \text{h.c.}. \tag{6.37}$$

This scenario is well known as the Inert Doublet model [100, 101]. In the MSSM this possibility is realised if η is a sfermion multiplet with an sneutrino, selectron and χ

being the bino. In this case η^0 can also be considered as a dark matter candidate. There also exist interactions between the scalar particle η and the Higgs doublet Φ. But we will neglect them, since we assume them not to contribute in the dark matter scattering. So, generally speaking we assume that the couplings $|\lambda_i| \ll 1$, such that the Majorana fermion mass m_χ, the scalar mass m_η and the Yuwaka coupling y are the relevant parameters of this model. By demanding that the dark matter abundance matches the observed dark matter density $\Omega_{\mathrm{DM}} = 0.120 \pm 0.001$, we can fix one remaining parameter in the model. Hence, the Yukawa coupling can be expressed in terms of the masses $y(m_\chi, m_\eta)$. This is shown in Fig. 6.5. Thus, we are only left with two open parameters of the model [99].
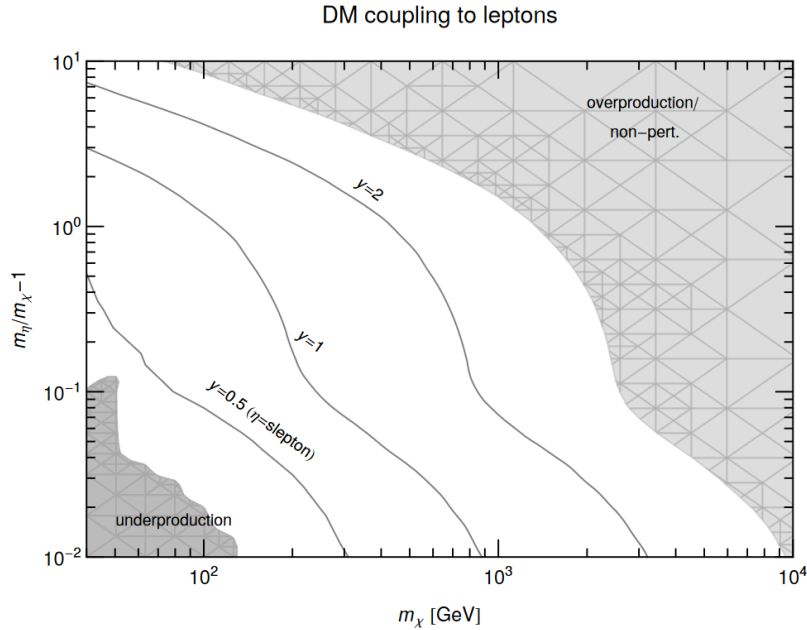
Figure 6.5: Parameter space for the Majorana fermion χ being the dark matter that couples to leptons. Here η is the mediator. The Yukawa couplings y are shown as contour lines requiring that dark matter density is $\Omega_{\mathrm{DM}} = 0.1198 \pm 0.0015$[1]. The dark matter is produced in the early universe via thermal freeze-out. The upper right regions lead to overproduction of the dark matter density, while the lower left region leads to underproduction. Figure is taken from [99].

6.2.1 Coannihilation in the t-channel Mediator Model

The t-channel mediator model is a perfect example for coannihilation. As we have seen in previous sections is the main mechanism to produce the correct dark matter abundance is the freeze-out mechanism in the early universe (see ch. 3). One exception to the standard scenario is, when the dark matter mass is close to the mass of another particle in the dark sector. This scenario can be achieved in the t-channel mediator model, if for example $m_\eta/m\chi \lesssim 1.2$ [99].

---

[1]Note that the dark matter density in [99] is from the year 2015. There exists newer results of the Planck collaboration [22] from 2018 where $\Omega_{\mathrm{DM}} = 0.120 \pm 0.001$ which is in good agreement with the value used in [99].

Let us simply assume that the lightest particle is the χ particle in the t-channel mediator model and that the mass of the mediator particle m_η is bigger than m_χ. Both, the χ and η particle live in the dark sector. We further assume that η is a singlet and interacts with χ through the following vertex:
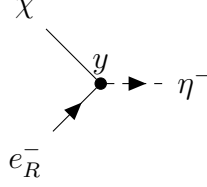
In the following discussion we will not write explicitly the electron as the right handed one. The t-channel model has an ad hoc introduced Z_2 symmetry under which the SM model particles are even and the dark sector particles η and χ are odd. Therefore, the remaining reactions relevant in the early universe are

The interactions are the annihilation of $\chi\chi \to e_R^+ e_R^-$, the inelastic scattering $\chi\eta^- \to e_R^-\gamma$ and the annihilation of $\eta\eta \to \gamma\gamma$. In the region of coannihilation we have to use the effective thermal avveraged cross section which is given by

$$\langle \sigma_{\text{eff}} v \rangle = \langle \sigma v_{\chi\chi} \rangle \left(\frac{n_\chi^{\text{eq}}}{n^{\text{eq}}} \right)^2 + \langle \sigma v_{\chi\eta} \rangle \left(\frac{n_\chi^{\text{eq}} n_\eta^{\text{eq}}}{(n^{\text{eq}})^2} \right) + \langle \sigma v_{\eta\eta} \rangle \left(\frac{n_\eta^{\text{eq}}}{n^{\text{eq}}} \right)^2, \tag{6.38}$$

where $n^{\text{eq}} = n_\chi^{\text{eq}} + n_\eta^{\text{eq}} = n_\chi^{\text{eq}}(1 + R)$ with $R \sim \exp(-(m_\eta - m_\chi)/T)$. Thus, we can reduce the equation by using the cross section from the annihilation and scattering to obtain [99, 102]

$$\langle \sigma_{\text{eff}} v \rangle \approx \frac{y^4 \langle C_{\chi\chi} \rangle + y^2 e^2 \langle C_{\chi\eta} \rangle R + e^4 \langle C_{\eta\eta} \rangle R^2}{m_\chi^2}. \tag{6.39}$$

Since, we know that the dark matter abundance is inversely proportional to the effective averaged thermal cross section we get that

$$\Omega_\chi h^2 \sim \frac{m_\chi^2}{y^4 \langle C_{\chi\chi} \rangle + y^2 e^2 \langle C_{\chi\eta} \rangle R + e^4 \langle C_{\eta\eta} \rangle R^2} \tag{6.40}$$

We can think about the coannihilation as buckets. We have a bucket full of dark matter particles χ. This bucket has only one tube to the standard model, namely over the annihilation channel into two electron pairs. If we only had this one opening, the bucket would empty too slowly and we would have a dark matter abundance that is to high. But in the coannihilation regime we also have a tube that goes from the χ bucket to the bucket filled with standard model particles over the η bucket via the inelastic scattering process of $\chi\nu \to e\gamma$. With this pipeline we can deplete the dark matter abundance sufficiently to obtain the correct dark matter abundance. In a very extreme case where $m_\eta/m_\chi \approx 1.1$ the lower limit on the mass of dark matter is $m_\chi \geq 50$ GeV for the scenario of dark matter coupling to leptons [99].

6.3 The Scotogenic Model

A special class of the t-channel mediator model is the Scotogenic Model [103, 104]. The model extends the SM by an inner doublet η and a fermion singlet χ. The new particles are odd under an imposed Z_2 symmetry, while the SM remains even. But, the main difference to the t-channel mediator model is that in the Scotogenic Model we are dealing with different flavours. The dark matter particle does not couple only to one generation of fermions but to all three of them. Hence, the Lagrangian reads [103]

$$\mathcal{L} \supset -\frac{1}{2}M_i\overline{\chi_i^c}\chi_i - (y_{i\alpha}\overline{\chi_i}L_\alpha\eta + h.c.), \qquad (6.41)$$

where $L_\alpha = \begin{pmatrix} \nu_L \\ e_L \end{pmatrix}_\alpha$ denotes the SM doublet with the generations labelled by greek letters $\alpha = e, \mu, \tau$ and $y_{i\alpha}$ the coupling constant. We will only consider neutrinos in general and do not separate between the electron, muon and tau neutrino. Furhter, we will only consider Standard Model neutrinos without a mass and that are only left handed. So, we may write ν instead of ν_L in the lepton doublet L. Furthermore, we will work with Majorana spinors which full fill the charge conjugation condition $\psi_\chi^c = \psi_\chi$. We can write the interaction Lagrangian for the neutrinos as

$$\mathcal{L}_{\text{int}} = -y_{i\alpha}\overline{\chi_i}\nu_\alpha\eta + h.c., \qquad (6.42)$$

which looks quite similar to the interaction that we have looked at in our toy model. Actually, the Scotogenic Model motivated us to introduce the toy model in the first place.

Originally, the Scotogenic Model or Minimal Scotogenic Model (if we want to be more precise) was introduced to add mass to the neutrinos via radiative corrections. But is was soon realised that the model could also be used to tackle the dark matter problem [105, 106, 107].

In the Scotogenic we could assume that either the χ or the η can be the dark matter, depending on the mass hierarchy. But, in the Scotogenic Model we have to take into account that we have lepton number or Lepton Flavour Violation (LFV) processes $\mu \to e\gamma$ given by the following diagrams [108]:
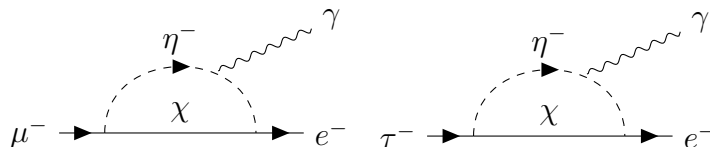
These processes limit our model. In the case of χ being the dark matter and $m_\chi < m_\eta$ we need large Yukawa couplings of $\mathcal{O}(1)$ to obtain the correct relic abundance of $\Omega h^2 \approx 0.12$. Because the only annihilation channel is $\chi\chi \to l_\alpha \bar{l}_\beta$ with l being a SM lepton. The annihilation cross section for WIMPs with mass m_{DM} scales as [39]

$$\sigma_{\mathrm{ann}} \propto \frac{y^4}{m_{\mathrm{DM}}} \qquad (6.43)$$

Hence, we need large Yukawa couplings to not overproduce the DM. But this will lead to conflicts with the LFV bounds [108]. In the case of η being the DM we do not stay in conflict with the LFV bounds. The η particle has additionally gauge and scalar interactions to deplete the relic abundance [108]. Thus, the dark matter candidate in the Scotogenic Model can only be the lightest neutral component of the η doublet.

However, this is only the case if we assume that the dark matter particle is a thermal relic. There are various ways to get out of this situation [109]. But, we will focus on dark matter particles as thermal relics and therefore χ is contrived as a DM candidate in the Scotogenic Model. So, we will only treat the case where the lightest CP even scalar η^0 is the dark matter candidate in the Scotogenic Model.

We want to mention one extension of the Scotogenic Model which is called the Scale Invariant Scotogenic Model [107, 110]. The Minimal Scotogenic Model has some disadvantages. The origin of the Z_2 symmetry is unclear and cumbersome. Further, we do not have fermions as DM candidate. It would be nice to solve this issues. In the Scale Invariant Scotogenic Model we replace the Lagrangian term $M_i \overline{\chi_i^c} \chi_i$ by $\lambda_i \phi \overline{\chi_i^c} \chi_i$, where ϕ is a complex field. Hence, the Lagrangian reads [110]

$$\mathcal{L} \supset i\overline{\chi}\gamma^\mu \partial_\mu \chi + \frac{1}{2}(\partial^\mu \phi)^2 + |D^\mu \eta|^2 - \frac{\lambda_i}{2}\phi\overline{\chi_i^c}\chi_{iR} - y_{i_\alpha}\overline{\chi_{iR}}L_\alpha \eta, \qquad (6.44)$$

where D_μ denotes the covariant derivative which couples the η particle to the gauge bosons. If we consider χ_i and η with charge $+1$ and ϕ with a charge of -2 under a global $U(1)$ symmetry and require a vacuum expectation value for ϕ, then the Z_2 symmetry is a remnant after symmetry breaking. Hence, we solved the problem of the origin of the Z_2 symmetry. Furthermore, we can have new annihilation channels for the singlet fermion χ_i. Before we only had the usual channel of $\chi\chi \to l^+l^-$, where l is a SM lepton. But now we can decompose the complex field ϕ into the real and imaginary part such that $\phi = \rho + ia$, where ρ is a scalar and a a pseudoscalar. So, we also have the channels of $\chi\chi \to \rho\rho, aa, \rho a$. With these new channels one is able to avoid overproduction of χ as dark matter candidate because one can deplete the abundance of χ even for small Yukawa couplings $y_{i\alpha}$. Hence, in the Scale Invariant extension of the Scotogenic Model we can have fermionic DM as a thermal relic and obey the limits of LFV processes.

6.4 Cross Section between Dark Matter and Neutrinos or Photons

As we did in the toy model before, we now want to discuss the cross section for the t-channel mediator model and for its special case, the Scotogenic Model. We remember that the difference between these two models lies in the coupling of the

Majorana fermion to the leptons. In the t-channel mediator model the Majorana fermion only couples to one flavour, while in th Scotogenic Model it couples to all lepton flavours. Thus, in the t-channel mediator model we examine two dark matter candidates. The η^0, which is the lightest neutral particle of the η doublet and the Majorana fermion χ. In the Scotogenic Model we only assume η^0 to be the dark matter candidate. In the Scale Invariant Scotogenic Model also χ can be the dark matter. Note also, that we have different values of the Yukawa couplings and different values for the masses. In the t-channel mediator model the Yukawa couplings can be largish, while in the Scotogenic case they are at $\mathcal{O}(y) \sim 10^{-2}$ to avoid the LFV processes. We take the mass of the dark matter particle is in the order of $\mathcal{O}(m_{\mathrm{DM}}) \sim$ TeV in the Scotogenic Model and in the order of $\mathcal{O}(m_{\mathrm{DM}}) \sim 100$ GeV in the t-channel mediator model. Hence, the cross section are supposed to be smaller in the Scotogenic Model compared to the t-channel mediator model. We first want to look at the case of scalar dark matter and then have a glance at fermionic dark matter.

All of the diagrams were generated and calculated with Mathematica and the help of the MSSM package by relabelling the particles and indices. With the MSSM package one can use, as scalar dark matter, the sneutrino $\tilde{\nu}$ because it is the uncharged component of a scalar doublet. For the fermionic dark matter one can use the neutralino χ which is a Majorana fermion. This is motivated by the fact that the t-channel mediator model can be realised in the MSSM. Also, the imposed Z_2 symmetry in the t-channel model is the R-parity in the MSSM. After calculating the matrix element and the phase factor, the remaining differential cross section was integrated numerically with the help of Python. The full Feynman rules of the MSSM can be looked up in [111].

We denote two different scenarios for scalar dark matter particles. The first scenario where we have a dark matter mass with $m_{\eta^0} = 100$ GeV and small mass splittings between the mediator mass m_χ and the dark matter particle and a Yukawa coupling of $y = 0.7$. In Fig. 6.5 we see that for small mass splittings and a dark matter mass of 100 GeV, we lie between $y = 1$ and $y = 0.5$. This scenario can be realised in the t-channel mediator model and we therefore call it the t-channel mediator scenario, or shorter the t-channel scenario. In the second scenario we look at a dark matter mass of $m_{\eta^0} = 1$ TeV and a larger mass splitting between the mediator mass and the dark matter mass at $\mathcal{O}(m_\chi - m_{\eta^0}) > 10$ and a Yukawa coupling of $\mathcal{O}(y) = 10^{-2}$. This scenario can be realised in the Scotogenic Model. That is why we call this scenario simply the Scotogenic case.
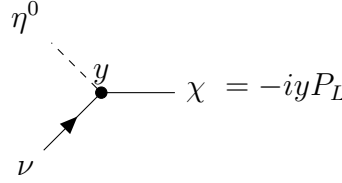
For the case of χ as dark matter candidate, we mainly look at the t-channel mediator scenario. Thus, where $m_\chi = 100$ GeV and small mass splittings between η and χ. But, out of curiosity, we will also slightly vary the masses of the η doublet. And we take a Yukawa coupling of $y = 0.7$.

So, let us start with the scalar dark matter candidate.

6.4.1 Scalar Dark Matter

In the case of scalar dark matter we can have either elastic or inelastic scattering between the dark matter particle and neutrinos or photons. The Scotogenic Model does include inelastic scattering as well as its scale invariant extension [110]. The

interaction Lagrangian between η^0 and neutrinos reads $\mathcal{L}_{\text{int}} = -y\bar{\chi}P_L\nu\eta^0$. Hence, the vertex is given by:

$$
\begin{array}{c}
\eta^0 \\
\diagup y \\
\bullet \!\!\!\!- \chi \\
\diagup \\
\nu
\end{array}
\quad = -iyP_L
\tag{6.45}
$$

So, we get exactly the same results as in our toy model case. The relevant diagrams for the process of $\nu\eta^0 \to \nu\eta^0$ are shown in Fig. 6.1. We have an s and a u channel. We explicitly calculated the cross section for the elastic process (see ch. 6.1). We find that the cross section in the rest frame of η^0 is given by Eq. (6.27):

$$
\begin{aligned}
\left.\frac{d\sigma}{d\cos\theta}\right|_{\nu\eta^0\to\nu\eta^0} &= \frac{y^4}{8\pi m_{\eta^0}^2}\frac{E_\nu'^2}{E_\nu^2}\frac{m_{\eta^0}^4 E_\nu E_\nu'(1+\cos\theta)(E_\nu+E_\nu')^2}{(s-m_\chi^2)^2(u-m_\chi^2)^2} \\
&= \frac{y^4 m_{\eta^0}^2}{8\pi}\frac{E_\nu'^2}{E_\nu^2}\frac{E_\nu E_\nu'(1+\cos\theta)(E_\nu+E_\nu')^2}{(m_\eta^2+2E_\nu m_\eta - m_\chi^2)^2(m_\eta^2-2E_\nu' m_\eta - m_\chi^2)^2},
\end{aligned}
$$

Here again the energy of the incoming neutrino is E_ν, the energy of the outgoing neutrino E_ν' and θ the scattering angle in the rest frame of the dark matter particle. But now, we have a more sophisticated model with concrete values for the dark matter and the Yukawa couplings. The results are shown in Fig. 6.6.
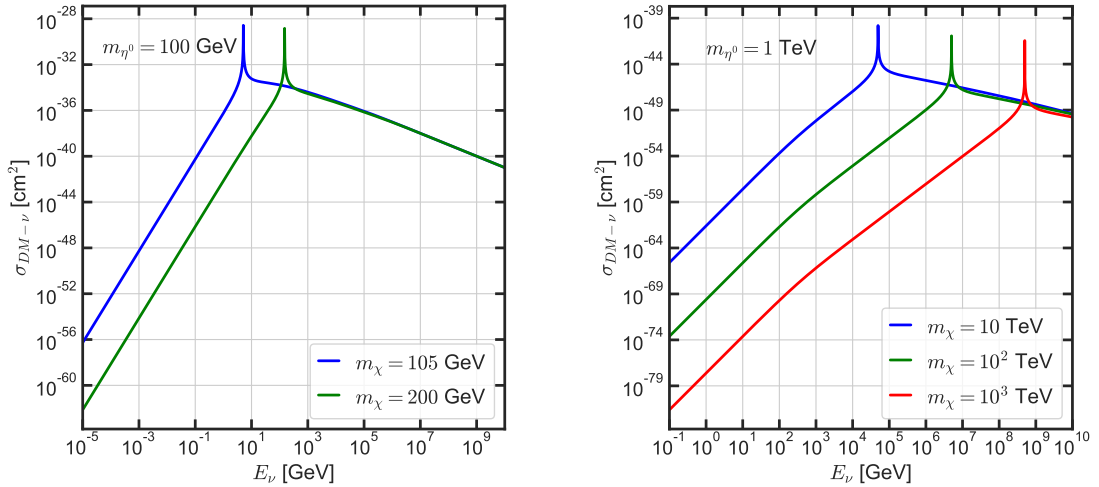
Figure 6.6: *Left panel*: Elastic scattering cross section of the dark matter particle η^0, namely $\nu\eta^0 \to \nu\eta^0$, in the t-channel mediator scenario. The mass of $m_\eta^0 = 100$ GeV and $y = 0.7$. Two different cases are shown for the mediator mass $m_\chi = 105$ GeV and $m_\chi = 200$ GeV. *Right panel*: The same elastic scattering cross section for the Scotogenic scenario, where $m_{\eta^0} = 1$ TeV and $y = 10^{-2}$. The mediator masses are $m_\chi = 10, 10^2, 10^3$ TeV.

For the t-channel mediator scenario the cross section for a given energy is larger than in the Scotogenic scenario because $\sigma \propto y^4$. Thus, the cross section of the Scotogenic scenario is suppressed by 7 orders of magnitude compared to the t-channel mediator scenario. Furthermore, for low energies we have already seen in

ch. 6.1 that the cross section scales with m_η^2/m_χ^8. Thus, the Scotogenic scenario is further suppressed by 8 orders of magnitude. In total the spectrum of the Scotogenic Model is suppressed by 15 orders of magnitude for low energies. For example, if we fix the energy $E_\nu = 10^{-1}$ GeV and look at the blue curves of each of the panels in Fig. 6.6 we see that $\sigma \sim 10^{-40}$ cm^2 in the t-channel mediator scenario and $\sigma \sim 10^{-65}$ cm^2 for the Scotogenic scenario. The resonance energy is $(m_\chi^2 - m_{\eta^0}^2)/(2m_{\eta^0})$. In the t-channel mediator scenario we reach earlier the resonance because we have lower dark matter and mediator masses. This further implies that we reach the domain where $\sigma \sim E_\nu^{-1}$ for lower energies than in the Scotogenic scenario. For detailed scaling relations in the different energy regimes and more dicussion see ch. 6.1.

In the Scale Invariant Scotogenic Model we have an additional inelastic term that does not appear in the t-channel mediator model. Remember that the Lagrangian term $M_i\overline{\chi^c}_i\chi_i$ is replaced by $\lambda_i\phi\overline{\chi^c}_i\chi_i$, with ϕ being a complex field. We can decompose the field $\phi = \rho + ia$. Hence, we also have the channel where $\chi \to \chi\rho/a$. So, we get in addition to the elastic scattering the inelastic $\nu\eta^0 \to \chi\rho/a$ scattering. The diagram of this process is shown in Fig. 6.7.
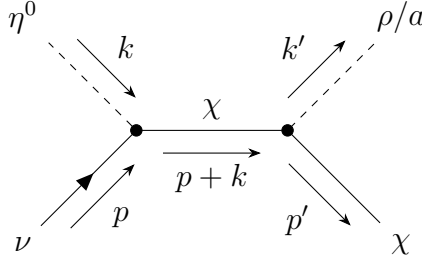
Figure 6.7: Feynman diagram of the inelastic $\nu\eta \to \chi\rho/a$ scattering in the Scale Invariant Scotogenic Model.

The matrix element of process is given by

$$iT = \overline{u}_\chi(p', s')(-i\lambda)P_R\frac{i(\slashed{p} + \slashed{k} + m_\chi)}{(p + k)^2 - m_\chi^2 + i\epsilon}(-iy)P_L u(p, s).$$ (6.46)

Evaluating this matrix element in terms of the Mandelstam variables yields

$$\overline{|T|^2} = \lambda^2 y^2 2\frac{(s - m_{\eta^0}^2)(s + m_\chi^2 - m_\rho^2) + s(t - m_\chi^2)}{(s - m_\chi^2)^2}.$$ (6.47)

In this case it is easier to work in the centre of mass frame and then transform back into the rest frame of η^0. The mass of the incoming particles does not equal the mass of the outgoing particles and we do not have the simple relation of $E_\nu' = E_\nu/(1 + \frac{E_\nu}{m_\eta}(1 - \cos\theta))$ anymore. Hence, we use the well known formula that we derived in ch. 4.2

$$\frac{d\sigma}{dt} = \frac{1}{64\pi s}\frac{1}{|p_{1cm}|^2}\overline{|T|^2}.$$ (6.48)

By applying this formula we obtain after some intermediate steps the following:

$$
\begin{aligned}
\sigma\big|_{\nu\eta\to\chi\rho} &= \lambda^2 y^2 \left[\frac{m_{\eta^0}^2 t(m_\rho^2 - m_\chi^2 - s) + st(s - m_\rho^2) + st^2/2}{32\pi(m_{\eta^0}^2 - s)^2(m_\chi^2 - s)^2} \right]_{t_1}^{t_0} \\
&= \lambda^2 y^2 \frac{(s - m_{\eta^0}^2)^2(s - m_\rho^2 + m_\chi^2)\sqrt{m_\rho^4 - 2m_\rho^2(m_\chi^2 + s) + (m_\chi^2 - s)^2}}{64\pi s(s - m_{\eta^0}^2)(s - m_\chi^2)^2} \\
&= \lambda^2 y^2 \frac{2E_\nu^3(E_\nu m_{\eta^0} + m_{\eta^0}^2 + m_\chi^2)}{64\pi \left(\frac{E_\nu^2 m_{\eta^0}}{2E_\nu + m_{\eta^0}}\right)^{3/2} (2E_\nu + m_{\eta^0})^3 \sqrt{\frac{(2E_\nu m_{\eta^0} + m_{\eta^0}^2 - m_\chi^2)^2}{m_{\eta^0}(2E_\nu + m_{\eta^0})}}}.
\end{aligned}
\tag{6.49}
$$

In the last step we used that $s = m_{\eta^0}^2 + 2E_\nu m_{\eta^0}$ in the rest frame of the DM particle η^0 and set $m_\rho = 0$ for simplicity. Fig. 6.8 shows the cross section of the equation for two different masses m_χ and a fixed dark matter mass m_{η^0}.
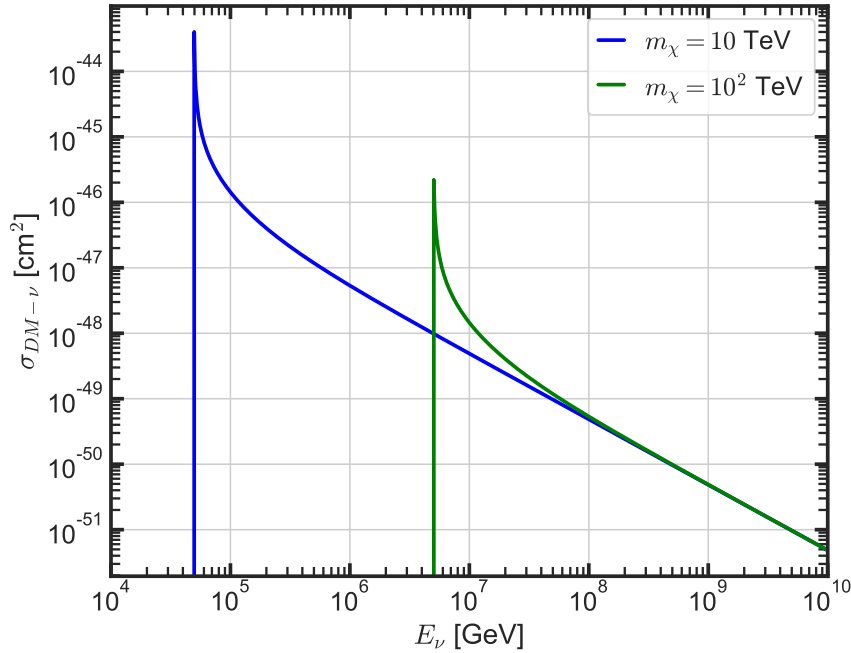
Figure 6.8: The figure shows the scattering cross section of the process $\eta^0\nu \longrightarrow \chi\rho$ in the Scale Invariant Scotogenic Model for two cases in terms of the energy E_ν of the incoming neutrino. The blue curve shows the cross section for $m_\chi = 10$ TeV and the green one for $m_\chi = 10^2$ TeV. The dark matter is the lightest scalar particle η^0 of the $SU(2)_L$ doublet with mass $m_{\eta^0} = 1$ Tev for both cases. For simplicity we have chosen that the two couplings to be the same, namely that $\lambda = y = 10^{-2}$ and we have set $m_\rho = 0$.

The two plots of Fig. 6.8 show the two cases where $m_\chi = 10$ TeV and $m_\chi = 10^2$ TeV. Whereby, the dark matter mass $m_{\eta^0} = 1$ TeV because the Scale Invariant Scotogenic Model predicts new physics in the TeV scale [112]. When we look again at Eq. (6.49) we see that for energies larger than any mass involved in the process the cross section scales as

$$
\sigma\big|_{\nu\eta\to\chi\rho} \approx \frac{\lambda^2 y^2}{128\pi m_{\eta^0} E_\nu}.
\tag{6.50}
$$

Hence, the cross section decreases as the energy increases. Furthermore we notice that in the graph we have an onset for both cases. This due to the fact that this time the χ particle is not an imaginary particle. Therefore the process is kinematically allowed if $\sqrt{s} > m_\chi$ (for $m_\rho = 0$). This translates into the condition of $E_\nu > (m_\chi^2 - m_{\eta^0})^2/(2m_\eta^0)$. Therefore, only after the resonance peak the process of $\eta^0 \nu \to \chi \rho$ opens. For the case of $m_\chi = 10$ TeV and $m_{\eta^0} = 1$ TeV the energy mus be larger than $E_\nu > 50$ TeV. Thus, for larger masses of m_χ the onset shifts to larger energies, as we can see in the plot. Furthermore, the behaviour of the cross section for large energies is independent of the mass m_χ. Note that ρ can have a mass that is smaller than the dark matter mass because it is even under the imposed Z_2 symmetry. Hence, the dark matter can not decay into a pair of ρ's.

The scattering of $\eta^0 \nu \to \chi a$ should work analogously. One just have to keep in mind that a is a pseudoscalar an that the Feynman rules are different than for ρ. It is left over for future work.

Next, we want to consider the case of inelastic scattering for a general extension of the SM by an $SU(2)_L$ doublet. Since η is a doublet under $SU(2)_L$ it interacts with the gauge bosons W^+, W^- and Z. We will now investigate these scatterings. They can occour in the t-channel mediator model and in the Scotogenic Model.

Let us start with the scatterings between neutrinos and the dark matter η^0. We have a glance at this scenario with different dark matter masses m_{η^0}. The inelastic channels are $\nu \eta^0 \to \eta^+ e^-$, $\nu \eta^0 \to \chi Z$ and $\nu \eta^0 \to \nu A^0$. The diagrams are shown in Fig. 6.9, 6.10 and Fig. 6.11.
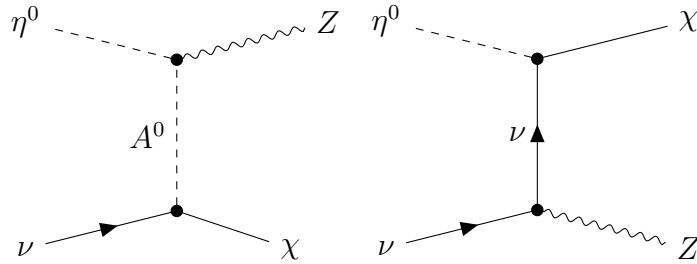
Figure 6.9: Feynman diagram of the $\nu \eta^0 \to Z\chi$ scattering in the t-channel mediator model. Note that the left diagram with η^0 as mediator is forbidden by parity because we do not have a $\eta^0 \eta^0 Z$ vertex.
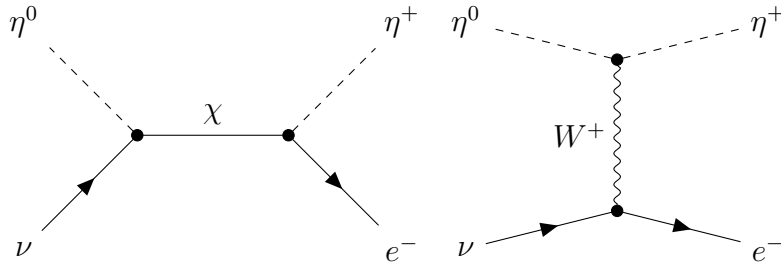
Figure 6.10: Feynman diagram of the $\nu \eta^0 \longrightarrow \eta^+ e^-$ scattering in the t-channel mediator model.
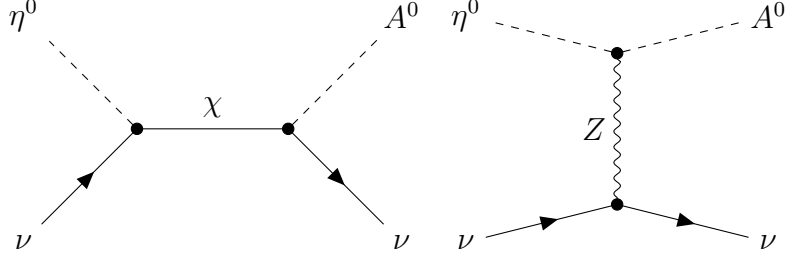
Figure 6.11: Feynman diagram of the $\nu\eta^0 \to \nu A^0$ scattering in the t-channel mediator model.

Interestingly, we have diagrams, were we do not have the unknown Yukawa coupling and only gauge couplings g. See for example the right diagram of Fig. 6.10 or the right diagram of Fig. 6.11. The cross section is expected so scale with g^4 instead of $y^2 g^2$ or y^4 which makes them very attractive. Note that the diagrams might not be complete. It could be that there are some diagrams missing that one has to include for future calculations. The MSSM also includes the Goldstone bosons as an additional diagram. But we have neglected it because it is suppressed by m_e and therefore negligible.

The differential cross section of the first diagrams (Fig. 6.9) in terms of the Mandelstam variables is given by

$$
\left.\frac{\mathrm{d}\sigma}{\mathrm{d}t}\right|_{\nu\eta^0 \to \chi Z} = \frac{e^2 y^2}{128\pi t^2 m_Z^2 t^2 (s - m_{\eta^0}^2)^2 (s + t - m_Z^2 - m_{\eta^0}^2 - m_\chi^2 + m_A^2)^2 \sin^2\theta_W \cos^2\theta_W} \cdot
$$

$$
\begin{aligned}
\Big[&-m_Z^6 (4m_A^2(m_{\eta^0}^2 - m_\chi^2) - 4m_{\eta^0}^4 + 4m_{\eta^0}^2 s + 4m_\chi^4 - 4m_\chi^2 s - 6m_\chi^2 t \\
&+ 2st + t^2) - tm_Z^2(m_A^4(-2m_\chi^2 + 2s + t) + 2m_A^2(2m_{\eta^0}^4 - 4m_{\eta^0}^2(s+t) \\
&+ 2m_\chi^4 - 2m_\chi^2(s+t) + 2s^2 + 3st + t^2) - 4m_{\eta^0}^6 + m_{\eta^0}^4(-2m_\chi^2 + 10s + 7t) \\
&+ 2m_{\eta^0}^2(s+t)(2m_\chi^2 - 4s - t) - 2m_\chi^6 + 2m_\chi^4(s+2t) - 2m_\chi^2(s+t)^2 \\
&+ 2s(s+t)^2) + m_Z^4(2m_A^4(m_{\eta^0}^2 - m_\chi^2) + m_A^2(-4m_{\eta^0}^4 + 4m_{\eta^0}^2 s + 4m_\chi^4 \\
&- 4m_\chi^2(s+2t) + 2t(2s+t)) + 2m_{\eta^0}^6 + 2m_{\eta^0}^4(m_\chi^2 - 2s + 2t) \\
&+ m_{\eta^0}^2(-2m_\chi^4 + 4m_\chi^2 t + 2s^2 - 8st - 5t^2) - 2m_\chi^6 + 4m_\chi^4 s + 8m_\chi^4 t \\
&- 2m_\chi^2 s^2 - 8m_\chi^2 st - 6m_\chi^2 t^2 + 4s^2 t + 5st^2 + t^3) + 2m_Z^8(m_{\eta^0}^2 - m_\chi^2) \\
&- t^2(m_A^2 - m_{\eta^0}^2)^2(m_{\eta^0}^2 - s - t) \Big],
\end{aligned}
$$

$$(6.51)$$

where we have replaces the variable u. We can again integrate this equation numerically to obtain the full cross section. This is shown in Fig. 6.12. In Fig. 6.12 we can see the t-channel mediator scenario with $m_{\eta^0} = 100$ GeV, $m_\chi = 105, 200$ GeV and $y = 0.7$ (left panel) and the Scotogenic scenario with $m_{\eta^0} = 1$ TeV, $m_\chi = 10, 10^2, 10^3$ TeV. In bot scenarios we assumed that the mass of A^0 is a bit larger than η^0 such that $m_{\eta^0} \leq m_{A^0}$. In both panels the cross section scales with E_ν^{-1} for large energies which is consistent with unitary. The cross section can be approximated by

$$
\sigma\big|_{\nu\eta^0 \to \chi Z} \simeq \frac{y^2 e^2}{256\pi E_\nu m_{\eta^0} \sin^2\theta_W \cos^2\theta_W},
$$

$$(6.52)$$

69
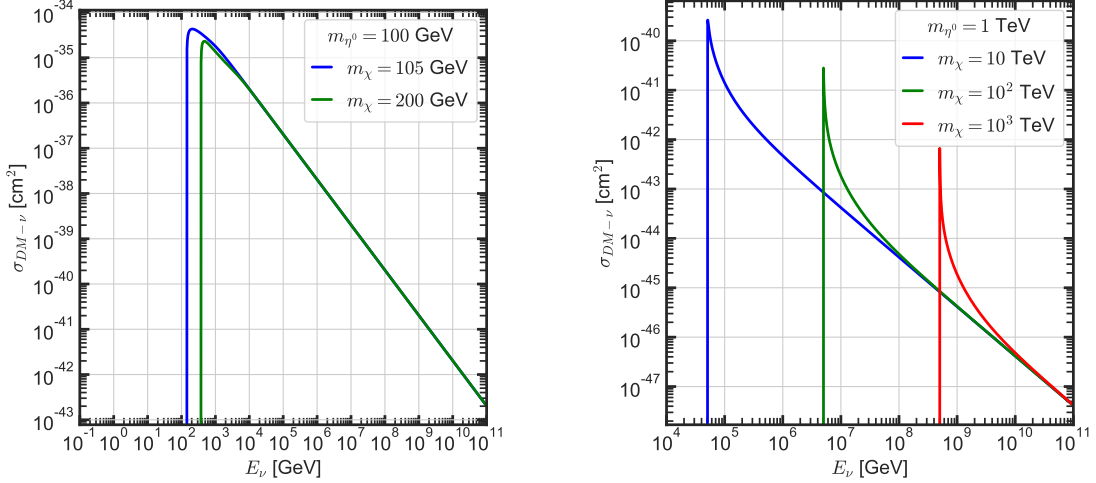
Figure 6.12: *Left panel*: Inelastic scattering cross section between the dark matter particle η^0 and the neutrino given by the $\nu\eta^0 \to Z\chi$ in the t-channel mediator scenario. The mass of $m_{\eta^0} = 100$ GeV and $y = 0.7$. Two different cases are shown for the mediator mass $m_\chi = 105$ GeV and $m_\chi = 200$ GeV. *Right panel*: The same inelastic scattering cross section than in the left panel but for the Scotogenic scenario, where $m_{\eta^0} = 1$ TeV and $y = 10^{-2}$. The mediator masses are $m_\chi = 10, 10^2, 10^3$ TeV.

where θ_W is the Weinberg angle with $\cos\theta_W = m_W/m_Z$ and $e = g\sin\theta_W$. For large mass differences between the mediator mass m_χ and the dark matter mass m_{η^0}, the cross section approaches a resonance close to the threshold of the scattering. This is the case because for large energies we obtain an overall factor of $1/(u - m_{A^2})^2 = 1/(s + t - m_Z^2 - m_\chi^2 - m_{\eta^0}^2 + m_{A^2})$. For small mass differences between m_{η^0} and m_χ this factor is proportional to $1/s$ because the masses cancel. But if $m_\chi \gg m_{\eta^0}$, we approach a resonance when $s = m_\chi^2$ when t is small compared to s and m_χ^2. This is the reason why we have a resonance feature in the right but not in the left panel. We further notice, that the cross section only depends on the mass of the dark matter particle m_{η^0} and not the mass of the other particles involved in the process. This is reasonable because for large energies the cross section should scale with $1/s$ and the masses should be irrelevant.

The two other processes, namely $\nu\eta^0 \to \eta^+ e^-$ and $\eta^0\nu \to \nu A^0$, should have the same order of magnitude than $\nu\eta^0 \to \chi Z$. During the calculation we encountered some problems. Due to unitarity the cross section should scale in both processes with $1/s$ for large energies. The phase space factor always scales with $1/s^2$ in our processes. But, we obtained a matrix amplitude that has a term which is proportional to s^2. Hence, for large energies the cross section becomes constant. This is very odd, because it was not expected and violates the unitarity condition. Consequently, we do not fully understand the process or there is something wrong in the calculations. But our calculation were fine for the previous scatterings and is also valid for the case of χ being the dark matter. For the process of $\eta^0\nu \to \chi Z$ we also would have a constant term if we only include the right diagram if Fig. 6.9. By including the left diagram with A^0 as mediator the constant term cancelled out. Therefore, the constant cross section might be due to the fact that we are missing some diagrams. However, finding those diagrams is left over for future work.

Nevertheless, the magnitude of the cross section should be comparable to that of the $\eta^0 \nu \to \chi Z$ scattering. The interesting part of the diagrams with the bosons as mediator is that we have a cross section that is proportional to the known gauge boson coupling g^4 and independent of the unknown coupling Yukawa coupling y. Note that there could also be diagrams with the Goldstone boson that we neglected for simplicity and because we think they are suppressed by m_e.

So, let us continue by only taking the diagrams into account that scale with $g^2 y^2$ and y^4. Thus, we drop the right diagrams of Fig. 6.20 and Fig. 6.11 which are proportinal to g^4. For the cross sections we obtain

$$\frac{\mathrm{d}\sigma}{\mathrm{d}t}\bigg|_{\nu\eta^0\to\eta^+e^-} = \frac{y^4(m_{\eta_0}^2(-m_e^2 + m_\eta^2 - s) + s(-m_\eta^2 + s + t))}{32\pi(s - m_{\eta_0}^2)^2(m_\chi^2 - s)^2}, \qquad (6.53)$$

where m_η denotes the mass of the charged η particle and

$$\frac{\mathrm{d}\sigma}{\mathrm{d}t}\bigg|_{\nu\eta^0\to\nu A^0} = \frac{y^4(m_{A^0}^2 + m_\eta^2 - 2s - t)^2((m_{A^0}^2 - s)(m_\eta^2 - s) + st)}{32\pi(m_\chi^2 - s)^2(m_\eta^2 - s)^2(-m_{A^0}^2 + m_\chi^2 - m_\eta^2 + s + t)^2}. \qquad (6.54)$$

The results are shown in Fig. 6.13 and Fig. 6.14.
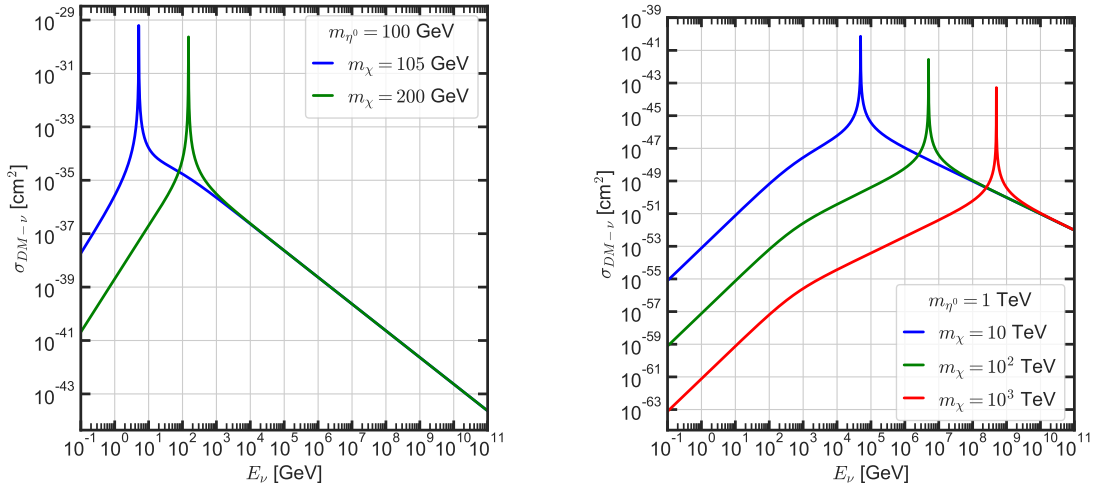
Figure 6.13: *Left panel*: Inelastic scattering cross section of the dark matter particle η^0 and the neutrino given by the $\nu\eta^0 \to \eta^+e^-$ in the t-channel mediator scenario but only for the s-channel diagram. The mass of $m_{\eta^0} = 100$ GeV and $y = 0.7$. Two different cases are shown for the mediator mass $m_\chi = 105$ GeV and $m_\chi = 200$ GeV. *Right panel*: The same inelastic scattering cross section than in the left panel but for the Scotogenic scenario, where $m_{\eta^0} = 1$ TeV and $y = 10^{-2}$. The mediator masses are $m_\chi = 10, 10^2, 10^3$ TeV. For simplicity we set the masses of the η doublet to be equal.

In Fig. 6.13 we can see the inelastic scattering $\nu\eta^0 \to \eta^+e^-$ but only in the s-channel. We dropped the diagram, where the mediator is the W boson because we encountered some problems. In the left panel the scenario with $m_{\eta^0} = 100$ GeV, $m_\chi = 105, 200$ GeV and $y = 0.7$ is shown which can be realised in the t-channel mediator model. The right panel shows the Scotogenic scenario for $m_{\eta^0} = 1$ TeV, $m_\chi = 10, 10^2, 10^3$ TeV and $y = 10^{-2}$. We chose for both panels the same mass for

the η particles for simplicity which means that $m_{\eta^0} = m_\eta$. Strictly we must use that $m_{\eta^0} \lesssim m_{\eta^+}$ but it only makes a difference in the onset of the scattering. That is why we neglected the mass difference here. For both scenarios we see that the cross section decreases with $1/E_\nu$ if $E_\nu \gg (m_{\eta^0} - m_\chi^2)/(2m_{\eta^0})$ as in the elastic scattering, namely:

$$\sigma_{\nu\eta^0 \to \eta^+ e^-}\big|_{E \gg m_\chi} \widetilde{\simeq} \frac{y^4}{128\pi E_\nu m_{\eta^0}} \tag{6.55}$$

This should be the case because the scattering is comparable to the elastic scattering if we set $m_e = 0$ and $m_{\eta^0} = m_\eta$. But we note some difference for $E_\nu < (m_{\eta^0} - m_\chi^2)/(2m_{\eta^0})$. Here the cross section scale with E_ν between $m_{\eta^0} < E_\nu < (m_{\eta^0} - m_\chi^2)/(2m_{\eta^0})$ and with E_ν^2 for $E_\nu \ll m_{\eta^0}$. More precisely they are given by:

$$\sigma_{\nu\eta^0 \to \eta^+ e^-}\big|_{E_\nu \gg m_{\eta^0}} \widetilde{\simeq} \frac{y^4 E_\nu^2}{16\pi m_\chi^4} \tag{6.56}$$

and

$$\sigma_{\nu\eta^0 \to \eta^+ e^-}\Big|_{m_{\eta^0} < E_\nu < \frac{m_\chi^2 - m_{\eta^0}^2}{2m_\chi}} \widetilde{\simeq} \frac{y^4 m_{\eta^0} E_\nu}{32\pi m_\chi^4}, \tag{6.57}$$

where we set $m_e = 0$ and $m_{\eta^0} = m_\eta$. In the elastic scattering the cross section scales with E_ν^4 and E_ν^3 in those regimes. The reason for this is that we are only dealing with the s-channel here. In the elastic scattering we also have the u-channel which leads to different scaling behaviours. One can simply check that by only using the s-channel for the elastic scattering and compare the two matrix elements. They are equal if one sets $m_e = 0$ and $m_{\eta^0} = m_\eta$. We will not check it explicitly here because it is straightforward and only takes a few steps of computation. Otherwise, we just have to believe the words of the thesis writer who checked it. For small mass differences between the dark matter particle and the mediator we do not have the intermediate scaling regime and the cross section scales with E_ν^2 if $E_\nu < (m_{\eta^0} - m_\chi^2)/(2m_{\eta^0})$.

In Fig. 6.14 we can see the cross section of $\nu\eta^0 \to \nu A^0$. We once again the usual scenarios of $m_{\eta^0} = 100$ GeV, $m_\chi = 105, 200$ GeV (left panel) and $y = 0.7$ and $m_\chi = 1$ TeV with $m_\chi = 10, 10^2, 10^3$ TeV and $y = 10^{-2}$ (right panel) are shown. For simplicity we chose $m_{\eta^0} = m_{A^0}$. Here the cross section is similar to the elastic cross section despite the fact that the pseudoscalar follows different Feynman rules. But the scattering becomes quite similar when we equal the masses of η^0 and A^0. For energies with $E_\nu \gg m_\chi$ we have

$$\sigma\big|_{E_\nu \gg m_\chi} \widetilde{\simeq} \frac{y^4}{16\pi E_\nu m_{\eta^0}} \tag{6.58}$$

and

$$\sigma\big|_{E_\nu \ll m_{\eta^0}} \widetilde{\simeq} \frac{y^4 E_\nu^4 m_{\eta^0}}{\pi m_\chi^8} \tag{6.59}$$

Thus, the large and low scaling behaviours are similar to the elastic scattering. Due to that fact, we will not comment further on the plots because we would just repeat what we have written in ch. 6.1. But we want to mention again that there are still some diagrams missing that one has to include for the inelastic scattering. Now, we want to turn our interest to the scattering between photons and the dark matter particles.
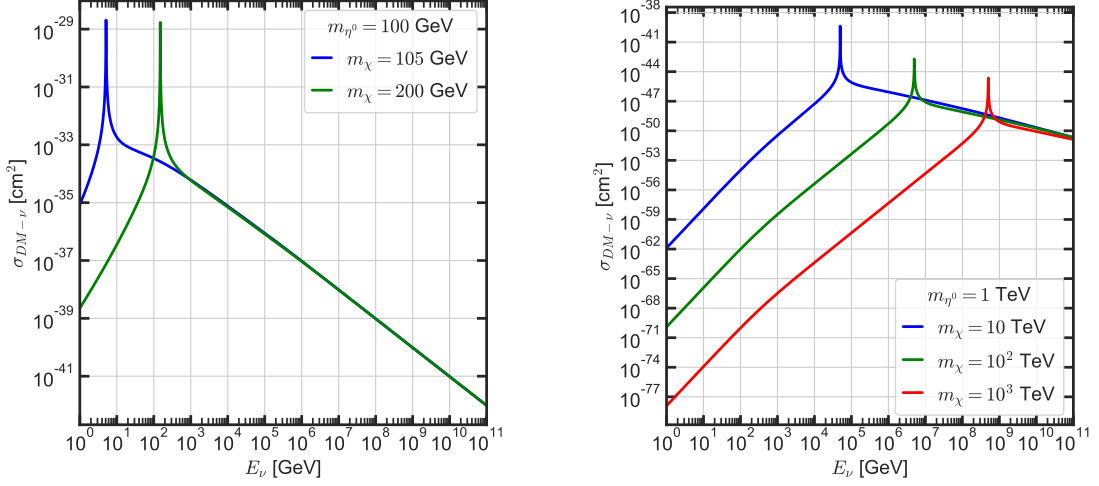
Figure 6.14: *Left panel*: Inelastic scattering cross section of the dark matter particle η^0 and the neutrino given by the $\nu\eta^0 \to \nu A^0$ in the t-channel mediator scenario but without the Z boson as mediator. The mass of $m_{\eta^0} = 100$ GeV and $y = 0.7$. Two different cases are shown for the mediator mass $m_\chi = 105$ GeV and $m_\chi = 200$ GeV. *Right panel*: The same inelastic scattering cross section than in the left panel but for the Scotogenic scenario, where $m_{\eta^0} = 1$ TeV and $y = 10^{-2}$. The mediator masses are $m_\chi = 10, 10^2, 10^3$ TeV.

In the scenario of η^0 being the dark matter we could also have an interaction between the photons and the dark matter particles at tree level via the process $\eta^0\gamma \longrightarrow \eta^+W^-$ which is shown in Fig. 6.15.
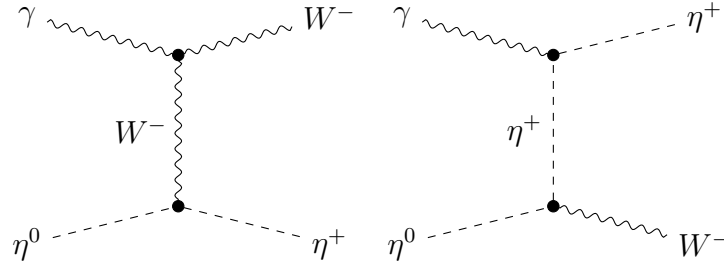
Figure 6.15: Feynman diagram of the $\eta^0\gamma \longrightarrow \eta^+W^-$ scattering in the t-channel mediator model.

During the calculation of the cross section of the diagrams in Fig. 6.15 we also encountered the same problem than in the processes $\nu\eta^0 \to \eta^+e^-$ and $\eta^0\nu \to \nu A^0$. As mentioned earlier the cross section becomes constant which violates unitarity. We discussed this problem above, so we will not discuss it further. The problem could be that there are still diagrams missing for the process. Solving this issue is left over for future work. But we want to highlight that the left diagram only depends on g^4 which makes it an attractive interaction because we do not have the unknown Yukawa coupling y. Also, we have interference terms between the two channels. It might be that they are the reason for a constant cross section. Nevertheless, we will not continue with the calculations and turn now our interest into the case of fermionic dark matter.

6.4.2 Fermionic Dark Matter

After examining the case of scalar dark matter we now want to look at the case where the dark matter candidate is the χ particle. Here, we can also have elastic and inelastic scattering between the neutrinos or photons. This scenario can be realised in the Scale Invariant Scotogenic Model as well as in the t-channel mediator model.

The interaction term of the elastic scattering is the same than above with $\mathcal{L}_{\text{int}} = -y\overline{\chi}P_L\nu\eta^0$. Thus, we obtain the following two Feynman diagram ms for the $\nu\chi \to \nu\chi$ scattering shown in Fig. 6.16. The fermion dark matter χ is a Majorana fermion which is its own antiparticle. Because of that we also have to take the s channel for the scattering.
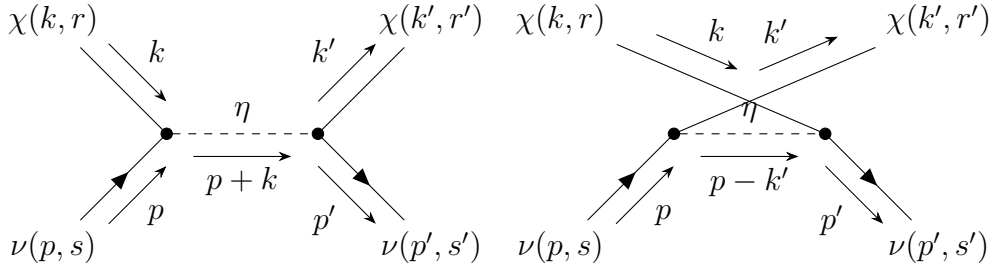
Figure 6.16: Feynman diagram of the $\nu\chi \to \nu\chi$ scattering in the s and u channel. Here the η is strictly speaking an η^0.

Note that we also could have the same diagrams with the A^0 instead of the η^0 as mediator. But, by neglecting these terms we implicitly assume that $m_{\eta^0} < m_{A^0}$. The diagrams scale with $1/m_{\text{med}}^2$ and therefore the contributions from A^0 can be neglected because they are supposed to be smaller. For the matrix amplitude we obtain the following:

$$
\begin{aligned}
iT = &\overline{u}_\nu(p',s')(-iy)P_R v_\chi(k',r')\frac{i}{(p+k)^2 - m_\eta^2}\overline{v}_\chi(k,r)(-iy)P_L u_\nu(p,s) \\
&+ \overline{u}_\nu(p',s')(-iy)P_R u_\chi(k,r)\frac{i}{(p-k')^2 - m_\eta^2}\overline{u}_\chi(k',r')(-iy)P_L u_\nu(p,s).
\end{aligned}
\tag{6.60}
$$

Note that we have to take the Feynman rules for Majorana particles which can be found in [113]. Luckily, this feature is implemented in Mathematica, such that one can simply evaluate the cross section. Notice, that Mathematica automatically transposes spinor chains in order to perform the spin sums [53], e.g. $v^T(p,s) = -\overline{u}(p,s)C$, where C is the charge conjugated operator.

This time we have to take the spin average to be $1/4$ for the two fermions because we assume that the dark matter particle is a spin $1/2$ particle. Thus, after some calculations we obtain that cross section in of the dark matter particle χ in terms of the Mandelstam variables is given by

$$
\left.\frac{d\sigma}{dt}\right|_{\nu\chi\to\nu\chi} = \frac{y^4}{128\pi(s-m_\chi^2)^2}\left\{\frac{(s-m_\chi^2)^2}{2(s-m_{\eta^0}^2)^2} + \frac{(m_\chi^2-u)^2}{2(u-m_{\eta^0}^2)^2} - \frac{m_\chi^2 t}{(s-m_{\eta^0}^2)(u-m_{\eta^0}^2)}\right\}
\tag{6.61}
$$

We can replace the Mandelstam variable u with $u = -s-t+2m_\chi^2$ and integrate Eq. (6.61) numerically over dt from $-(s-m_\chi)^2/s$ to 0 with Python. The results are

shown in Fig. 6.17. Note that we used the different expression for the cross section this time than in the case for scalar dark matter elastic scattering. The numerical integration over $\mathrm{d}t$ with Python is more time efficient than the integration over the angle θ.
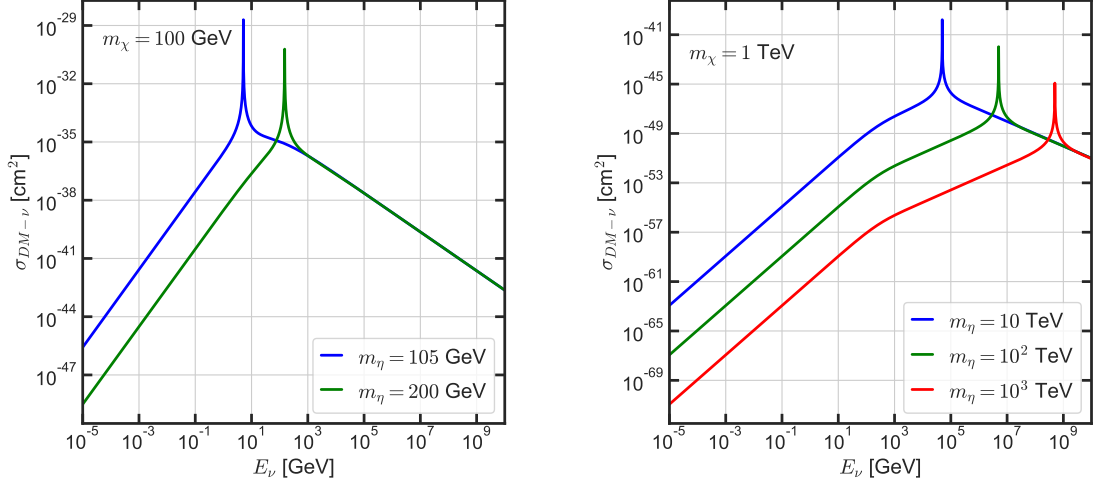
Figure 6.17: *Left panel*: Elastic scattering cross section of the dark matter particle χ and the neutrino given by $\nu\chi \to \nu\chi$ in the t-channel mediator model. The mass of $m_\chi = 100$ GeV and $y = 0.7$. Two different cases are shown for the mediator mass $m_{\eta^0} = 105$ GeV and $m_{\eta^0} = 200$ GeV. *Right panel*: The same elastic scattering cross section than in the left panel but for the Scotogenic scenario, where $m_\chi = 1$ TeV and $y = 10^{-2}$. The mediator masses are $m_{\eta^0} = 10$ TeV, $m_{\eta^0} = 10^2$ TeV and $m_{\eta^0} = 10^3$ TeV.

In Fig. 6.17 we see twp different scenarios. In the left panel the scenario for the dark matter mass of $m_\chi = 100$ GeV and two different mediator masses m_{η^0}, namely 105 GeV and 200 GeV are shown. This mass splitting is compatible with the Yukawa coupling of $y = 0.7$. We notice the low and large scale behaviours which are given by

$$\sigma_{\nu\chi\to\nu\chi}\big|_{E_\nu \ll m_\chi} \simeq \frac{y^4 E_\nu^2}{32\pi m_{\eta^0}^4}. \tag{6.62}$$

and

$$\sigma_{\nu\chi\to\nu\chi}\big|_{E_\nu \gg m_\chi} \simeq \frac{y^4}{128\pi E_\nu m_\chi^2}. \tag{6.63}$$

So, for $E_\nu \ll m_\chi$ the cross section scales with E_ν^2 and for $E_\nu \gg (m_{\eta^0}^2 - m_\chi^2)/(2m_\chi^2)$ the cross sections is proportional to E_ν^{-1}. This scaling behaviour is in good agreement with [96]. Furthermore, we notice again the resonance peak for $E_\nu \approx (m_{\eta^0}^2 - m_\chi^2)/(2m_\chi^2)$. Hence, the cross section increases with E_ν^2 until the resonance peak and then after the resonance the cross section decreases with E_ν^{-1}. We can also see that in the large energy regime the cross section is independent of the mediator mass which only plays a role in the low energy regime and for the resonance peak. The resonance is due to the s channel and can be a good feature for probing the model.
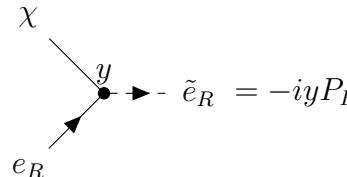
In the Scotogenic scenario, which is given in the right panel of Fig. 6.17, we use a dark matter mass of $m_\chi = 1$ TeV and three different mediator masses m_{η^0}, namely

10 TeV, 10^2 TeV and 10^3 TeV. The Yukawa coupling was chosen to be $y = 10^{-2}$. Here we notice a third energy regime which is between the resonance peak and the low energy regime, namely when $m_\chi < E_\nu < (m_{\eta^0}^2 - m_\chi^2)/(2m_\chi)$. In this regime the cross section scales with E_ν and is given by

$$\sigma_{\nu\chi \to \nu\chi}\Big|_{m_\chi < E_\nu < \frac{m_{\eta^0}^2 - m_\chi^2}{2m_\chi}} \simeq \frac{y^4 m_\chi E_\nu}{64\pi E_\nu m_{\eta^0}^4}. \tag{6.64}$$

In the t-channel scenario we do not have this scaling behaviour because we are already in the regime where $\sigma \sim E - \nu^{-1}$ after the resonance peak when $E_\nu \sim m_\chi$. Thus, only for large mass splittings we have this feature in the cross section because for low mass differences between the mediator and the dark matter mass the resonance peak shifts to energies lower than the dark matter mass. For a large mass difference the resonance peak is approximately given by $E_\nu \sim m_{\eta^0}^2/(2m_\chi)$ which is larger than m_χ for $m_{\eta^0} \gg m_\chi$. After the resonance peak, the cross section scales again with E_ν^{-1} as in the t-channel scenario. We once again remark that the cross section in the Scotogenic scenario is reduced by at least 8 order of magnitude because the cross section is proportional to y^4. It is further reduced because we have chosen a higher dark matter and mediator mass than in the t-channel mediator scenario. Notice, that in the Scale Invariant Scotogenic Model there is also a parameter space for a dark matter mass at $m_\chi \sim \mathcal{O}(100 \text{ GeV})$ [107] but the cross section would still be smaller than in the t-channel mediator scenario because of the small Yukawa coupling y. We further remark that in the Scotogenic Model the dark matter particle χ is very much contrived and ruled out. Nevertheless, we wanted to present the scenario for the elastic scattering because fermionic dark matter is allowed for the scale invariant extension [112] and because we wanted to show the new energy region where $\sigma \sim E_\nu$.

Next we want to take inelastic scattering into account. If χ is our dark matter particle, we could have inelastic scatterings between the dark matter particle and the neutrino and the photon. We first look at the photon dark matter interaction. Remember that in t-channel mediator model we can either choose the scalar particle η as a singlet or doublet under $SU(2)_L$. In the case for the photon let us treat η as a scalar singlet. Then, the interaction between the dark matter Majorana fermion χ, the scalar singlet η and the right-handed fermion f_R can be realised in the the MSSM, when η is the selectron $\tilde{e}$. So, the interaction Lagrangian reads $\mathcal{L}_{\text{int}}^{\text{fermion}} = -y\bar{\chi}e_R^-\tilde{e}_R^+ + \text{h.c.}$ [99]. Thus, we have the following vertex:

$$\tilde{e}_R = -iyP_R \tag{6.65}$$

Hence, we obtain the process of $\gamma\chi \to e_R\tilde{e}_R$ which is shown in Fig. 6.18.
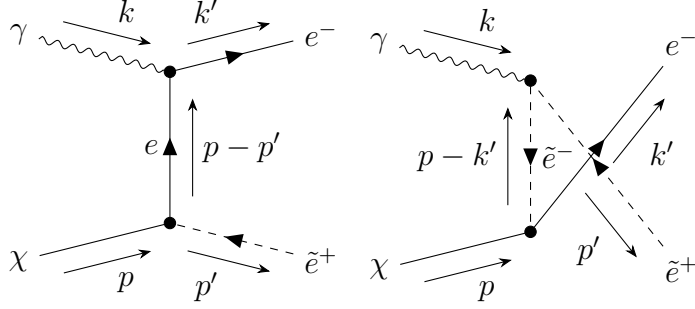
Figure 6.18: Feynman diagram for the inelastic scattering between the dark matter particle χ and a photon γ, namely $\gamma\chi \longrightarrow e^-\tilde{e}^+$. The diagram for the process $\gamma\chi \to e^+\tilde{e}^-$ is analogously with the charge flow going in the opposite direction.

We want to remark that just now we implicitly chose the η particle to be the selectron. The inelastic scattering process can be implemented in Mathematica and we obtain the following matrix element:

$$\overline{|T^2|} = \frac{e^2 y^2}{6}\left[\frac{(u - m_e^2 - m_\chi^2)(m_e^2 + 3m_\eta^2 + m_\chi^2 - s - t + u)}{(u - m_\eta^2)^2}\right.$$
$$- \frac{2(m_e^2(m_\chi^2 + t - u) + m_e^4 + m_\eta^2(4m_\chi^2 - 2u) - 2m_\chi^2 s - m_\chi^2 t + tu)}{(u - m_\eta^2)(t - m_e^2)}$$
$$- \frac{2(m_e^2(-2m_\eta^2 + m_\chi^2 + 3t + u) - m_e^4 + m_\eta^4 - m_\eta^2(s + t + u) - m_\chi^4}{(t - m_e^2)^2}$$
$$\left. - \frac{2(m_\chi^2 s + m_\chi^2 u + st)}{(t - m_e^2)^2}\right].$$

$$(6.66)$$

Note that for the mass of the selectron we have used m_η because we want to highlight that the singlet particle can but must not be the selectron. We can simplify this expression further by setting $m_e = 0$ and use $s + t + u = m_\chi^2 + m_\eta^2$. Hence, we get for the differential cross section in the rest frame of the dark matter particle χ the following expression:

$$\left.\frac{d\sigma}{dt}\right|_{\gamma\chi \to \gamma\chi} = \frac{e^2 y^2}{48\pi(s - m_\chi^2)^2}\left[\frac{2m_\eta^4(m_\chi^2 - s) + m_\eta^2(2s(s + t) - 2m_\chi^4)}{t(s + t - m_\chi^2)^2}\right.$$
$$\left. + \frac{m_\chi^6 - m_\chi^4(s + 2t) + m_\chi^2(s + t)^2 - s(s + t)^2}{t(s + t - m_\chi^2)^2}\right].$$

$$(6.67)$$

The mass of the electron is small compared to the mass of the other particles involved in the process. Thus, it is valid to set the electron mass equal to zero. Also, it makes the calculations easier and is less time consuming for the Python program. Now, we can again integrate the differential cross section numerically. The result is shown in Fig. 6.19.
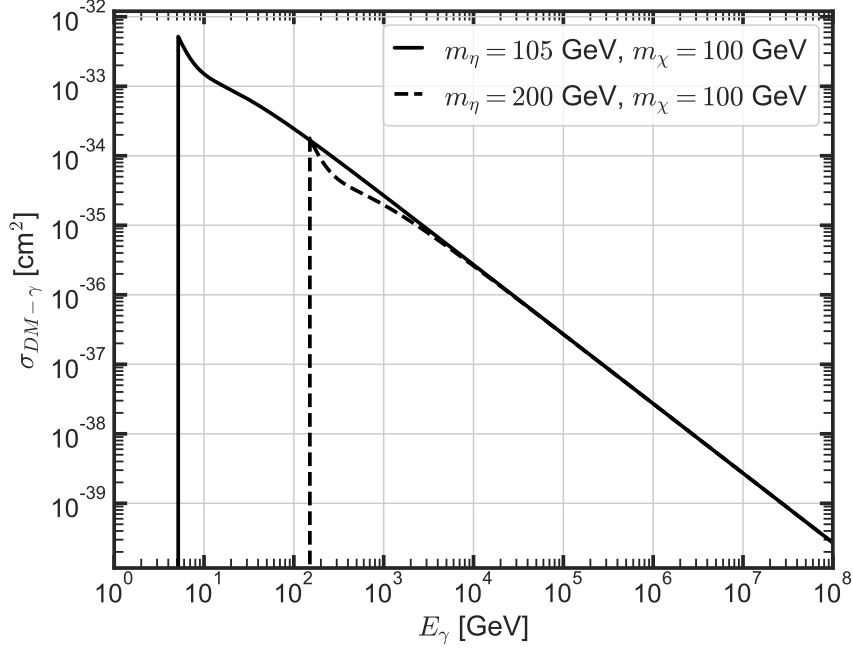
Figure 6.19: The figure shows the inelastic scattering cross section $\gamma\chi \to e\eta$ of fermionic dark matter with a high energetic photon, where we assumed that $m_e \approx 0$, $y \approx 0.5$. Here y is the Yukawa coupling between the DM, the electron and the scalar singlet particle η which can be the selectron $\tilde{e}$. The t-channel mediator model can be realised in the MSSM. The dark matter mass $m_\chi = 100$ GeV and $m_\eta = 105, 200$ GeV.

In Fig. 6.19 we see two different graphs. The solid line indicates the case where the mediator mass $m_\eta = 105$ GeV and the dashed line stands for the case where $m_\eta = 200$ GeV. For both cases the dark matter is $m_\chi = 100$ GeV. We have an an onset which makes sense because the process is kinematically allowed when $\sqrt{s} > m_\eta + m_e$. This translates into $E_\gamma \approx (m_\eta^2 - m_\chi^2)/(2m_\chi)$. Hence, for larger mediator masses the channel opens for larger energies as we can see in the figure. The Yukawa coupling is $y = 0.5$ and therefore corresponds to the case where the η can be the selectron of the MSSM. We can approximate the cross section for $E \gg m_\eta$ as follows:

$$\sigma\big|_{\gamma\chi \to e\eta} \underset{\sim}{\simeq} \frac{e^2 y^2 \log\left(\frac{2E_\gamma m_\chi}{m_e^2}\right)}{96\pi m_\chi E_\gamma}. \tag{6.68}$$

Interestingly, the cross section does not depend on the mass of the η (or selectron). But, if we look again at the two diagrams that are involved in our process in Fig. 6.18, we realise that the diagrams are proportional to $1/m_{\text{med}}^2$. The η or selectron has masses at around hundred GeV, while the mass of the electron is 511 keV. Thus, $m_e \ll m_\eta$ and therefore the cross section of the right diagram in Fig. 6.18 is suppressed compared to the left diagram. That is why for large energies the cross section scales only with the electron mass because the electron is the mediator in the left diagram. We also remark that the cross section scales basically with E_γ^{-1} because the logarithm grows slowly as the energy increases. We do not have an increase of the cross section because for $E_\gamma < (m_\eta^2 - m_\chi^2)/(2m_\chi)$ the process is kinematically forbidden.

78

Also, we only looked at the t-channel scenario because we do not have η as a singlet under $SU(2)_L$ in the Scotogenic scenario. But in the t-channel mediator it is possible that η is a singlet. Note, that in this process we only have right-handed electrons as selectrons because the fermions which couples to the η singlet must also be a singlet (because χ is a singlet too).

Note that we could also have the elastic scattering of $\chi\gamma \to \chi\gamma$ in the t-channel mediator model as follows:
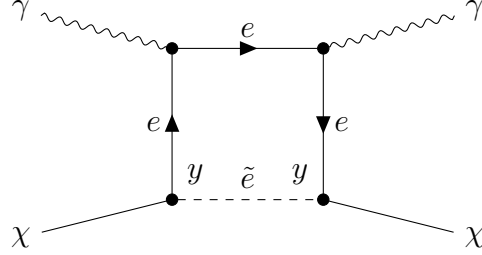
But since it has terms with y^2 and e^2 it will be highly suppressed compared to the inelastic scattering. Therefore we neglected this term´. But one can calculate his diagram as future work.

Next, we want to consider the inelastic scatterings for the case where η is a scalar doublet under $SU(2)_L$. As doublet it can interact with the gauge bosons W^+, W^- and Z. Here, we once again want to look at the scenario of the t-channel mediator with Yukawa coupling y and small mass splitting between the scalar doublet η and the Majorana singlet χ. The two inelastic channels that we have are $\chi\nu \to \eta^0 Z$ and $\chi\nu \to \nu^- W^+$ or $\chi\nu \to \eta^+ W^-$. The diagrams of these processes are shown in Fig. 6.20 and Fig. 6.21.
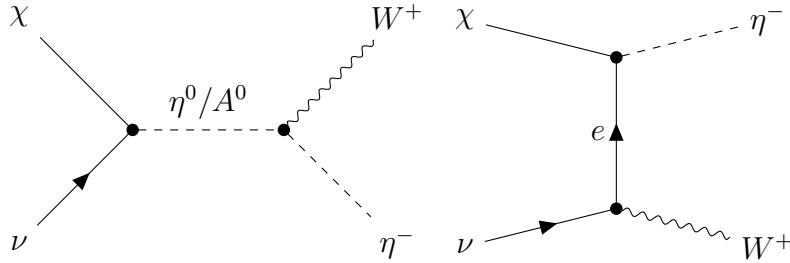
Figure 6.20: Feynman diagram of the $\nu\chi \longrightarrow \eta^- W^+$ scattering in the t-channel mediator model.
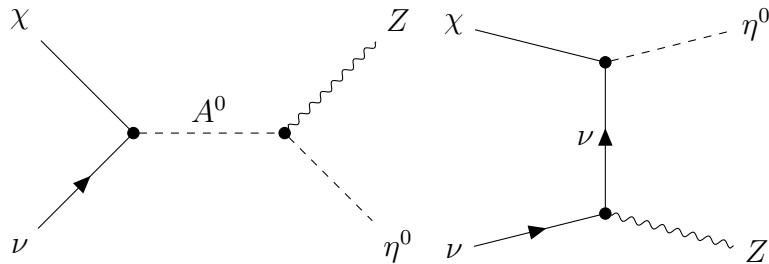
Figure 6.21: Feynman diagram of the $\nu\chi \longrightarrow \eta^0 Z$ scattering in the t-channel mediator model. Note that we can not have a s channel with η^0 because the $\eta^0\eta^0 Z$ vertex is forbidden by parity. See the Appendix in [101] for the Feynman rules.

The cross section of the process $\nu\chi \to \eta^- W^+$ is given by

$$\frac{d\sigma}{dt}\bigg|_{\nu\chi\to\eta^- W^+} = \frac{e^2 y^2}{128\pi t^2 m_W^2 (s-m_{\eta^0}^2)^2 (s-m_\chi^2)^2 \sin^2\theta_W}\cdot$$
$$\Bigg[m_W^4 \big(4m_{\eta^0}^2(m_\eta^2 s + m_\chi^2(t-s) - st) + 2m_{\eta^0}^4(-m_\eta^2 + m_\chi^2 + t)$$
$$- 2m_\eta^2 s^2 + 2m_\chi^2 s^2 - 4m_\chi^2 st - m_\chi^2 t^2 + 2s^2 t + st^2\big)$$
$$+ 2tm_W^2 \big(m_\eta^2(m_\chi^2(2s+t) - s(s+t)) + m_{\eta^0}^2(-2m_\eta^2 m_\chi^2 + 2m_\chi^4$$
$$- m_\chi^2(2s+t) + s(2s+t)) + m_{\eta^0}^4(m_\eta^2 - s - t)$$
$$- s(2m_\chi^4 - 2m_\chi^2(s+t) + s(s+t))\big) - (m_\eta^2 - m_{\eta^0}^2)^2 t^2 (m_\chi^2 - s)\Bigg]$$

(6.69)

Note that we have set the mass of the electron $m_e = 0$ because it is small compared to the other masses. Furthermore, we already expressed u in terms of s, t and the masses m_χ, m_η and m_W where m_η the mass of the charged component of the doublet η. Furthermore, we focused on the diagram, where the η^0 is the mediator for simplicity. Including the diagram with the pseudoscalar A^0 as mediator is left over for future work. Once again, θ_W is the Weinberg angle with $\cos\theta_W = m_W/m_Z$ and $e = g\sin\theta_W$ with g being the gauge coupling.

The cross section of the analogous process $\nu\chi \to \eta^0 Z$ reads

$$\frac{d\sigma}{dt}\bigg|_{\nu\chi\to\eta^0 Z} = \frac{e^2 y^2}{256\pi t^2 m_Z^2 (s-m_{A^0}^2)^2 (s-m_\chi^2)^2 \sin^2\theta_W \cos^2\theta_W}\cdot$$
$$\Bigg[m_Z^4 \big(2m_{A^0}^4(-m_{\eta^0}^2 + m_\chi^2 + t) + 4m_{A^0}^2(m_{\eta^0}^2 s + m_\chi^2(t-s) - st)$$
$$- 2m_{\eta^0}^2 s^2 + 2m_\chi^2 s^2 - 4m_\chi^2 st - m_\chi^2 t^2 + 2s^2 t + st^2\big)$$
$$- 2tm_Z^2 \big(m_{A^0}^4(-m_{\eta^0}^2 + s + t) + m_{A^0}^2(2m_{\eta^0}^2 m_\chi^2 - 2m_\chi^4 + m_\chi^2(2s+t)$$
$$- s(2s+t)) + m_{\eta^0}^2(s(s+t) - m_\chi^2(2s+t)) + s(2m_\chi^4 - 2m_\chi^2(s+t)$$
$$+ s(s+t))\big) - t^2(m_{A^0}^2 - m_{\eta^0}^2)^2 (m_\chi^2 - s)\Bigg],$$

(6.70)

where we have once again replaced u with s, t, m_χ, m_η^0 and m_Z. Note that this cross section has an additional $\cos^2\theta_W$ in the denominator due to the coupling of the Z boson to the neutrino. The Z bosons couples with $e/(2\sin\theta_W \cos\theta_W)$ while the W couples with $e/(\sqrt{2}\sin\theta_W)$. This is also the reason why the cross section of the Z process is divided by 256 instead of 128. We can again integrate over dt with Python to obtain the full cross section. This is shown in Fig. 6.22.

In Fig. 6.22 we can see both cross section for the inelastic scattering between the dark matter particle χ and the neutrino into a final state with a Z or W boson. Two cases are shown for $m_\chi = 100$ GeV and $m_\eta = 105$ GeV (left panel) and $m_\chi = 100$ GeV and $m_\eta = 200$ GeV (right panel). For simplicity we assumed that all masses of the $SU(2)_L$ doublet are the same and given by m_η. The only difference between these two cases is that the cross section shifts to larger energies as the mass m_η increases and that the cross section is more suppressed due to the higher mass of
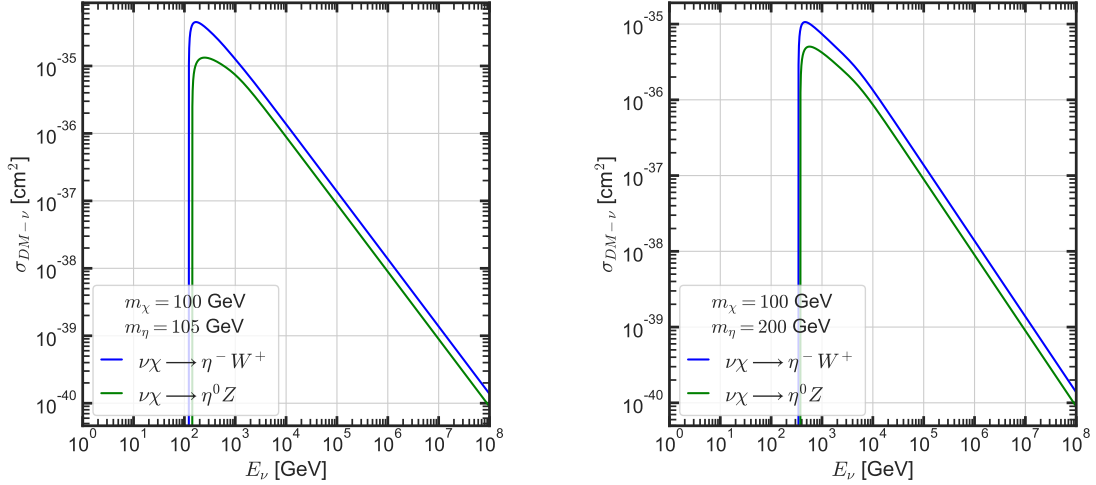
Figure 6.22: *Left panel*: The figure shows the scattering cross section $\nu\chi \longrightarrow \eta^0 Z$ and $\nu\chi \longrightarrow \eta^- W^+$. Here we choose $m_\chi = 100$ GeV, $m_\eta = 105$ and $y = 0.7$. For simplicity the masses of the η doublet are set equal so that $m_{\eta^0} = m_{A^0} = m_\eta = 105$ GeV. *Right panel*: The same cross section than the left panel but with $m_\chi = 100$ GeV, $m_{\eta^0} = m_{A^0} = m_\eta = 200$ GeV and $y = 0.7$.

m_η. The cross section shifts to larger energies because the channel opens when $\sqrt{s} > m_{W/Z} + m_\eta$ which translates into $E_\nu > ((m_{W/Z} + m_\eta)^2 - m_\chi^2)/(2m_\chi)$. For large energies, where $E_\nu \gg m_\eta$, we obtain the following behaviour for the cross sections:

$$\sigma|_{\nu\chi \longrightarrow \eta^- W^+} \widetilde{\approx} \frac{e^2 y^2}{128\pi E_\nu m_\chi \sin^2\theta_W} \tag{6.71}$$

$$\sigma|_{\nu\chi \longrightarrow \eta^0 Z} \widetilde{\approx} \frac{e^2 y^2}{256\pi E_\nu m_\chi \sin^2\theta_W \cos^2\theta_W} \tag{6.72}$$

Hence, both cross sections scale with E_ν^{-1} for large energies and only depend on the unknown dark matter mass m_χ. We also remark that for large energies $\sigma|_{\nu\chi \longrightarrow \eta^- W^+} = (\cos^2\theta_W/2) \cdot \sigma|_{\nu\chi \longrightarrow \eta^0 Z}$. This relation can be understand physically. The diagrams in Fig. 6.20 and Fig. 6.21 are $SU(2)_L$ related. The Lorentz structure of the particles is identical. The only difference are the masses and the charge which are irrelevant for high energies. Hence, it makes sense that both processes have the same scaling behaviours and the simple relation for large energies.

Note that we could also plot the cross section for larger values of m_χ and m_η, namely for $m_\chi = 1$ TeV and $m_\eta = 10$ TeV. But the graphs would look identical. The only difference would be that the value for the cross section decreases and gets shifted to larger energies because the channel opens for larger energies. It would not give more insights as we now so far. That is why we do not treat this case here, unlike in the elastic scattering. We obtain larger cross sections for lower dark matter and mediator masses.

Let us also take a look at the cross section for different mass splittings in the $SU(2)_L$ doublet. The masses of m_{η^-}, m_{η^0} and m_{A^0} are strictly speaking not identical. So, lets keep the dark matter mass m_χ fixed and vary the scalar doublet masses. We
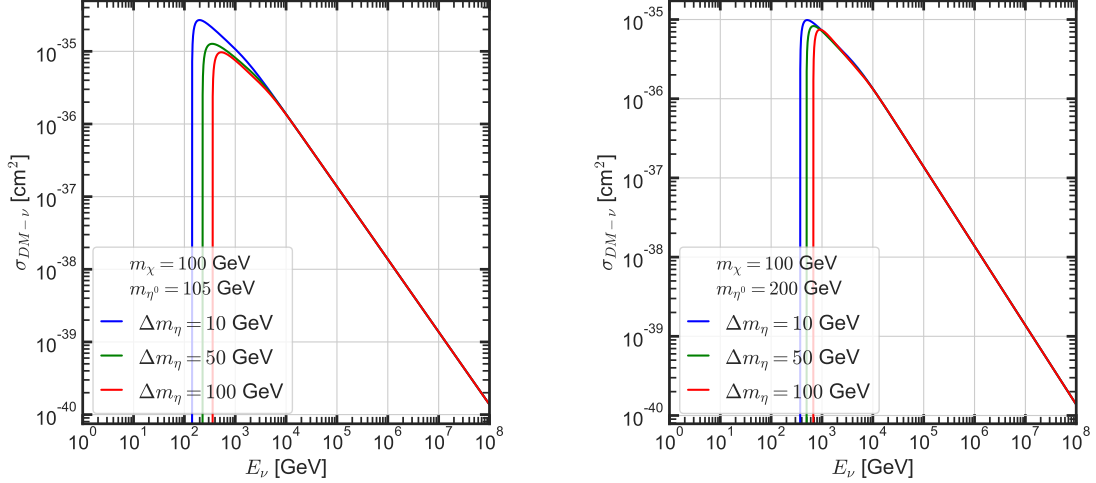
Figure 6.23: *Left panel*: Cross section of $\nu\chi \longrightarrow \eta^- W^+$ with $m_\chi = 100$ GeV the dark matter mass, $m_{\eta^0} = 105$ GeV and $y = 0.7$ as function of the neutrino energy E_ν. The cross section is shown for three different mass splittings $\Delta m_\eta = m_{\eta^-} - m_\eta^0$.*Right panel*: The same cross section than the left panel but with $m_\chi = 100$ GeV and $m_{\eta^0} = 200$ GeV.

define the mass splitting $\Delta m_\eta = m_{\eta^-} - m_\eta^0$ and $\Delta m_{A^0} = m_{A^0} - m_{\eta^0}$. The results of the mass splitting are shown in Fig. 6.23 and in Fig. 6.24.

So, in Fig. 6.23 we can see the the cross section of the $\nu\chi \to \eta^- W^+$ process with the dark matter mass $m_\chi = 100$ GeV and the mass of the neutral component of the scalar doublet $m_{\eta^0} = 105$ GeV (left panel) and $m_{\eta^0} = 200$ GeV (right panel). The three different colours stand for the mass splittings of $\Delta m_\eta = 10$ GeV (blue), $\Delta m_\eta = 50$ GeV (green) and $\Delta m_\eta = 100$ GeV (red). We can see that the mass splitting only is relevant for energies lower than 10^3 GeV. But even there the cross section does not change in one order of magnitude. For large energies above 10^3 GeV the mass splitting is totally irrelevant. If we increase the mass of the η^0 particle, the mass splitting does not play a significant role anymore and gets more negligible. Hence, we can set the masses of the η^0 and the charged η^- to be equal with a clear conscience.

In Fig. 6.24 we can see the the cross section of the $\nu\chi \longrightarrow \eta^0 Z$ process with the dark matter mass $m_\chi = 100$ GeV and the mass of the neutral component of the scalar doublet $m_{\eta^0} = 105$ GeV (left panel) and $m_{\eta^0} = 200$ GeV (right panel). The two three different colours stand for the mass splittings of $\Delta m_{A^0} = 10$ GeV (blue) and $\Delta m_{A^0} = 100$ GeV (green). In both panels we see an interesting feature which is due to the resonance peak of the s channel, namely when $s = m_{A^0}$. This feature becomes visible when the mass splitting Δm_{A^0} is at the order of m_Z. We know that the inelastic channel is kinematically allowed when $\sqrt{s} > m_{\eta^0} + m_Z$. This gives a threshold energy of $E_{\text{th}} = ((m_{\eta^0} + m_Z)^2 - m_{\eta^0}^2)/(2m_{\eta^0})$. The cross section hits the resonance when $E_{\text{res}} = (m_{A^0}^2 - m_\chi^2)/(2m_\chi)$. By demanding that $E_{\text{res}} > E_{\text{th}}$ we obtain that $m_{A^0} > m_{\eta^0} + m_Z$ which we can further simplify to $\Delta m_{A^0} > m_Z$. Therefore, when the mass splitting Δm_{A^0} is larger than the mass of the Z boson we get a resonance peak in our inelastic cross section. Such features are always nice to have. But unfortunately, we do not expect such high mass splittings between the
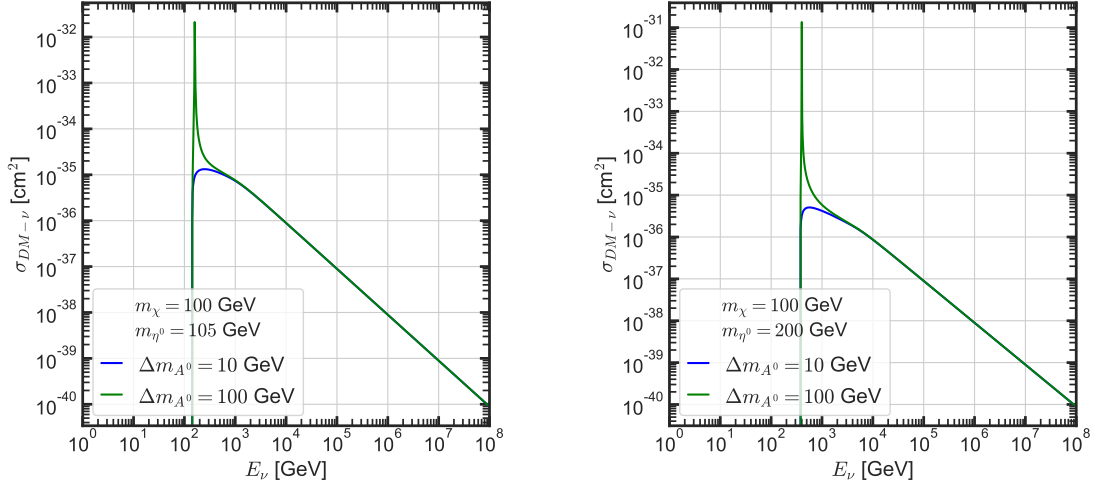
Figure 6.24: *Left panel*: Cross section of $\nu\chi \longrightarrow \eta^0 Z$ with the dark matter mass $m_\chi = 100$ GeV, the scalar particle mass $m_{\eta^0} = 105$ GeV and $y = 0.7$ as function of the neutrino energy E_ν. The cross section is shown for three different mass splittings $\Delta m_{A^0} = m_{A^0} - m_{\eta^0}$ between the scalar η^0 and the pseudoscalar A^0. *Right panel*: The same cross section than the left panel but with $m_\chi = 100$ GeV and $m_{\eta^0} = 200$ GeV.

scalar η^0 and the pseudoscalar A^0 [100, 101].

So, as expected the mass splitting does not play a crucial role for the cross section despite of the resonant peak. Hence, it is a good approximation to set the masses equal.

In the end, we are only interested in the rate of absorption that comes from the inelastic scattering between the neutrinos and the dark matter particles (see ch. 6.5). Therefore, we are only interested in the total inelastic cross section. The final state is irrelevant for the absorption rate. Also, the final states are distinguishable from each other and we do not expect them to interfere among themselves. Thus, we can express the total cross section as a incoherent sum of the processes which reads

$$\sigma_{\text{DM}-\nu}^{\text{tot}} = \sigma_{\nu\chi\to\eta^- W^+} + \sigma_{\nu\chi\to\eta^+ W^-} + \sigma_{\nu\chi\to\eta^0 Z} \tag{6.73}$$

Note that we could also have the channel of $\nu\chi \to A^0 Z$ which we did not treat in our analysis. Including this channel is left over for future work. So finally, we can simply add all of the inelastic channels together. The result is shown in Fig. 6.25.

In Fig. 6.25 we can see the total inelastic cross section of the scattering between the dark matter particle χ and the neutrino ν as a function of the neutrino energy E_ν for a dark matter mass $m_\chi = 100$ GeV (left panel) and $m_\chi = 300$ GeV (right panel). We varied the mass of the scalar doublet m_η between 105 GeV and 400 GeV in the left and between 450 GeV and 900 GeV in the right panel. We set all masses of the η doublet equal. The variations correspond to the cases of $m_\eta/m_\chi - 1 = 0.5, 1, 2$ in the right panel and to $m_\eta/m_\chi - 1 = 0.05, 1, 3$ in the left panel. Note that for some of the cases we have to chose a different value of the Yukawa coupling y (see Fig. 6.5). For the cases where the Yukawa coupling lies between $y = 1 - 2$ we chose that $y \approx 1.5$. We see in both panels that for large energies the total inelastic cross section is independent of the scalar doublet mass m_η and only depends on the dark
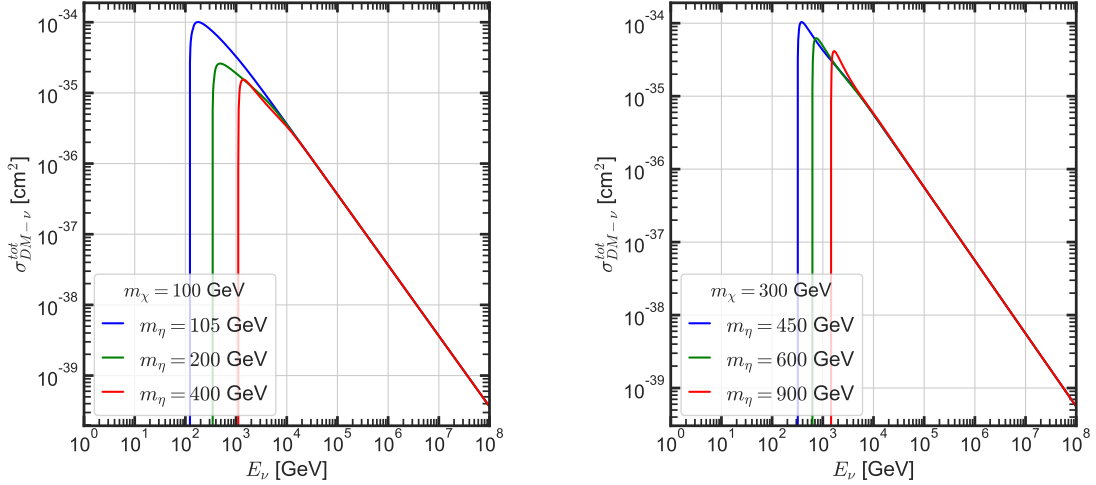
Figure 6.25: *Left panel*: The total inelastic cross section of the scattering between the neutrinos and the dark matter particle χ with $m_\chi = 100$ GeV. We set all masses of the η doublet to be equal at $m_\eta = 105$ GeV (blue curve), $m_\eta = 200$ GeV (green curve) and $m_\eta = 450$ GeV (red curve). *Right panel*: Also, the total inelastic cross section of the scattering between the neutrinos and χ but for $m_\chi = 300$ and $m_\eta = 450$ GeV (blue curve), $m_\eta = 600$ GeV (green curve) and $m_\eta = 900$ GeV (red curve). Note that in this mass regime the value of the Yukawa coupling y ranges between $y = 1 - 2$ (see Fig. 6.5) and we therefore chose $y \approx 1.5$.

matter mass m_χ, as expected. The cross section decreases with E_ν^{-1} because all of the separate cross sections decrease with E_ν^{-1} for large energies. We can approximate the cross section by

$$\sigma_{\text{DM}-\nu}^{tot}\bigg|_{E \gg m_\eta} \approx 2.5 \cdot 10^{-2} \frac{y^2}{E_\nu m_\chi}. \tag{6.74}$$

The cross section in the high energy regime depends linearly on m_χ and therefore weakens when increasing m_χ. The cross section on the right panel is also slightly lager because the Yukawa coupling y is larger than in the left panel even though the dark matter mass is larger. We also want to highlight that the cross section only depends on two unknown variables, namely y and m_χ in the high energy regime. This is interesting to know because on excepts neutrinos from AGNs to be emitted at the order of several TeVs [81, 82]. Thus, for neutrinos from AGNs we are left with two unknown parameters. We further remark that the cross section scales with y^2. To achieve high values for the cross section one either needs large Yukawa couplings or small dark matter masses which can be realised in the t-channel mediator model.

6.5   Flux Attenuation of the Neutrinos or Photons

Ultimately, we are interested in the rate of absorption and therefore in the total cross section. For the total inelastic cross section the final state is irrelevant. The final states are indistinguishable from each other and do not interfere. Therefore, the total cross section is an incoherent sum of the rates. With this cross section we can determine the absorption rate.

Remember, that we can approximate the reduction of the neutrino or photon flux in the vicinity of a black hole by (see ch. 5.4):

$$\frac{\Phi_\nu^{\text{obs}}}{\Phi_\nu^{\text{em}}} = e^{-\mu_\nu} = e^{-\frac{\sigma_{\text{DM-}\nu}\Sigma_{\text{DM}}}{m_{\text{DM}}}}. \qquad (6.75)$$

This equation results from the cascade equation which can be simplified for the case of inelastic scattering because we do not have any final neutrino energy E_ν' anymore. Let us start our investigations for the absorption rate with the case of fermionic dark matter χ and then continue with the scalar dark matter η. Note, that we switch the order.

6.5.1 Fermionic Dark Matter

We are now in the position that we have the total inelastic cross section for the interaction between ν and χ shown in Fig. 6.25. Furthermore we can approximate the dark matter density as a dense dark matter spike with Eq. 5.21. So, let us take the column density of the blazar TXS 0506 + 056 (see Fig. 5.4) and evaluate Eq. 6.75 as a function of the neutrino energies E_ν. The result is shown in Fig. 6.26.
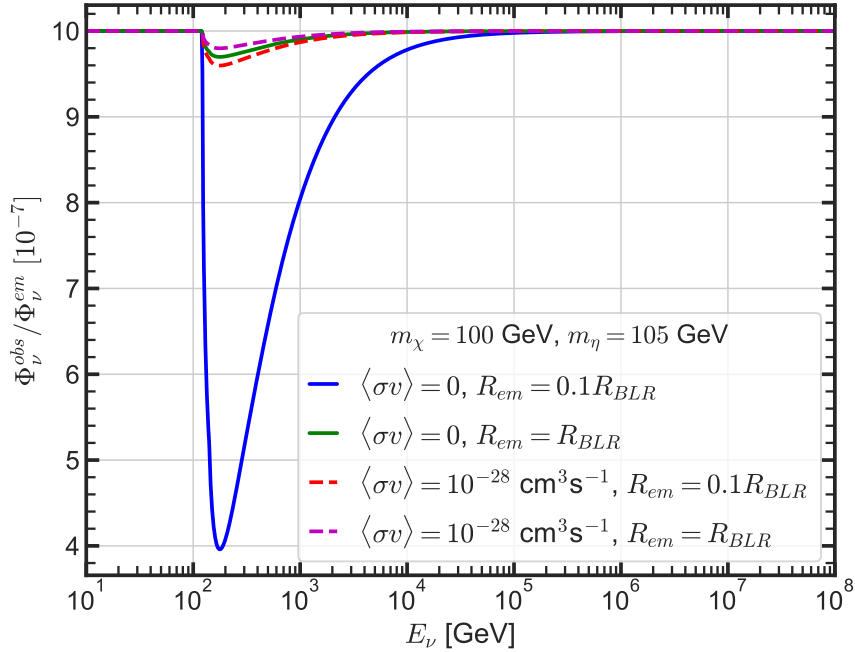
Figure 6.26: Flux attenuation of the neutrinos in vicinity of the blazar TXS 0506 + 056 as a function of the neutrino energy E_ν for. The column density given by Fig. 5.4.

In Fig. 6.26 we can see that the rate of absorption of the total inelastic scattering between the neutrino and the dark matter particle χ. The dark matter mass was chosen to be $m_\chi = 100$ GeV and $m_\eta = 105$ GeV is the mass of the $SU(2)_L$ doublet, where we set all of the masses in the doublet to be equal. The four different colours indicate four different column densities, due to the emission region R_{em} of the neutrino and the annihilation cross section of the dark matter particles. Note that the y-axis only shows magnitude of 10^{-7}. Hence, for the balzar TXS 0506+056

we only have an impact on the absorption in the seventh digit. Thus, we can clearly say that we would not expect any reduction of the neutrino flux on earth with our t-channel mediator model for the blazar TXS $0506 + 056$. The column density of TXS $0506 + 056$ is simply to small. Therefore, we do not have a sizeable interaction between the dark matter particles and the neutrinos.

However, we can continue our investigations by varying the column density of the dark matter mass Σ_{DM}. The result is shown in Fig. 6.27.
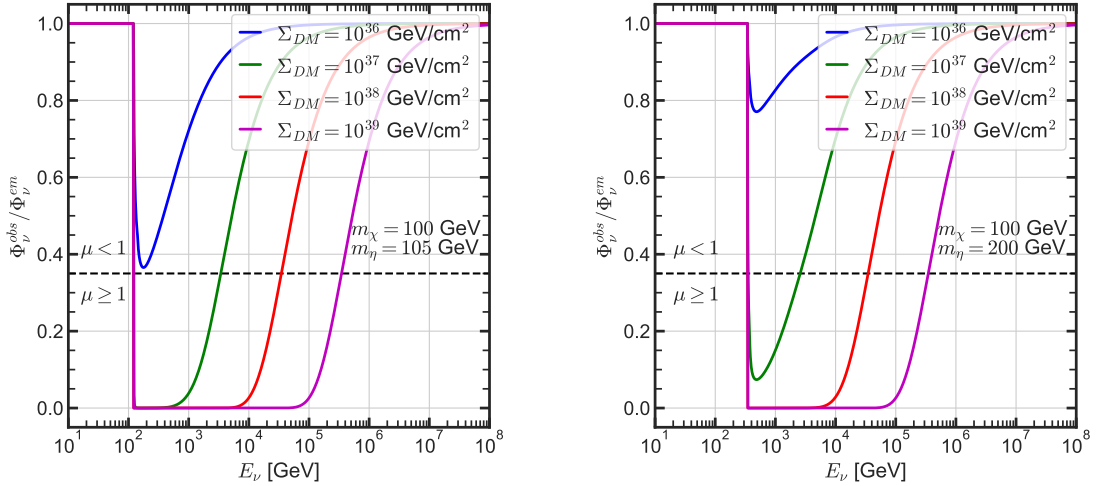
Figure 6.27: *Left panel*: The observed neutrino flux normalised to the emitted neutrino flux as a function of the neutrino energy E_ν given by Eq. (6.75). The cross section was calculated with Eq. (6.73) for a dark matter mass of $m_\chi = 100$ GeV and a scalar doublet mass of $m_\eta = 105$ GeV. All of the masses of the scalar doublet are chosen to have the same mass. *Right panel*: The same than in the left panel but with $m_\eta = 200$ GeV.

In Fig. 6.27 we used Eq. (6.75) together with the cross section of Eq. (6.73) for both panels. We show the emitted neutrino flux over the observed neutrino for different values of the dark matter column density Σ_{DM}, namely $\Sigma_{\mathrm{DM}} = 10^{36}, 10^{37}, 10^{38}, 10^{39}$ GeV/cm^2. For both panels we use $m_\chi = 100$ GeV and chose $m_\eta = 105$ GeV for the left panel and $m_\eta = 200$ GeV for the right one. In the high energy regime the mass differences of the η particles is irrelevant for the cross section. That is why we have chosen all of the masses of the η doublet to be equal. We can see that the absorption starts for $E_\nu > 10^2$ GeV because the inelastic channel is kinematically forbidden before. In the left panel the absorption is over 90% for $E_\nu \sim 10^2 - 10^3$ GeV for $\Sigma_{\mathrm{DM}} = 10^{37}$ GeV/cm^2, between $E_\nu \sim 10^2 - 10^4$ GeV if $\Sigma_{\mathrm{DM}} = 10^{38}$ GeV/cm^2 and between $E_\nu \sim 10^2 - 10^5$ GeV if $\Sigma_{\mathrm{DM}} = 10^{39}$ GeV/cm^2.

If we want to have the attenuation coefficient at least at order one or greater we demand that $\Phi_\nu^{\mathrm{obs}}/\Phi_\nu^{\mathrm{em}} \leq 0.35$. Which is an absorption rate of at least 65%. This is indicated in Fig. 6.27 as dashed line which separates the plot in a regime where $\mu < 1$ and $\mu \geq 1$. For the scenario of $m_\chi = 100$ GeV and $m_\eta = 105$ GeV this is realised between 100 GeV and a few TeV if $\Sigma_{\mathrm{DM}} = 10^{37}$ GeV/cm^2, between 100 GeV and several 10 TeV if $\Sigma_{\mathrm{DM}} = 10^{38}$ GeV/cm^2, between 100 GeV and several 100 TeV if $\Sigma_{\mathrm{DM}} = 10^{39}$ GeV/cm^2. For the scenario of $m_\chi = 100$ GeV and $m_\eta = 200$ GeV between 200 GeV and 3 TeV if $\Sigma_{\mathrm{DM}} = 10^{38}$ GeV/cm^2, between 200 GeV and 30 TeV

Neutrino energy E_ν range for an absorption rate of at least 65%						
m_χ [GeV]	m_η [GeV]	Σ_{DM} [GeV/cm^2]	μ	$\Phi^{\text{obs}}/\Phi^{\text{em}}$	E_ν [TeV]
100	105	10^{36}	≥ 1	≤ 0.35	0
		10^{37}	≥ 1	≤ 0.35	$0.12 - 3.5$
		10^{38}	≥ 1	≤ 0.35	$0.12 - 35$
		10^{39}	≥ 1	≤ 0.35	$0.12 - 350$
	200	10^{36}	≥ 1	≤ 0.35	0
		10^{37}	> 1	≤ 0.35	$0.34 - 2.5$
		10^{38}	≥ 1	≤ 0.35	$0.34 - 35$
		10^{39}	≥ 1	≤ 0.35	$0.34 - 350$

Table 6.1: Summary of the neutrino energy range E_ν for which we have at least an absorption of 65% for the inelastic scattering with the dark matter particle χ.

and between 200 GeV and 300 TeV if $\Sigma_{\text{DM}} = 10^{39}$ GeV/cm^2. In both scenarios the rate of absorption is below 65% for 100 TeV if $\Sigma_{\text{DM}} < 10^{37}$ GeV/cm^2. A concrete summary of the energies ranges can be found in Tab. 6.1. For lower dark matter densities than $\Sigma_{\text{DM}} = 10^{37}$ GeV/cm^2 the rate of absorption is for both scenarios not sufficient enough to probe the model.

One expects blazars to emit neutrinos in the regime of several hundreds of TeV. To achieve absorption for neutrino energies of hundred TeV one has to increase the dark matter column density up to $\Sigma_{\text{DM}} = 10^{39}$ GeV/cm^2. This is nearly ten orders of magnitude larger than the dark matter spike that we expected around the blazar TXS $0506 + 056$ [3]. In the case of the galaxy NGC we might have larger column density than for TXS $0506 + 056$ [4] but still the spike density is less than 10^{32} GeV/cm^2 which is still 5 to 6 orders of magnitude lower than we need. Nevertheless, it could still be possible that there are AGNs in the universe that have a large enough column density to probe the t-channel mediator model but it has yet to be found. We also want to mention that the formation of a spike is rather unclear and that it is covered with a lot of astrophysical uncertainties. So, once again, particle physicists have to rely on astrophysicists and both have to work together. Note that we also did not include the inelastic scattering channel of the Scale Invariant Scotogenic Model which can be included in a future work. Let us now look at the dark matter-photon interaction.

We can do the same analysis for the photon and dark matter interaction. Remember, that in this case the η is a singlet under $SU(2)_L$ and interacts with the right handed fermions. The total inelastic cross section is also a sum of the single processes and given by

$$\sigma^{\text{tot}}_{\text{DM}-\gamma} = \sigma_{\chi\gamma \to \tilde{e}^+ e^-} + \sigma_{\chi\gamma \to \tilde{e}^- e^+}, \tag{6.76}$$

where we once again have chosen the η singlet to be the selectron. We will also denote the mass of the selctron with m_η to highlight that the η must not be the selectron.

As for the neutrinos, we can investigate if the column density of the TXS $0506 + 056$ is large enough to deplete the photon flux sufficiently. The result is shown in Fig. 6.28.
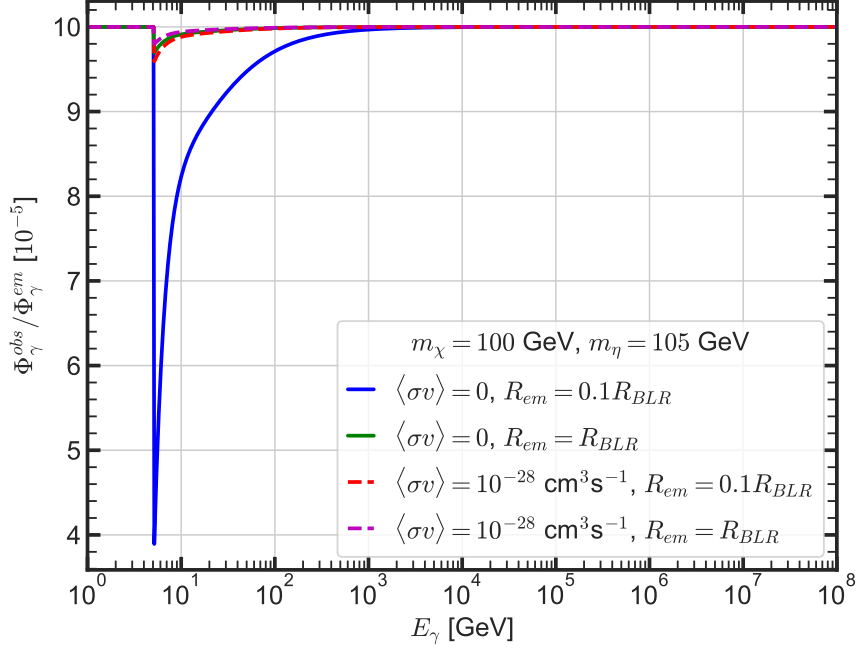
Figure 6.28: Flux attenuation of the photons in vicinity of the blazar TXS $0506 + 056$ as a function of the photon energy E_γ. The column density given by Fig. 5.4.

In Fig. 6.28 we show the expected photon flux divided by the emitted photon flux for different emission regions and annihilation cross sections. Due to the different emission regions and the annihilation cross sections, the column density for the photon changes (see Fig. 5.4). We see one again that the flux only gets attenuated in the 5th digit which is too small for sizeable absorption effects. Nevertheless, we can continue with the analysis by looking at different values of the column density for fixed dark and mediator mass.

So let us vary the column density Σ_{DM}. We once again assume that the model is probable if the attenuation coefficient is at least at the order of one. The rate of absorption is shown in Fig. 6.29 for different values of the column density Σ_{DM}.

So, in Fig. 6.29 we see the rate of absorption due to the inelastic scattering between the dark matter particle χ with the photons. The rate of absorption is energy dependent because the cross section depends on the energy. The absorption rate is shown for four different column densities Σ_{DM}. The absorption begins as the channels opens kinematically. In the left panel we have chosen $m_\chi = 100$ GeV and $m_\eta = 105$ GeV and $m_\chi = 100$ GeV with $m_\eta = 200$ GeV in the right panel. We demand that the rate of absorption is once at least 65% which is indicated with the dashed black line. For $\Sigma_{DM} = 10^{36}$ GeV/cm^2 we have over 65% absorption between $E_\gamma \sim 5 - 10^3$ GeV in the left panel and between $E_\gamma \sim 150 - 630$ GeV in the right panel. Consequently, as the column density increases by one order of magnitude, also the energy range for the absorption increases by one order of magnitude. A summary of the photon energy ranges is shown in Tab. 6.2. The total inelastic cross section is independent of the mediator mass m_η for large energies. Thus, only the lower limit of the energy range for an absorption greater than 65% changes but not the upper limit. For a dark matter column density Σ_{Dm} at the order of 39, the absorption rate is greater than 65% for energies up to even $E \sim 10^3$ TeV.
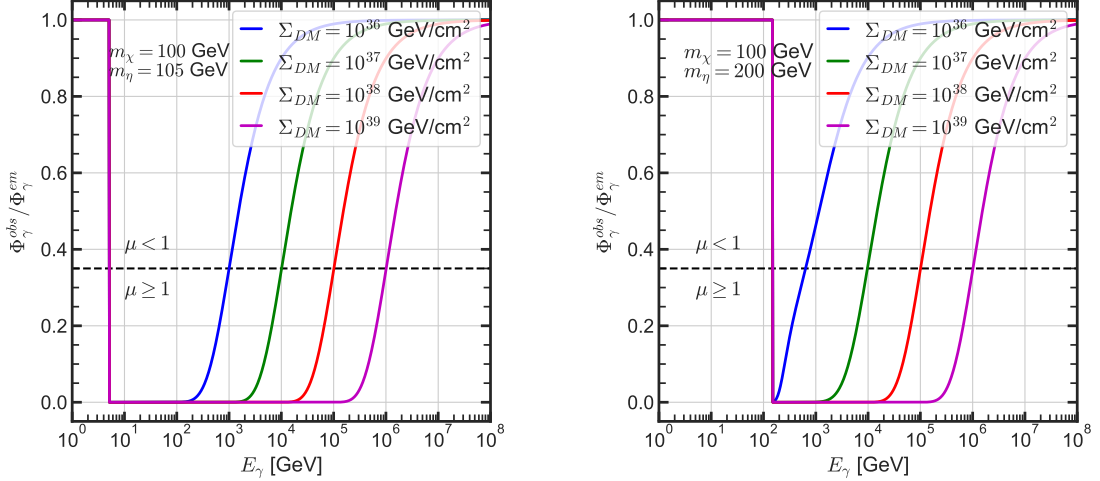
Figure 6.29: *Left panel*: The observed gamma-ray flux normalised to the emitted gamma-ray flux as a function of the photon energy E_γ given by Eq. (6.75) for the total inelastic scattering between γ and χ with $m_\chi = 100$ GeV and $m_\eta = 105$ GeV. Note that here η is a singlet under $SU(2)_L$. *Right panel*: The same than in the left panel but with $m_\eta = 200$ GeV.

Photon energy range E_γ for an absorption rate of at least 65%					
m_χ [GeV]	m_η [GeV]	$\Sigma_{\rm DM}$ [GeV/cm^2]	μ	$\Phi^{\rm obs}/\Phi^{\rm em}$	E_ν [TeV]
100	105	10^{36}	≥ 1	≤ 0.35	$0.005 - 1$
		10^{37}	≥ 1	≤ 0.35	$0.005 - 10$
		10^{38}	≥ 1	≤ 0.35	$0.005 - 100$
		10^{39}	≥ 1	≤ 0.35	$0.005 - 1000$
	200	10^{36}	≥ 1	≤ 0.35	$0.15 - 0.63$
		10^{37}	> 1	≤ 0.35	$0.15 - 10$
		10^{38}	≥ 1	≤ 0.35	$0.15 - 100$
		10^{39}	≥ 1	≤ 0.35	$0.15 - 1000$

Table 6.2: Summary of the photon energy range E_γ for which we have at least an absorption of 65% for the inelastic scattering with the dark matter particle χ.

In summary, we have seen that for the dark matter interaction with neutrinos or photons we could have an rate of absorption over 65%. Nevertheless, the column density in both cases must be at least 8 magnitudes larger than the column density of the balzar TXS $0506 + 056$. We can try to estimate the black hole mass that one needs in order to obtain such a large column density. If we assume that the dark matter profile is a NFW profile with $\gamma = 1$ and a spike parameter of $y_{\rm sp} = 7/3$, we can use Eq. 5.20 to evaluate the black hole mass. We can naively take the values of the TXS $0506 + 056$ for ρ_0, r_0, α_γ together with $R_{\rm em} = R_{\rm BLR} \sim 0.021$ pc. By rearranging the equation we obtain $M_{\rm BH} \sim 10^{18} M_\odot$ if $\Sigma_{\rm DM} = 10^{36}$ GeV/cm^2 and $M_{\rm BH} \sim 10^{23} M_\odot$ if $\Sigma_{\rm DM} = 10^{39}$ GeV/cm^2. Which is larger than the currently known supermassive black holes of about $10^{10} - 10^{11} M_\odot$ [114, 115]. It is questionable if a black hole even can be that big because there exist theoretical limits on the growth of a black hole [116]. Nonetheless, it might be possible that in our universe there

exits so called stupendously large black holes which masses exceed $M_\odot > 10^{11} M_\odot$ [117]. But they have never been observed and it is far from being clear, if they reach such high masses of $10^{18} M_\odot$.

We could also try to increase the spike parameter in order to achieve a higher dark matter column density for lower black hole masses. If we take $\gamma = 4/3$, we obtain $\gamma_{\mathrm{sp}} = 19/8$. Together with Eq. (5.21), the values of TXS 0506 + 056 and $R_{\mathrm{em}} = R_{\mathrm{BLR}}$ we can again evaluate the black holes mass. We obtain the range of $M_{\mathrm{BH}} \sim 10^{18} - 10^{22} M_\odot$ which is more or less the same result from above with $\gamma_{\mathrm{sp}} = 7/3$. So, varying the spike parameter is not promising.

Note, that there are many more uncertainties to play with. The emission region R_{em} and the normalisation factor ρ_0, for example. But checking on all of these quantities is left over for future work and will not be treated in this master thesis. We just want to highlight that the photon or neutrino flux can be reduced due to their interactions with the dark matter particles, at least theoretically. If dark matter column densities of the size between $10^{36} - 10^{39}$ GeV/cm^2 really exit, is a question that must be answered by astrophysicist. Maybe they will observe some large and dense astrophysical objects that could achieve such large column densities. But currently, we do not know of any AGN with such a large dark matter column density.

6.5.2 Scalar Dark Matter

After carefully looking at the fermionic dark matter candidate we now want to turn our interest to the scalar dark matter candidate η^0. We can also calculate the flux attenuation of the neutrinos, due to their inelastic scattering of the η^0 particle. But, in this case we are only left with one process because we were not able to calculate all of the processes properly. Nevertheless, we can just compute the rate of absorption due to the inelastic scattering $\eta^0 \nu \to \chi Z$. If all of the other processes are of the same magnitude we can approximate the total cross section by simply multiplying $\sigma_{\eta^0 \nu \to \chi Z}$ by a factor of 4. So, let us approximate the total cross section by

$$\sigma_{\mathrm{DM}-\nu}^{tot} = \sigma_{\eta^0 \nu \to \chi Z} + \sigma_{\eta^0 \nu \to \eta^+ e^-} + \sigma_{\eta^0 \nu \to \eta^- e^+} + \sigma_{\eta^0 \nu \to \nu A^0} \approx 4 \cdot \sigma_{\eta^0 \nu \to \chi Z}. \quad (6.77)$$

We again want to highlight that this approximation only holds, when all of the processes are of the same order of magnitude which was the case for χ as dark matter candidate. This is what inspired this assumption and is the reason why we are motivated to continue with the calculations, even though, we encountered some problems with the particular processes. However, this approximation or assumption might not be valid and is highly uncertain. On the other side, we can say that a factor of four is not expected to make a huge difference in the absorption rate because the cross section still has the same order of magnitude than for the single process of $\sigma_{\eta^0 \nu \to \chi Z}$. The crucial quantity of our analysis will again be the column density Σ_{DM}.

At first, we can once again look at the flux attenuation of the blazar TXS 0506 + 056 which is shown in Fig. 6.30. Not surprisingly, we only have an attenuation in the 7th digit. Therefore, we have no sizeable flux attenuation. This was expected because we do not have a sizeable attenuation in the case of fermionic dark matter and the cross section for scalar dark matter ins not sufficiently larger.
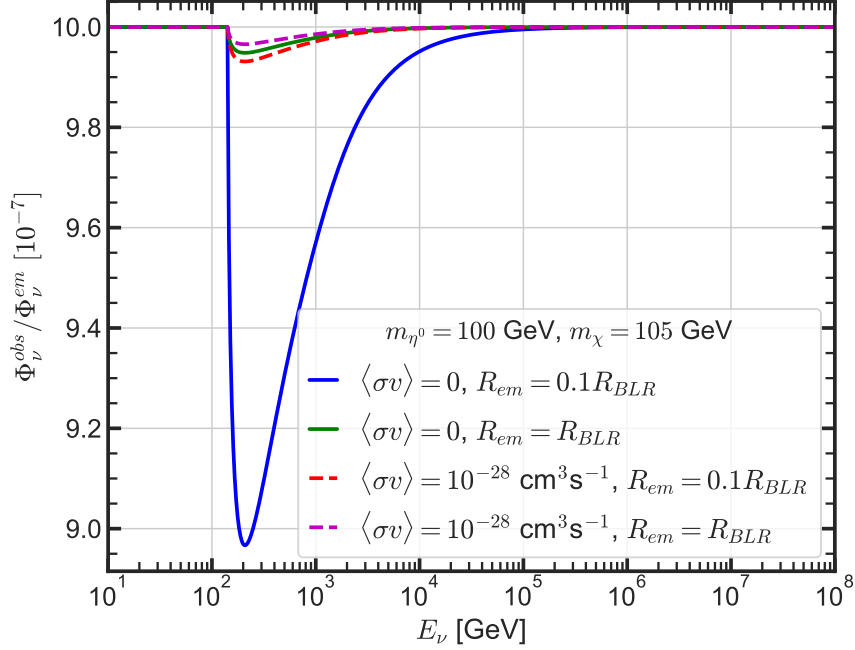
Figure 6.30: Flux attenuation of the neutrinos in vicinity of the blazar TXS 0506 + 056 as a function of the neutrino energy E_ν for the column density given by Fig. 5.4.

But, as in the fermionic case, we can continue the analysis by varying the magnitude of the dark matter column density Σ_{DM}. The result are shown in Fig. 6.31 and in Fig. 6.32.
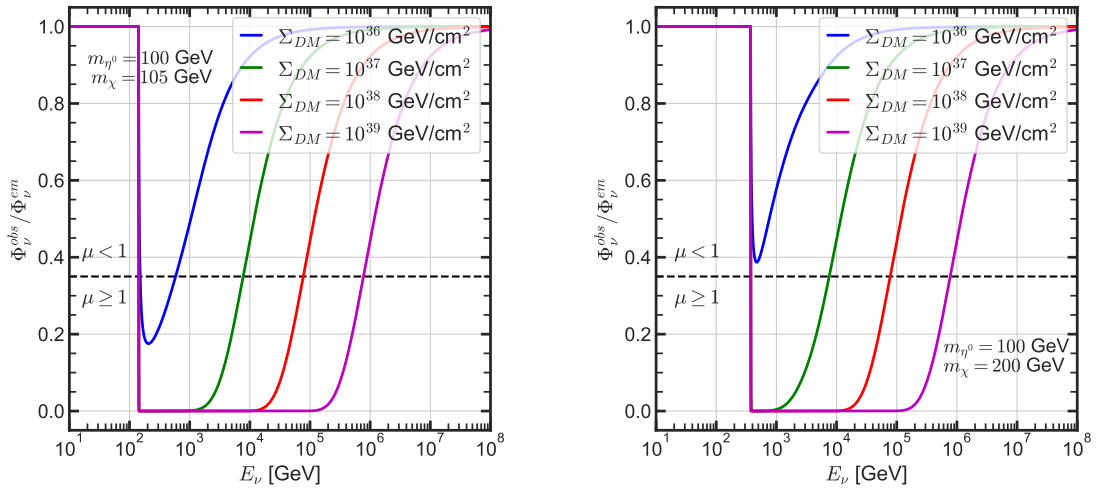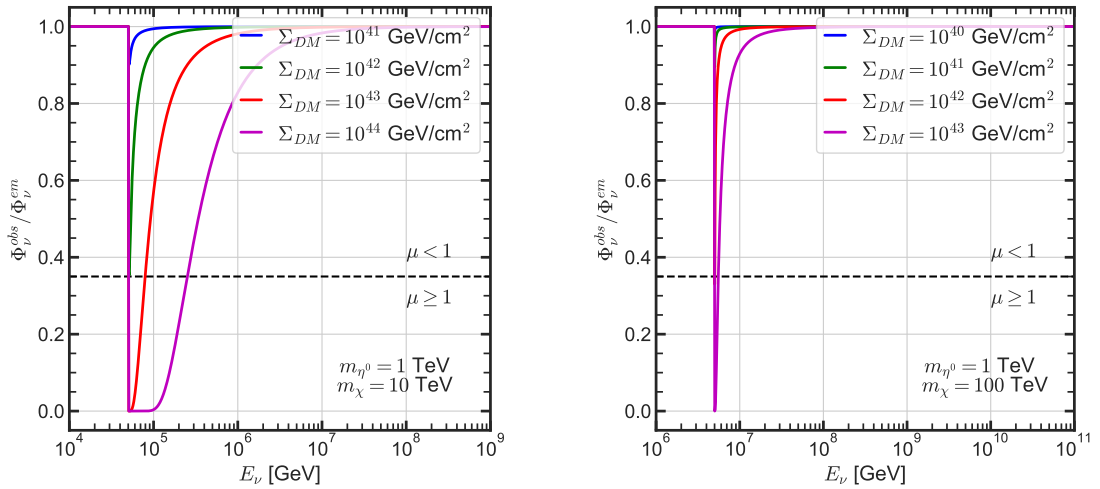

Figure 6.31: *Left panel*: The observed neutrino flux normalised to the emitted neutrino flux as a function of the neutrino energy E_ν given by Eq. (6.75) for the total inelastic scattering between the neutrino and χ with $m_{\eta^0} = 100$ GeV and $m_\chi = 105$ GeV. Note that we set the masses of the η particle to be equal for simplicity. *Right panel*: The same than in the left panel but with $m_\chi = 200$ GeV.

In Fig. 6.31 we can see the expected absorption rate of the neutrinos due to their interaction with dark matter for different values of the column density, namely

$\Sigma_{\mathrm{DM}} = 10^{36}, 10^{37}, 10^{38}, 10^{39}$ GeV/cm^2. The left panel shows the case where $m_{\eta^0} = 100$ GeV and $m_\chi = 105$ GeV and the right panel the case where $m_\chi = 200$ GeV. The dashed line indicates an absorption rate of 65% for which the attenuation coefficient needs to be at the order of one. As we increase the column density the energy range increases for which the absorption is more than 65%. Which makes sense, because the attenuation coefficient deepens linearly on the column density. The cross section is independent on the mediator mass for large energies. Also, the lower energy limit for the absorption stays the same for $\Sigma_{\mathrm{DM}} > 10^{36}$ GeV/cm^2. For $\Sigma_{\mathrm{DM}} = 10^{36}$ we only have an absorption that is greater than 65%, when the mass splitting between m_{η^0} and m_χ is $m_\chi/m_{\eta^0} < 2$.

We expect that AGNs emitt high energetic neutrinos in the range of several hundreds of TeV. To achieve an absorption in the range of $E_\nu \sim 10^2 - 10^3$ TeV we would need a column density at least of the order of 39. Note, that we have not include all of the diagrams for the scattering. We simply assumed that all of the processes are of the same order of magnitude. Hence, it could be that with the bosons as mediator we achieve larger cross sections. This would mean that we could have an absorption rate of 65% for lower dark matter densities.

We also want to quickly check the Scotogenic scenario, where the masses of the dark matter particle and the mediator lie in the range of TeV and not GeV. The result is visualised in Fig. 6.32.

Figure 6.32: *Left panel*: The observed neutrino flux normalised to the emitted neutrino flux as a function of the neutrino energy E_ν given by Eq. (6.75) for the total inelastic scattering between the neutrino and χ with $m_{\eta^0} = 1$ TeV and $m_\chi = 10$ TeV. Note that we set the masses of the η particle to be equal for simplicity. *Right panel*: The same than in the left panel but with $m_\chi = 100$ TeV.

As above, we see in Fig. 6.32 the possible flux attenuation of the neutrinos as the function of the energy E_ν. This time we have a larger dark matter mass of $m_{\eta^0} = 1$ TeV and mediator masses $m_\chi = 10$ TeV (left panel) and $m_\chi = 10^2$ TeV (right panel). Note that the column densities now vary between $10^{41} - 10^{44}$ GeV/cm^2. We can clearly see that even for this high column densities, which are 12 to 15 order large than for TXS 0506 + 056, we only have an absorption over

Neutrino energy range E_ν for an absorption rate of at least 65%					
m_{η^0} [GeV]	m_χ [GeV]	Σ_{DM} [GeV/cm^2]	μ	$\Phi^{\text{obs}}/\Phi^{\text{em}}$	E_ν [TeV]
100	105	10^{36}	≥ 1	≤ 0.35	$0.14 - 0.57$
		10^{37}	≥ 1	≤ 0.35	$0.14 - 7.5$
		10^{38}	≥ 1	≤ 0.35	$0.14 - 75$
		10^{39}	≥ 1	≤ 0.35	$0.14 - 750$
	200	10^{36}	≥ 1	≤ 0.35	0
		10^{37}	> 1	≤ 0.35	$0.37 - 7.5$
		10^{38}	≥ 1	≤ 0.35	$0.37 - 75$
		10^{39}	≥ 1	≤ 0.35	$0.37 - 750$
10^3	10^{41}	10^{41}	≥ 1	≤ 0.35	0
		10^{42}	≥ 1	≤ 0.35	0
		10^{43}	≥ 1	≤ 0.35	$50 - 80$
		10^{44}	≥ 1	≤ 0.35	$50 - 250$
	10^5	10^{41}	≥ 1	≤ 0.35	0
		10^{42}	> 1	≤ 0.35	0
		10^{43}	≥ 1	≤ 0.35	5000
		10^{44}	≥ 1	≤ 0.35	$5000 - 5500$

Table 6.3: Summary of the neutrino energy range E_ν for which we have at least an absorption of 65% for the inelastic scattering with the dark matter particle η^0. The t-channel mediator scenario is shown as well as the Scotogenic scenario

65% between 50 TeV and 250 TeV (see left panel for $\Sigma_{\text{DM}} = 10^{42}$ GeV/cm^2). If the mass splitting between the mediator and the dark matter particle is over two orders of magnitude, the absorption becomes very narrow. A summary of the energy ranges can be seen in Tab. 6.3 for the t-channel mediator scenario, as well as for the Scotogenic scenario. In the case of fermionic dark matter we have already estimated the black hole masses for column densities between $\Sigma_{\text{DM}} = 10^{36} - 10^{39}$ GeV/cm^2. We need black hole masses between $M_{\text{BH}} \sim 10^{18} - 10^{23} M_\odot$. In our universe, we know of no AGN with such a high mass.

To conclude this chapter, we have seen that absorption might also be possible for the scalar dark matter candidate η^0. But, as for the other candidate χ, we also have to pay the price of a large dark matter column density. As discussed earlier, the mass of currently known supermassive black holes are not sufficient enough to achieve such large column densities. But, it could be that we observe even larger black holes masses than currently known. Or, we discover other astrophysical objects that achieve column densities of about $\Sigma_{\text{DM}} \geq 10^{36}$ GeV/cm^2. So, let us keep our eyes open for future astrophysical observations.

Chapter 7

Conclusion

For over several decades the searches for dark matter is ongoing. But the nature of dark matter is still unknown and we have neither produced, nor detected dark matter directly or indirectly. Despite the constant efforts of physicists to solve the dark matter puzzle, there is still no proof of any dark matter model. Nevertheless, researchers will continue to do their best and mankind will sooner or later have an answer to the dark matter questions. One just hast to be patient and continue with the research.

In this master thesis we looked at dark matter interactions between neutrinos and photons and the possible flux attenuation in the vicinity of a black hole due to their scatterings. We aimed to calculate the cross section of the dark matter and neutrino interactions and investigated the flux attenuation resulting from the scatterings.

Since, this thesis is about particle dark matter we started by introducing some basic theory of particle dark matter. We have shown that WIMPs are very well motivated in theory. We discussed the production mechanism in the early universes and its exceptions. These effects could lead to larger couplings between standard model particles and the dark matter for a given dark matter mass by still giving the correct dark matter relic abundance.

After this brief introduction we discussed the possible flux attenuation of neutrinos and photons in the vicinity of black holes. Close to a black hole the dark matter profile steepens compared to the ordinary NFW profile, due to the gravitational attraction of the black hole. The result is a dense dark matter spike. Thereby, one assumes that the black hole growths adiabatic. Another uncertainty for the spike formation is the location of the black hole. The black hole has to be located at the centre of the initial dark matter cusp. As an example we calculated the dark matter spike and the dark matter column density of the blazar TXS $0506 + 056$. We presented the newest constrains on the dark matter cross section with photons and neutrinos. This motivated us to look at dark matter scatterings for a particular model toy model example.

Then, we studied the possible flux attenuation of neutrino-dark matter interactions given by a fairly simple toy model, where we assumed the dark matter to be a scalar dark matter particle η and a fermionic mediator χ. We calculated the elastic scattering between the dark matter and the neutrino in the s- and u-channel. By assuming that the outgoing energy of the neutrino becomes irrelevant, we calculated the flux attenuation of the neutrinos in the vicinity of TXS $0506 + 056$. Due to the s-channel we have a resonance which could lead to an attenuation of the flux of over

65% close to the resonance for a dark matter mass of $m_\eta = 1$ GeV and a mediator mass of $m_\chi = 10$ GeV. For dark matter masses of $m_\eta > 1$ GeV or larger mass splittings between m_χ and m_η, we only detected an attenuation directly at the resonance peak.

The results motivated us to continue with a more general and sophisticated model, namely the t-channel mediator model which has as subclass the Scotogenic Model and its Scale Invariant extension. The Scotogenic Model is model for neutrinos that tries to explain the neutrino masses. But it can also be used for generating dark matter candidates. We introduced the two models briefly. The t-channel mediator model allows for either fermionic dark matter χ, as well as, for scalar dark matter η. For the case of scalar dark matter and η being a $SU(2)_L$ doublet we chose η^0 as the dark matter candidate. But the dark matter candidate could also be the pseudoscalar A^0, if it is lighter than η^0. In the Scotogenic Model χ as dark matter is very contrived. After introducing the model we discussed the neutrino- or photon-dark matter interaction for the two cases of fermionic and scalar dark matter.

For the scalar dark matter η^0 we denoted two different scenarios. First, the scenario where $m_{\eta^0} = 100$ GeV and $m_\chi = 105, 200$ GeV which is motivated by the t-channel mediator model. Second, the scenario where $m_{\eta^0} = 1$ TeV and $m_\chi = 10, 10^2, 10^3$ TeV motivated by the Scotogenic Model. We remark, that also the Scale Invariant Scotogenic Model can allow for fermionic dark matter. For the Majorana dark matter particle χ we mainly looked at the scenario, where $m_\chi = 100$ GeV and $m_{\eta^0} = 105, 200$ GeV.

In the case of the scalar dark matter m_η^0 we first looked at the elastic scattering between the dark matter and neutrinos which we already studied in the simple toy model. Then, we continued by studying the inelastic cross section of the processes $\nu\eta^0 \rightarrow \chi Z$, $\nu\eta^0 \rightarrow \eta^+ e^- / \eta^- e^+$ and $\nu\eta^0 \rightarrow \nu A^0$. The last two scatterings are interesting because they both have diagrams involved that scale with g^4 instead of $g^2 y^2$ and y^4. Therefore, they are independent of the unknown Yukawa coupling y. But we focused on the diagrams with $g^2 y^2$ and y^4 instead. Including the g^4 diagrams is left over as a future work. Also, the process of $\gamma\eta^0 \rightarrow e^-\eta^+ / e^+\eta^-$ which is proportional to g^4 has to be calculated and analysed in the future. We carefully studied the cross section produced by the $g^2 y^2$ and y^4 diagrams and obtained cross section for $E_\nu \gg m_\chi, m_{\eta^0}$ which scale as $\sigma \sim E_\nu^{-1}$ in accordance with unitarity.

In the case of χ being the dark matter candidate we also calculated the elastic scattering mediated by the scalar η^0. Then, we studied the inelastic scattering processes between the dark matter particles and the neutrino given by $\nu\chi \rightarrow \eta^0 Z$ and $\nu\chi \rightarrow W^-\eta^+ / W^+\eta^-$. These interactions also scale with $y^2 g^2$. Also, we computed the cross section behaviour for $E_\nu \gg m_\chi, m_{\eta^0}$ and saw that $\sigma \sim E^{-1}$. Furthermore, we varied the masses of the η doublett, namely $\Delta(m_\eta - m_{\eta^0})$ and $\Delta(m_{A^0} - m_{\eta^0})$, where m_η was the mass of the charged scalar particle, to see their impact on the cross section. We have seen that for large cross section the mass splitting in the doublet is negligible.

We continued with examining the inelastic scattering process between gamma-rays and dark matter given by $\gamma\chi \rightarrow \tilde{e}^+ e^- / \tilde{e}^- e^+$. In this case η is a singlet under $SU(2)_L$. To be more concrete, we chose the η particle to be the selectron $\tilde{e}$ of the MSSM as our mediator particle and calculated the cross section. Furthermore, we have calculated the total inelastic cross section of the neutrino-dark matter interaction as an incoherent sum of the three single processes.

As a last step, we used the calculated cross section to investigate the rate of absorption $\Phi^{\mathrm{obs}}/\Phi^{\mathrm{em}}$ of photons and neutrinos. Due to the inelastic scattering the cascade equation reduces to an exponential decrease because the neutrinos or photons get absorbed. Only for fermionic dark matter we investigated the possible flux attenuation of photons. We demanded that the flux should be attenuated to 65% of its initial value which gives an attenuation coefficient of $\mu \geq 1$. In the vicinity of the blazar TXS $0506 + 056$ the attenuation is for both dark cases, the scalar and fermionic dark matter, less than 65%, regardless if the dark matter interacts with photons or neutrinos. The column density of TXS $0506 + 056$ is to small in order to lead to high absorption. This motivated us to determine the neutrino and photon energy ranges for flux reduction of at least 65%, due to their interaction with dark matter. This was done by varying the dark matter column density Σ_{DM} for the total inelastic scattering cross section. For the scalar dark matter scenario and the fermionic dark matter scenario we found energy ranges between ~ 100 GeV up to 750 TeV (scalar dark matter) or 1000 TeV (fermionic dark matter) for a dark matter mass of $m_{\mathrm{DM}} = 100$ GeV and column densities between $\Sigma_{\mathrm{DM}} = 10^{36} - 10^{39}$ GeV/cm^2. For a dark matter mass of $m_{\mathrm{DM}} = 1$ TeV (scalar dark matter) we only found very tiny energy ranges for even larger column densities.

Furthermore, we estimated the black holes mass for the column densities that given absorption of at least 65% with the values of TXS $0506 + 056$ and a dark matter spike index $\gamma_{\mathrm{sp}} = 7/3$. We found that $M_{\mathrm{BH}} \sim 10^{18} - 10^{23} M_{\odot}$. The estimations showed that the black hole masses would exceed the current known black hole masses by 7-12 orders of magnitude. Nevertheless, it was only an estimation and not a strict analysis. We did not take into account all of the astrophysical uncertainties. Working out the black hole masses more precisely for the different variable astrophysical properties could be done in the future. Moreover, it is not entirely impossible that such high black hole masses or let us say such high column densities are realised in our universe.

All together, hopefully this thesis has shown that AGNs are powerful probes of dark matter properties. They give a good opportunity to test specific dark matter models and their interactions with standard model particles. As future work, we leave the occasion to probe more dark matter models with AGNs and the method presented in this thesis.

Bibliography

[1] Gregor Schiemann, ed. *Was Ist Natur? Klassische Texte Zur Naturphilosophie.* Deutscher Taschenbuchverlag, 1996.

[2] Jens Erler and Matthias Schott. "Electroweak precision tests of the Standard Model after the discovery of the Higgs boson". In: *Progress in Particle and Nuclear Physics* 106 (May 2019), pp. 68–119. DOI: 10.1016/j.ppnp.2019.02.007. URL: https://doi.org/10.1016%2Fj.ppnp.2019.02.007.

[3] Francesc Ferrer, Gonzalo Herrera, and Alejandro Ibarra. "New constraints on the dark matter-neutrino and dark matter-photon scattering cross sections from TXS 0506+056". In: *Journal of Cosmology and Astroparticle Physics* 2023.05 (May 2023), p. 057. DOI: 10.1088/1475-7516/2023/05/057. URL: https://doi.org/10.1088%5C%2F1475-7516%5C%2F2023%5C%2F05%5C%2F057.

[4] James M. Cline and Matteo Puel. "NGC 1068 constraints on neutrino-dark matter scattering". In: *Journal of Cosmology and Astroparticle Physics* 2023.06 (June 2023), p. 004. DOI: 10.1088/1475-7516/2023/06/004. URL: https://doi.org/10.1088%5C%2F1475-7516%5C%2F2023%5C%2F06%5C%2F004.

[5] F. Zwicky. "Die Rotverschiebung von extragalaktischen Nebeln". In: *Helvetica Physica Acta* 6 (Jan. 1933), pp. 110–127.

[6] Vera C. Rubin and Jr. Ford W. Kent. "Rotation of the Andromeda Nebula from a Spectroscopic Survey of Emission Regions". In: *Astrophys. J.* 159 (Feb. 1970), p. 379. DOI: 10.1086/150317.

[7] Gianfranco Bertone, Dan Hooper, and Joseph Silk. "Particle dark matter: evidence, candidates and constraints". In: *Physics Reports* 405.5-6 (Jan. 2005), pp. 279–390. DOI: 10.1016/j.physrep.2004.08.031. URL: https://doi.org/10.1016%2Fj.physrep.2004.08.031.

[8] M. Milgrom. "A modification of the Newtonian dynamics as a possible alternative to the hidden mass hypothesis." In: *Astrophys. J.* 270 (July 1983), pp. 365–370. DOI: 10.1086/161130.

[9] F. Zwicky. "On the Masses of Nebulae and of Clusters of Nebulae". In: *Astrophys. J.* 86 (Oct. 1937), p. 217. DOI: 10.1086/143864.

[10] J. G. de Swart, G. Bertone, and J. van Dongen. "How dark matter came to matter". In: *Nature Astronomy* 1.3 (Mar. 2017). DOI: 10.1038/s41550-017-0059. URL: https://doi.org/10.1038%2Fs41550-017-0059.

[11] Sinclair Smith. "The Mass of the Virgo Cluster". In: *Astrophys. J.* 83 (Jan. 1936), p. 23. DOI: 10.1086/143697.

[12] Richard Massey, Thomas Kitching, and Johan Richard. "The dark matter of gravitational lensing". In: *Reports on Progress in Physics* 73.8 (July 2010), p. 086901. DOI: 10.1088/0034-4885/73/8/086901. URL: https://dx.doi.org/10.1088/0034-4885/73/8/086901.

[13] M. Markevitch et al. "A Textbook Example of a Bow Shock in the Merging Galaxy Cluster 1E 0657-56". In: *Astrophys. J. Lett.* 567.1 (Mar. 2002), pp. L27–L31. DOI: 10.1086/339619. arXiv: astro-ph/0110468 [astro-ph].

[14] *Credit: X-ray: NASA/CXC/CfA/ M.Markevitch et al.; Lensing Map: NASA/STScI; ESO WFI; Magellan/U.Arizona/ D.Clowe et al. Optical image: NASA/STScI; Magellan/U.Arizona/D.Clowe et al.* URL: https://chandra.harvard.edu/photo/2006/1e0657/more.html.

[15] *Credit: NASA/ESA/M.Bradac et al.* URL: https://chandra.harvard.edu/photo/2008/macs/more.html.

[16] Douglas Clowe et al. "A Direct Empirical Proof of the Existence of Dark Matter". In: *Astrophys. J.* 648.2 (Aug. 2006), pp. L109–L113. DOI: 10.1086/508162. URL: https://doi.org/10.1086%5C%2F508162.

[17] A. A. Penzias and R. W. Wilson. "A Measurement of Excess Antenna Temperature at 4080 Mc/s." In: *Astrophys. J.* 142 (July 1965), pp. 419–421. DOI: 10.1086/148307.

[18] Ruth Durrer. "The cosmic microwave background: the history of its experimental investigation and its significance for cosmology". In: *Classical and Quantum Gravity* 32.12 (June 2015), p. 124007. DOI: 10.1088/0264-9381/32/12/124007. URL: https://dx.doi.org/10.1088/0264-9381/32/12/124007.

[19] P. J. E. Peebles. "Large-scale background temperature and mass fluctuations due to scale-invariant primeval perturbations". In: *Astrophys. J. Lett.* 263 (Dec. 1982), pp. L1–L5. DOI: 10.1086/183911.

[20] N. Aghanim et al. "Planck 2018 results. I. Overview and the cosmological legacy of Planck". In: *Astron. Astrophys.* 641 (Sept. 2020), A1. DOI: 10.1051/0004-6361/201833880. URL: https://doi.org/10.1051%5C%2F0004-6361%5C%2F201833880.

[21] Wayne Hu, Naoshi Sugiyama, and Joseph Silk. "The physics of microwave background anisotropies". In: *Nature* 386.6620 (Mar. 1997), pp. 37–43. DOI: 10.1038/386037a0. URL: https://doi.org/10.1038%5C%2F386037a0.

[22] N. Aghanim et al. "Planck 2018 results. VI. Cosmological parameters". In: *Astron. Astrophys.* 641 (Sept. 2020), A6. DOI: 10.1051/0004-6361/201833910. URL: https://doi.org/10.1051%5C%2F0004-6361%5C%2F201833910.

[23] George F. Chapline and Paul H. Frampton. "A new direction for dark matter research: intermediate-mass compact halo objects". In: *Journal of Cosmology and Astroparticle Physics* 2016.11 (Nov. 2016), p. 042. DOI: 10.1088/1475-7516/2016/11/042. URL: https://dx.doi.org/10.1088/1475-7516/2016/11/042.

[24] Jaiyul Yoo, Julio Chaname, and Andrew Gould. "The end of the MACHO era: limits on halo dark matter from stellar halo wide binaries". In: *Astrophys. J.* 601 (2004), pp. 311–318. DOI: 10.1086/380562. arXiv: astro-ph/0307437.

[25] Massimo Ricotti, Jeremiah P. Ostriker, and Katherine J. Mack. "Effect of Primordial Black Holes on the Cosmic Microwave Background and Cosmological Parameter Estimates". In: *The Astrophysical Journal* 680.2 (June 2008), pp. 829–845. DOI: 10.1086/587831. URL: https://doi.org/10.1086%5C%2F587831.

[26] Jihn E. Kim and Gianpaolo Carosi. "Axions and the strong *CP* problem". In: *Rev. Mod. Phys.* 82 (1 Mar. 2010), pp. 557–601. DOI: 10.1103/RevModPhys.82.557. URL: https://link.aps.org/doi/10.1103/RevModPhys.82.557.

[27] Pierre Sikivie. "Invisible axion search methods". In: *Rev. Mod. Phys.* 93 (1 Feb. 2021), p. 015004. DOI: 10.1103/RevModPhys.93.015004. URL: https://link.aps.org/doi/10.1103/RevModPhys.93.015004.

[28] L. J. Rosenberg and K. A. van Bibber. "Searches for invisible axions." In: *Phys. Rep.* 325.1 (Feb. 2000), pp. 1–39. DOI: 10.1016/S0370-1573(99)00045-9.

[29] A. Bellerive et al. "The Sudbury Neutrino Observatory". In: *Nuclear Physics B* 908 (July 2016), pp. 30–51. DOI: 10.1016/j.nuclphysb.2016.04.035. URL: https://doi.org/10.1016%2Fj.nuclphysb.2016.04.035.

[30] Yu-Feng Li et al. "Unambiguous determination of the neutrino mass hierarchy using reactor neutrinos". In: *Phys. Rev. D* 88 (1 July 2013), p. 013008. DOI: 10.1103/PhysRevD.88.013008. URL: https://link.aps.org/doi/10.1103/PhysRevD.88.013008.

[31] M. Aker et al. "Direct neutrino-mass measurement with sub-electronvolt sensitivity". In: *Nature Phys.* 18.2 (2022), pp. 160–166. DOI: 10.1038/s41567-021-01463-1. arXiv: 2105.08533 [hep-ex].

[32] J. R. Bond, G. Efstathiou, and J. Silk. "Massive Neutrinos and the Large-Scale Structure of the Universe". In: *Phys. Rev. Lett.* 45 (24 Dec. 1980), pp. 1980–1984. DOI: 10.1103/PhysRevLett.45.1980. URL: https://link.aps.org/doi/10.1103/PhysRevLett.45.1980.

[33] P. J. E. Peebles. "The Origin of Galaxies and Clusters of Galaxies". In: *Science* 224.4656 (1984), pp. 1385–1391. DOI: 10.1126/science.224.4656.1385. eprint: https://www.science.org/doi/pdf/10.1126/science.224.4656.1385. URL: https://www.science.org/doi/abs/10.1126/science.224.4656.1385.

[34] Hasan Yüksel, John F. Beacom, and Casey R. Watson. "Strong Upper Limits on Sterile Neutrino Warm Dark Matter". In: *Physical Review Letters* 101.12 (Sept. 2008). DOI: 10.1103/physrevlett.101.121301. URL: https://doi.org/10.1103%2Fphysrevlett.101.121301.

[35] A. Boyarsky et al. "Sterile neutrino Dark Matter". In: *Progress in Particle and Nuclear Physics* 104 (Jan. 2019), pp. 1–45. DOI: 10.1016/j.ppnp.2018.07.004. URL: https://doi.org/10.1016%2Fj.ppnp.2018.07.004.

[36] Sacha Davidson and Alejandro Ibarra. "A lower bound on the right-handed neutrino mass from leptogenesis". In: *Physics Letters B* 535.1-4 (May 2002), pp. 25–32. DOI: 10.1016/s0370-2693(02)01735-5. URL: https://doi.org/10.1016%2Fs0370-2693%2802%2901735-5.

[37] Lars Bergström. "Dark matter candidates". In: *New Journal of Physics* 11.10 (Oct. 2009), p. 105006. DOI: 10.1088/1367-2630/11/10/105006. URL: https://dx.doi.org/10.1088/1367-2630/11/10/105006.

[38] Giorgio Arcadi et al. "The waning of the WIMP? A review of models, searches, and constraints". In: *The European Physical Journal C* 78.3 (Mar. 2018). DOI: 10.1140/epjc/s10052-018-5662-y. URL: https://doi.org/10.1140%5C%2Fepjc%5C%2Fs10052-018-5662-y.

[39] Leszek Roszkowski, Enrico Maria Sessolo, and Sebastian Trojanowski. "WIMP dark matter candidates and searches—current status and future prospects". In: *Reports on Progress in Physics* 81.6 (May 2018), p. 066201. DOI: 10.1088/1361-6633/aab913. URL: https://dx.doi.org/10.1088/1361-6633/aab913.

[40] G.C. Branco et al. "Theory and phenomenology of two-Higgs-doublet models". In: *Physics Reports* 516.1-2 (July 2012), pp. 1–102. DOI: 10.1016/j.physrep.2012.02.002. URL: https://doi.org/10.1016%2Fj.physrep.2012.02.002.

[41] Susana Cebrian. "Review on dark matter searches". In: *Journal of Physics: Conference Series* 2502.1 (May 2023), p. 012004. DOI: 10.1088/1742-6596/2502/1/012004. URL: https://doi.org/10.1088%2F1742-6596%2F2502%2F1%2F012004.

[42] Laura Baudis. "Dark matter searches". In: *Annalen der Physik* 528.1-2 (), pp. 74–83. DOI: https://doi.org/10.1002/andp.201500114. eprint: https://onlinelibrary.wiley.com/doi/pdf/10.1002/andp.201500114. URL: https://onlinelibrary.wiley.com/doi/abs/10.1002/andp.201500114.

[43] Edward W. Kolb and Michael S. Turner. *The Early Universe*. Vol. 69. 1990. ISBN: 978-0-201-62674-2. DOI: 10.1201/9780429492860.

[44] David Tong. *Lectures on Cosmology*. 2019. URL: http://www.damtp.cam.ac.uk/user/tong/cosmo/cosmo.pdf.

[45] Paolo Gondolo and Graciela Gelmini. "Cosmic abundances of stable particles: Improved analysis". In: *Nucl. Phys. B* 360 (1991), pp. 145–179. DOI: 10.1016/0550-3213(91)90438-4.

[46] Kim Griest and David Seckel. "Three exceptions in the calculation of relic abundances". In: *Phys. Rev. D* 43 (10 May 1991), pp. 3191–3203. DOI: 10.1103/PhysRevD.43.3191. URL: https://link.aps.org/doi/10.1103/PhysRevD.43.3191.

[47] Raffaele Tito D'Agnolo and Joshua T. Ruderman. "Light Dark Matter from Forbidden Channels". In: *Phys. Rev. Lett.* 115 (6 Aug. 2015), p. 061301. DOI: 10.1103/PhysRevLett.115.061301. URL: https://link.aps.org/doi/10.1103/PhysRevLett.115.061301.

[48] Steven Weinberg. *The Quantum Theory of Fields*. Vol. 1. Cambridge University Press, 1995.

[49]   B. A. Lippmann and Julian Schwinger. "Variational Principles for Scattering Processes. I". In: *Phys. Rev.* 79 (3 Aug. 1950), pp. 469–480. DOI: 10.1103/PhysRev.79.469. URL: https://link.aps.org/doi/10.1103/PhysRev.79.469.

[50]   Michael E. Peskin and Daniel V. Schroeder. *An Introduction to quantum field theory*. Reading, USA: Addison-Wesley, 1995. ISBN: 978-0-201-50397-5.

[51]   David Tong. *Lectures on Quantum Field Theory*. 2007. URL: http://www.damtp.cam.ac.uk/user/tong/qft/qft.pdf.

[52]   Thomas Hahn. "Generating Feynman diagrams and amplitudes with FeynArts 3". In: *Computer Physics Communications* 140.3 (Nov. 2001), pp. 418–431. DOI: 10.1016/s0010-4655(01)00290-9. URL: https://doi.org/10.1016%2Fs0010-4655%2801%2900290-9.

[53]   Vladyslav Shtabovenko, Rolf Mertig, and Frederik Orellana. "FeynCalc 9.3: New features and improvements". In: *Computer Physics Communications* 256 (Nov. 2020), p. 107478. DOI: 10.1016/j.cpc.2020.107478. URL: https://doi.org/10.1016%2Fj.cpc.2020.107478.

[54]   Vladyslav Shtabovenko, Rolf Mertig, and Frederik Orellana. "New developments in FeynCalc 9.0". In: *Computer Physics Communications* 207 (Oct. 2016), pp. 432–444. DOI: 10.1016/j.cpc.2016.06.008. URL: https://doi.org/10.1016%2Fj.cpc.2016.06.008.

[55]   R. Mertig, M. Böhm, and A. Denner. "Feyn Calc - Computer-algebraic calculation of Feynman amplitudes". In: *Computer Physics Communications* 64.3 (1991), pp. 345–359. ISSN: 0010-4655. DOI: https://doi.org/10.1016/0010-4655(91)90130-D. URL: https://www.sciencedirect.com/science/article/pii/001046559190130D.

[56]   R. L. Workman et al. "Review of Particle Physics". In: *PTEP* 2022 (2022), p. 083C01. DOI: 10.1093/ptep/ptac097.

[57]   *Particle Dark Matter: Observations, Models and Searches*. Cambridge University Press, 2010. DOI: 10.1017/CBO9780511770739.

[58]   Julio F. Navarro, Carlos S. Frenk, and Simon D. M. White. "The Structure of Cold Dark Matter Halos". In: *The Astrophysical Journal* 462 (May 1996), p. 563. DOI: 10.1086/177173. URL: https://doi.org/10.1086%2F177173.

[59]   Riccardo Catena and Piero Ullio. "A novel determination of the local dark matter density". In: *Journal of Cosmology and Astroparticle Physics* 2010.08 (Aug. 2010), pp. 004–004. DOI: 10.1088/1475-7516/2010/08/004. URL: https://doi.org/10.1088%2F1475-7516%2F2010%2F08%2F004.

[60]   Julio F. Navarro et al. "The diversity and similarity of simulated cold dark matter haloes". In: *Monthly Notices of the Royal Astronomical Society* 402.1 (Dec. 2009), pp. 21–34. DOI: 10.1111/j.1365-2966.2009.15878.x. URL: https://doi.org/10.1111%2Fj.1365-2966.2009.15878.x.

[61]   J. N. Bahcall and R. M. Soneira. "The universe at faint magnitudes. I. Models for the Galaxy and the predicted star counts." In: *Astrophys. J. Suppl. Ser.* 44 (Sept. 1980), pp. 73–110. DOI: 10.1086/190685.

[62]   Albert Einstein. "Die Feldgleichungen der Gravitation". In: *Sitzungsberichte der Koeniglich Preussischen Akademie der Wissenschaften (Berlin* (Jan. 1915), 844–847).

[63]   *Credit: EHT Collaboration.* URL: https://eventhorizontelescope.org/blog/astronomers-reveal-first-image-black-hole-heart-our-galaxy.

[64]   *Credit: EHT Collaboration.* URL: https://eventhorizontelescope.org/press-release-april-10-2019-astronomers-capture-first-image-black-hole.

[65]   R. Genzel et al. "On the nature of the dark mass in the centre of the Milky Way". In: *Monthly Notices of the Royal Astronomical Society* 291.1 (Oct. 1997), pp. 219–234. DOI: 10.1093/mnras/291.1.219.

[66]   A. M. Ghez et al. "High Proper-Motion Stars in the Vicinity of Sagittarius A*: Evidence for a Supermassive Black Hole at the Center of Our Galaxy". In: *Astrophys. J.* 509.2 (Dec. 1998), pp. 678–686. DOI: 10.1086/306528. arXiv: astro-ph/9807210 [astro-ph].

[67]   A. Eckart and R. Genzel. "Stellar proper motions in the central 0.1 pc of the Galaxy". In: *Monthly Notices of the Royal Astronomical Society* 284.3 (Jan. 1997), pp. 576–598. ISSN: 0035-8711. DOI: 10.1093/mnras/284.3.576. eprint: https://academic.oup.com/mnras/article-pdf/284/3/576/3065815/284-3-576.pdf. URL: https://doi.org/10.1093/mnra%20s/284.3.576.

[68]   Event Horizon Telescope Collaboration et al. In: 930.2 (May 2022), p. L12. DOI: 10.3847/2041-8213/ac6674. URL: https://dx.doi.org/10.3847/2041-8213/ac6674.

[69]   Event Horizon Telescope Collaboration et al. "First M87 Event Horizon Telescope Results. I. The Shadow of the Supermassive Black Hole". In: *Astrophysical Journal, Letters to the Editor* 875.1, L1 (Apr. 2019), p. L1. DOI: 10.3847/2041-8213/ab0ec7. arXiv: 1906.11238 [astro-ph.GA].

[70]   D. Lynden-Bell. "Galactic Nuclei as Collapsed Old Quasars". In: *Nature* 223.5207 (Aug. 1969), pp. 690–694. DOI: 10.1038/223690a0.

[71]   Max Planck Institute for extraterrestrial physics. *Galactic Center Research Overview.* 2021. URL: https://www.mpe.mpg.de/ir/GC.

[72]   C. Megan Urry and Paolo Padovani. "Unified Schemes for Radio-Loud Active Galactic Nuclei". In: *Publications of the Astronomical Society of the Pacific* 107 (Sept. 1995), p. 803. DOI: 10.1086/133630. URL: https://doi.org/10.1086%2F133630.

[73]   and Mark Aartsen et al. "Multimessenger observations of a flaring blazar coincident with high-energy neutrino IceCube-170922A". In: *Science* 361.6398 (July 2018). DOI: 10.1126/science.aat1378. URL: https://doi.org/10.1126%2Fscience.aat1378.

[74]   Mark Aartsen et al. "Neutrino emission from the direction of the blazar TXS 0506+056 prior to the IceCube-170922A alert". In: *Science* 361.6398 (July 2018), pp. 147–151. DOI: 10.1126/science.aat2890. URL: https://doi.org/10.1126%2Fscience.aat2890.

[75] R. Abbasi et al. "Evidence for neutrino emission from the nearby active galaxy NGC 1068". In: *Science* 378.6619 (Nov. 2022), pp. 538–543. DOI: 10.1126/science.abg3395. URL: https://doi.org/10.1126%2Fscience.abg3395.

[76] Marco Ajello, Kohta Murase, and Alex McDaniel. "Disentangling the Hadronic Components in NGC 1068". In: *The Astrophysical Journal Letters* 954.2 (Sept. 2023), p. L49. DOI: 10.3847/2041-8213/acf296. URL: https://doi.org/10.3847%2F2041-8213%2Facf296.

[77] Kohta Murase, Markus Ahlers, and Brian C. Lacki. "Testing the hadronuclear origin of PeV neutrinos observed with IceCube". In: *Physical Review D* 88.12 (Dec. 2013). DOI: 10.1103/physrevd.88.121301. URL: https://doi.org/10.1103%2Fphysrevd.88.121301.

[78] Walter Winter. "Photohadronic origin of the TeV-PeV neutrinos observed in IceCube". In: *Physical Review D* 88.8 (Oct. 2013). DOI: 10.1103/physrevd.88.083007. URL: https://doi.org/10.1103%2Fphysrevd.88.083007.

[79] N. I. Shakura and R. A. Sunyaev. "Black holes in binary systems. Observational appearance." In: *Astron. Astrophys.* 24 (Jan. 1973), pp. 337–355.

[80] Edward M. Cackett et al. "Accretion Disk Reverberation with Hubble Space Telescope Observations of NGC 4593: Evidence for Diffuse Continuum Lags". In: *The Astrophysical Journal* 857.1 (Apr. 2018), p. 53. DOI: 10.3847/1538-4357/aab4f7. URL: https://dx.doi.org/10.3847/1538-4357/aab4f7.

[81] F. W. Stecker et al. "High-energy neutrinos from active galactic nuclei". In: *Phys. Rev. Lett.* 66 (21 May 1991), pp. 2697–2700. DOI: 10.1103/PhysRevLett.66.2697. URL: https://link.aps.org/doi/10.1103/PhysRevLett.66.2697.

[82] and Mark Aartsen et al. "Neutrino emission from the direction of the blazar TXS 0506+056 prior to the IceCube-170922A alert". In: *Science* 361.6398 (July 2018), pp. 147–151. DOI: 10.1126/science.aat2890. URL: https://doi.org/10.1126%2Fscience.aat2890.

[83] Paolo Gondolo and Joseph Silk. "Dark Matter Annihilation at the Galactic Center". In: *Physical Review Letters* 83.9 (Aug. 1999), pp. 1719–1722. DOI: 10.1103/physrevlett.83.1719. URL: https://doi.org/10.1103%5C%2Fphysrevlett.83.1719.

[84] P. J. E. Peebles. "Gravitational collapse and related phenomena from an empirical point of view, or, black holes are where you find them." In: *General Relativity and Gravitation* 3.1-2 (June 1972), pp. 63–82. DOI: 10.1007/BF00755923.

[85] Gerald D. Quinlan, Lars Hernquist, and Steinn Sigurdsson. "Models of Galaxies with Central Black Holes: Adiabatic Growth in Spherical Galaxies". In: *The Astrophysical Journal* 440 (Feb. 1995), p. 554. DOI: 10.1086/175295. URL: https://doi.org/10.1086%2F175295.

[86] James M. Cline et al. "Blazar Constraints on Neutrino-Dark Matter Scattering". In: *Physical Review Letters* 130.9 (Feb. 2023). DOI: 10.1103/physrevlett.130.091402. URL: https://doi.org/10.1103%2Fphysrevlett.130.091402.

[87] Pierre Salati. "Indirect and direct dark matter detection". In: *PoS* CARGESE2007 (2007). Ed. by Jean Orloff, Geraldine Servant, and Gerard Smadja, p. 009. DOI: 10.22323/1.049.0009.

[88] Thomas Lacroix et al. "Unique probe of dark matter in the core of M87 with the Event Horizon Telescope". In: *Physical Review D* 96.6 (Sept. 2017). DOI: 10.1103/physrevd.96.063008. URL: https://doi.org/10.1103%2Fphysrevd.96.063008.

[89] Piero Ullio, HongSheng Zhao, and Marc Kamionkowski. "Dark-matter spike at the galactic center?" In: *Physical Review D* 64.4 (July 2001). DOI: 10.1103/physrevd.64.043504. URL: https://doi.org/10.1103%2Fphysrevd.64.043504.

[90] David Merritt, Licia Verde, and Raul Jimenez. "Dark Matter Spikes and Annihilation Radiation from the Galactic Center". In: *Physical Review Letters* 88.19 (Apr. 2002). DOI: 10.1103/physrevlett.88.191301. URL: https://doi.org/10.1103%2Fphysrevlett.88.191301.

[91] Shyam Balaji et al. *Dark Matter spikes around Sgr A* in γ-rays*. 2023. arXiv: 2303.12107 [hep-ph].

[92] Oleg Y. Gnedin and Joel R. Primack. "Dark Matter Profile in the Galactic Center". In: *Physical Review Letters* 93.6 (Aug. 2004). DOI: 10.1103/physrevlett.93.061302. URL: https://doi.org/10.1103%2Fphysrevlett.93.061302.

[93] Man Ho Chan and Chak Man Lee. "Indirect Evidence for Dark Matter Density Spikes around Stellar-mass Black Holes". In: *The Astrophysical Journal Letters* 943.2 (Jan. 2023), p. L11. DOI: 10.3847/2041-8213/acaafa. URL: https://doi.org/10.3847%2F2041-8213%2Facaafa.

[94] Carlos A. Argüelles, Ali Kheirandish, and Aaron C. Vincent. "Imaging Galactic Dark Matter with High-Energy Cosmic Neutrinos". In: *Physical Review Letters* 119.20 (Nov. 2017). DOI: 10.1103/physrevlett.119.201801. URL: https://doi.org/10.1103%2Fphysrevlett.119.201801.

[95] P Padovani et al. "TXS 0506+056, the first cosmic neutrino source, is not a BL Lac". In: *Monthly Notices of the Royal Astronomical Society: Letters* 484.1 (Jan. 2019), pp. L104–L108. ISSN: 1745-3925. DOI: 10.1093/mnrasl/slz011. eprint: https://academic.oup.com/mnrasl/article-pdf/484/1/L104/27711472/slz011.pdf. URL: https://doi.org/10.1093/mnrasl/slz011.

[96] Ki-Young Choi, Jongkuk Kim, and Carsten Rott. "Constraining dark matter-neutrino interactions with IceCube-170922A". In: *Physical Review D* 99.8 (Apr. 2019). DOI: 10.1103/physrevd.99.083018. URL: https://doi.org/10.1103%2Fphysrevd.99.083018.

[97] Carlos A. Argüelles, Ali Kheirandish, and Aaron C. Vincent. "Imaging Galactic Dark Matter with High-Energy Cosmic Neutrinos". In: *Physical Review Letters* 119.20 (Nov. 2017). DOI: 10.1103/physrevlett.119.201801. URL: https://doi.org/10.1103%2Fphysrevlett.119.201801.

[98] Kensuke Akita and Shin'ichiro Ando. *Constraints on dark matter-neutrino scattering from the Milky-Way satellites and subhalo modeling for dark acoustic oscillations*. 2023. arXiv: 2305.01913 [astro-ph.CO].

[99] Mathias Garny, Alejandro Ibarra, and Stefan Vogl. "Signatures of Majorana dark matter with t-channel mediators". In: *International Journal of Modern Physics D* 24.07 (May 2015), p. 1530019. DOI: 10.1142/s0218271815300190. URL: https://doi.org/10.1142%5C%2Fs0218271815300190.

[100] Laura Lopez Honorez et al. "The inert doublet model: an archetype for dark matter". In: *Journal of Cosmology and Astroparticle Physics* 2007.02 (Feb. 2007), pp. 028–028. DOI: 10.1088/1475-7516/2007/02/028. URL: https://doi.org/10.1088%5C%2F1475-7516%5C%2F2007%5C%2F02%5C%2F028.

[101] Daniel Dercks and Tania Robens. "Constraining the Inert Doublet Model using Vector Boson Fusion". In: *The European Physical Journal C* 79.11 (Nov. 2019). DOI: 10.1140/epjc/s10052-019-7436-6. URL: https://doi.org/10.1140%5C%2Fepjc%5C%2Fs10052-019-7436-6.

[102] Mathias Garny et al. "Majorana dark matter with a coloured mediator: collider vs direct and indirect searches". In: *Journal of High Energy Physics* 2014.6 (June 2014). DOI: 10.1007/jhep06(2014)169. URL: https://doi.org/10.1007%2Fjhep06%282014%29169.

[103] Devabrat Mahanta and Debasish Borah. "Fermion dark matter with N2 leptogenesis in minimal scotogenic model". In: *Journal of Cosmology and Astroparticle Physics* 2019.11 (Nov. 2019), pp. 021–021. DOI: 10.1088/1475-7516/2019/11/021. URL: https://doi.org/10.1088%2F1475-7516%2F2019%2F11%2F021.

[104] Debasish Borah, P. S. Bhupal Dev, and Abhass Kumar. "TeV scale leptogenesis, inflaton dark matter, and neutrino mass in a scotogenic model". In: *Phys. Rev. D* 99 (5 Mar. 2019), p. 055012. DOI: 10.1103/PhysRevD.99.055012. URL: https://link.aps.org/doi/10.1103/PhysRevD.99.055012.

[105] Jisuke Kubo, Ernest Ma, and Daijiro Suematsu. "Cold Dark Matter, Radiative Neutrino Mass, mu to e gamma, and Neutrinoless Double Beta Decay". In: *Physics Letters B* 642.1-2 (Nov. 2006), pp. 18–23. DOI: 10.1016/j.physletb.2006.08.085. URL: https://doi.org/10.1016%2Fj.physletb.2006.08.085.

[106] Ivania M Avila, Giovanna Cottin, and Marco A Diaz. "Revisiting the scotogenic model with scalar dark matter". In: *Journal of Physics G: Nuclear and Particle Physics* 49.6 (Apr. 2022), p. 065001. DOI: 10.1088/1361-6471/ac5fb4. URL: https://doi.org/10.1088%2F1361-6471%2Fac5fb4.

[107] Rachik Soualah and Amine Ahriche. "Scale invariant scotogenic model: Dark matter and the scalar sector". In: *Physical Review D* 105.5 (Mar. 2022). DOI: 10.1103/physrevd.105.055017. URL: https://doi.org/10.1103%2Fphysrevd.105.055017.

[108] Takashi Toma and Avelino Vicente. "Lepton flavor violation in the scotogenic model". In: *Journal of High Energy Physics* 2014.1 (Jan. 2014). DOI: 10.1007/jhep01(2014)160. URL: https://doi.org/10.1007%2Fjhep01%282014%29160.

[109] Joachim Kopp, Lisa Michaels, and Juri Smirnov. "Loopy constraints on leptophilic dark matter and internal bremsstrahlung". In: *Journal of Cosmology and Astroparticle Physics* 2014.04 (Apr. 2014), pp. 022–022. DOI: `10.1088/1475-7516/2014/04/022`. URL: `https://doi.org/10.1088%2F1475-7516%2F2014%2F04%2F022`.

[110] Amine Ahriche, Kristian L. McDonald, and Salah Nasri. "The scale-invariant scotogenic model". In: *Journal of High Energy Physics* 2016.6 (June 2016). DOI: `10.1007/jhep06(2016)182`. URL: `https://doi.org/10.1007%2Fjhep06%282016%29182`.

[111] Janusz Rosiek. "Complete set of Feynman rules for the minimal supersymmetric extension of the standard model". In: *Physical Review D* 41.11 (June 1990), pp. 3464–3501. DOI: `10.1103/physrevd.41.3464`. URL: `https://doi.org/10.1103%2Fphysrevd.41.3464`.

[112] Amine Ahriche et al. "Scale-invariant models with one-loop neutrino mass and dark matter candidates". In: *Phys. Rev. D* 94 (5 Sept. 2016), p. 053005. DOI: `10.1103/PhysRevD.94.053005`. URL: `https://link.aps.org/doi/10.1103/PhysRevD.94.053005`.

[113] Ansgar Denner et al. "Feynman rules for fermion number violating interactions". In: *Nucl. Phys. B* 387 (1992), pp. 467–481. DOI: `10.1016/0550-3213(92)90169-C`.

[114] Nicholas J. McConnell et al. "Two ten-billion-solar-mass black holes at the centres of giant elliptical galaxies". In: *Nature* 480.7376 (Dec. 2011), pp. 215–218. DOI: `10.1038/nature10636`. URL: `https://doi.org/10.1038%2Fnature10636`.

[115] Hagai Netzer. "The Largest Black Holes and the Most Luminous Galaxies". In: *The Astrophysical Journal* 583.1 (Dec. 2002), p. L5. DOI: `10.1086/368012`. URL: `https://dx.doi.org/10.1086/368012`.

[116] Andrew King. "How big can a black hole grow?" In: *Monthly Notices of the Royal Astronomical Society: Letters* 456.1 (Dec. 2015), pp. L109–L112. ISSN: 1745-3925. DOI: `10.1093/mnrasl/slv186`. eprint: `https://academic.oup.com/mnrasl/article-pdf/456/1/L109/8011346/slv186.pdf`. URL: `https://doi.org/10.1093/mnrasl/slv186`.

[117] Bernard Carr, Florian Kühnel, and Luca Visinelli. "Constraints on stupendously large black holes". In: *Monthly Notices of the Royal Astronomical Society* 501.2 (Nov. 2020), pp. 2029–2043. ISSN: 0035-8711. DOI: `10.1093/mnras/staa3651`. eprint: `https://academic.oup.com/mnras/article-pdf/501/2/2029/35347450/staa3651.pdf`. URL: `https://doi.org/10.1093/mnras/staa3651`.